

EUROPEAN ORGANISATION FOR NUCLEAR RESEARCH (CERN)



JHEP 06 (2018) 107
 DOI: [DOI:10.1007/JHEP06\(2018\)107](https://doi.org/10.1007/JHEP06(2018)107)



CERN-EP-2017-182
 27th July 2018

Search for supersymmetry in final states with missing transverse momentum and multiple b -jets in proton–proton collisions at $\sqrt{s} = 13$ TeV with the ATLAS detector

The ATLAS Collaboration

A search for supersymmetry involving the pair production of gluinos decaying via third-generation squarks into the lightest neutralino ($\tilde{\chi}_1^0$) is reported. It uses LHC proton–proton collision data at a centre-of-mass energy $\sqrt{s} = 13$ TeV with an integrated luminosity of 36.1 fb^{-1} collected with the ATLAS detector in 2015 and 2016. The search is performed in events containing large missing transverse momentum and several energetic jets, at least three of which must be identified as originating from b -quarks. To increase the sensitivity, the sample is divided into subsamples based on the presence or absence of electrons or muons. No excess is found above the predicted background. For $\tilde{\chi}_1^0$ masses below approximately 300 GeV, gluino masses of less than 1.97 (1.92) TeV are excluded at 95% confidence level in simplified models involving the pair production of gluinos that decay via top (bottom) squarks. An interpretation of the limits in terms of the branching ratios of the gluinos into third-generation squarks is also provided. These results improve upon the exclusion limits obtained with the 3.2 fb^{-1} of data collected in 2015.

1 Introduction

Supersymmetry (SUSY) [1–6] is a generalisation of space-time symmetries that predicts new bosonic partners for the fermions and new fermionic partners for the bosons of the Standard Model (SM). If R -parity is conserved [7], SUSY particles are produced in pairs and the lightest supersymmetric particle (LSP) is stable. The scalar partners of the left- and right-handed quarks, the squarks \tilde{q}_L and \tilde{q}_R , can mix to form two mass eigenstates \tilde{q}_1 and \tilde{q}_2 , ordered by increasing mass. SUSY can solve the hierarchy problem [8–11] reducing unnatural tuning in the Higgs sector by orders of magnitude, provided that the superpartners of the top quark have masses not too far above the weak scale. The large top Yukawa coupling results in significant \tilde{t}_L - \tilde{t}_R mixing so that the mass eigenstate \tilde{t}_1 is typically lighter than the other squarks [12, 13]. Because of the SM weak-isospin symmetry, the mass of the lightest bottom squark \tilde{b}_1 is also expected to be close to the weak scale. The fermionic partners of the gluons, the gluinos (\tilde{g}), are also motivated by naturalness [14] to have a mass around the TeV scale in order to limit their contributions to the radiative corrections to the top squark masses. For these reasons, and because the gluinos are expected to be pair-produced with a high cross-section at the Large Hadron Collider (LHC), the search for gluino production with decays via top and bottom squarks is highly motivated at the LHC.

This paper presents a search for pair-produced gluinos decaying via top or bottom squarks in events with multiple jets originating from the hadronisation of b -quarks (b -jets in the following), high missing transverse momentum of magnitude E_T^{miss} , and potentially additional light-quark jets and/or an isolated charged lepton.¹ The dataset consists of 36.1 fb^{-1} of proton–proton (pp) collision data collected with the ATLAS detector [15] at a centre-of-mass energy of 13 TeV in 2015 and 2016. Interpretations are provided in the context of several effective simplified models [16–18] probing various gluino decays into third-generation squarks and the LSP. The latter is assumed to be the lightest neutralino $\tilde{\chi}_1^0$, a linear superposition of the superpartners of the neutral electroweak and Higgs bosons. One model also features the lightest charginos $\tilde{\chi}_1^\pm$, which are linear superpositions of the superpartners of the charged electroweak and Higgs bosons. The results supersede the ones obtained using 3.2 fb^{-1} of data collected in 2015 using the same strategy [19]. Pair-produced gluinos with top-squark-mediated decays have also been searched for using events containing pairs of same-sign leptons or three leptons using 13 TeV data [20, 21]. The same-sign/three lepton search is comparable in sensitivity to the search presented in this paper only when the masses of the gluino and the LSP are very close to each other. Similar searches performed using the 13 TeV dataset collected in 2015 and 2016 by the CMS experiment have produced results comparable to the ATLAS searches [22–25].

2 SUSY signal models

Various simplified SUSY models [17, 18] are employed to optimise the event selection and/or interpret the results of the search. In terms of experimental signature, they all contain at least four b -jets originating from either gluino or top quark decays, and two $\tilde{\chi}_1^0$, which escape the detector unseen, resulting in high E_T^{miss} .

Gluinos are assumed to be pair-produced and to decay either as $\tilde{g} \rightarrow \tilde{b}_1 \bar{b}$ or $\tilde{g} \rightarrow \tilde{t}_1 \bar{t}$ (the charge conjugate process is implied throughout this paper). The following top and bottom squark decays are then

¹ The term “lepton” refers exclusively to an electron or a muon in this paper.

considered: $\tilde{t}_1 \rightarrow t\tilde{\chi}_1^0$, $\tilde{t}_1 \rightarrow b\tilde{\chi}_1^+$ and $\tilde{b}_1 \rightarrow b\tilde{\chi}_1^0$.² In all cases, the top or bottom squarks are assumed to be off-shell in order to have simplified models with only two parameters: the gluino and $\tilde{\chi}_1^0$ masses.³ All other sparticles are decoupled.

Two simplified models are used to optimise the event selection and to interpret the results. In the Gbb (Gtt) model, illustrated in Figure 1(a) (1(b)), each gluino undergoes an effective three-body decay $\tilde{g} \rightarrow b\bar{b}\tilde{\chi}_1^0$ ($\tilde{g} \rightarrow t\bar{t}\tilde{\chi}_1^0$) via off-shell bottom (top) squarks, with a branching ratio of 100%. The Gbb model is the simplest in terms of particle multiplicity, resulting in the minimal common features of four b -jets and two $\tilde{\chi}_1^0$. In addition to these particles, the Gtt model produces four W bosons originating from the top quark decays: $t \rightarrow Wb$. The presence of these four W bosons motivates the design of signal regions with a higher jet multiplicity than for Gbb models, and in some cases with at least one isolated electron or muon.

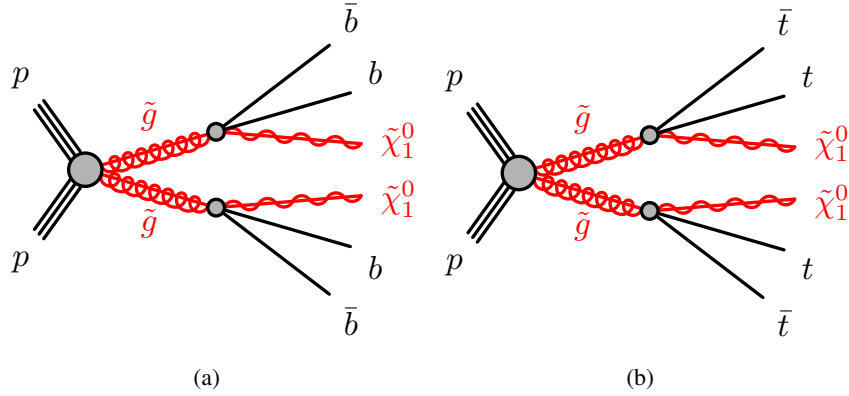


Figure 1: The decay topologies in the (a) Gbb and (b) Gtt simplified models.

This paper includes an interpretation that probes the sensitivity of the search as a function of the gluino branching ratio, in addition to the gluino and $\tilde{\chi}_1^0$ masses. Similar interpretations have been performed by the CMS collaboration [24, 27]. For that interpretation a third gluino decay is considered: $\tilde{g} \rightarrow t\bar{b}\tilde{\chi}_1^-$ (via the off-shell top squark decay $\tilde{t}_1^* \rightarrow \bar{b}\tilde{\chi}_1^-$). The $\tilde{\chi}_1^-$ is then forced to decay as $\tilde{\chi}_1^\pm \rightarrow W^*\tilde{\chi}_1^0 \rightarrow f\bar{f}'\tilde{\chi}_1^0$ (where f denotes a fermion). To keep the number of model parameters at only two, the mass difference between the $\tilde{\chi}_1^\pm$ and the $\tilde{\chi}_1^0$ is fixed to 2 GeV. Such a small mass-splitting between the $\tilde{\chi}_1^\pm$ and the $\tilde{\chi}_1^0$ is typical of models where the $\tilde{\chi}_1^0$ is dominated by the higgsinos, the superpartners of the neutral Higgs boson. Such models are well motivated by naturalness. The products of the decay $W^* \rightarrow f\bar{f}'$ are typically too soft to be detected, except for very large mass differences between the gluino and the $\tilde{\chi}_1^\pm$. Thus, in this model, the gluino can decay as either $\tilde{g} \rightarrow b\bar{b}\tilde{\chi}_1^0$, $\tilde{g} \rightarrow t\bar{b}\tilde{\chi}_1^-$ (with $\tilde{\chi}_1^- \rightarrow f\bar{f}'\tilde{\chi}_1^0$) or $\tilde{g} \rightarrow t\bar{t}\tilde{\chi}_1^0$, with the sum of individual branching ratios adding up to 100%. This model probes more realistic scenarios where the branching ratio for either $\tilde{g} \rightarrow b\bar{b}\tilde{\chi}_1^0$ or $\tilde{g} \rightarrow t\bar{t}\tilde{\chi}_1^0$ is not 100%, and where one, two or three top quarks, and thus on-shell W bosons, are possible in the final state, in between the Gbb (no top quarks) and Gtt (four top quarks) decay topologies. The decay topologies that are considered in the variable branching ratio model are illustrated in Figure 2. The model also includes the Gbb and Gtt decay topologies illustrated in

² The decay $\tilde{b}_1 \rightarrow t\tilde{\chi}_1^-$ is also possible but, following $\tilde{g} \rightarrow \tilde{b}_1\bar{b}$, it yields the same final state as $\tilde{g} \rightarrow \tilde{t}_1^*t \rightarrow (\bar{b}\tilde{\chi}_1^-)t$, which is already considered.

³ The analysis sensitivity is found to be mostly independent of the top and bottom squark masses, except when the top squark is very light [26].

Figure 1. A limited set of 10 mass points were generated for this variable branching ratio model with $m_{\tilde{g}}$ varying from 1.5 TeV to 2.3 TeV and $m_{\tilde{\chi}_1^0}$ varying from 1 GeV to 1 TeV.

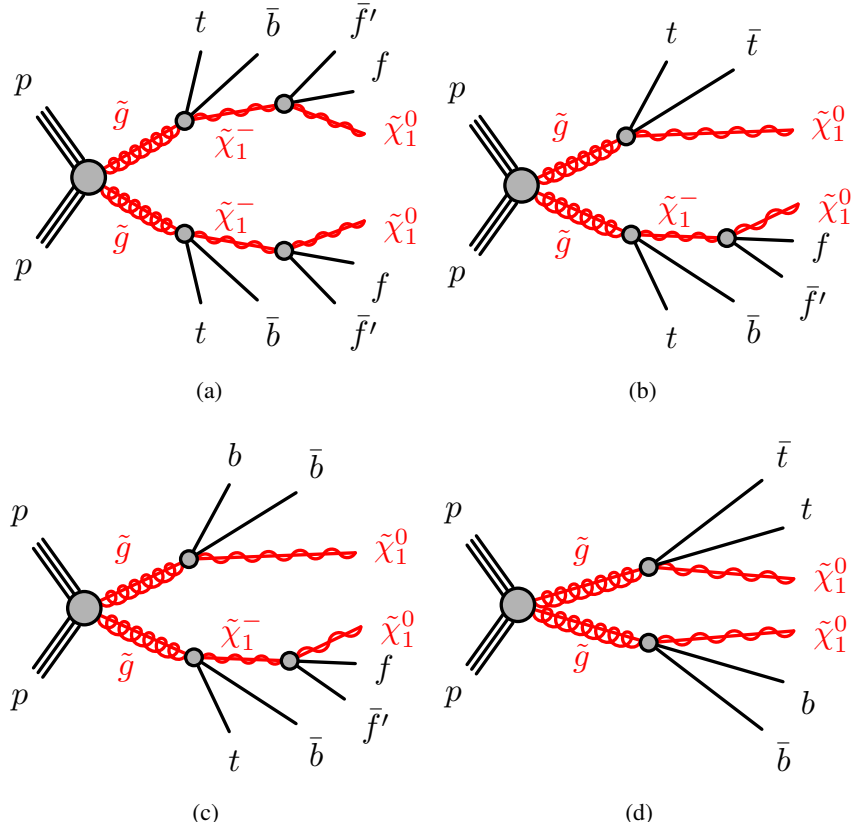


Figure 2: The additional decay topologies of the variable gluino branching ratio model in addition to the ones of Figure 1. (a) Both gluinos can decay as $\tilde{g} \rightarrow tb\tilde{\chi}_1^-$ with $\tilde{\chi}_1^- \rightarrow f\bar{f}\tilde{\chi}_1^0$, or only one can with the other decaying as (b) $\tilde{g} \rightarrow tt\tilde{\chi}_1^0$ or (c) $\tilde{g} \rightarrow bb\tilde{\chi}_1^0$. (d) Finally, one gluino can decay as $\tilde{g} \rightarrow tb\tilde{\chi}_1^-$ and the other as $\tilde{g} \rightarrow b\bar{b}\tilde{\chi}_1^0$. The charge conjugate processes are implied. The fermions originating from the $\tilde{\chi}_1^\pm$ decay are typically soft because the mass difference between the $\tilde{\chi}_1^\pm$ and the $\tilde{\chi}_1^0$ is fixed to 2 GeV.

The technical implementation of the simulated samples produced from these models is described in Section 4.

3 ATLAS detector

The ATLAS detector is a multipurpose particle physics detector with a forward-backward symmetric cylindrical geometry and nearly 4π coverage in solid angle.⁴ The inner tracking detector (ID) consists

⁴ ATLAS uses a right-handed coordinate system with its origin at the nominal interaction point in the centre of the detector. The positive x -axis is defined by the direction from the interaction point to the centre of the LHC ring, with the positive y -axis pointing upwards, while the beam direction defines the z -axis. Cylindrical coordinates (r, ϕ) are used in the transverse plane, ϕ being the azimuthal angle around the z -axis. The pseudorapidity η is defined in terms of the polar angle θ by $\eta = -\ln(\tan(\theta/2))$. Rapidity is defined as $y = 0.5 \ln[(E + p_z)/(E - p_z)]$ where E denotes the energy and p_z is the component of the momentum along the beam direction.

of silicon pixel and microstrip detectors covering the pseudorapidity region $|\eta| < 2.5$, surrounded by a transition radiation tracker, which enhances electron identification in the region $|\eta| < 2.0$. Before the start of Run 2, the new innermost pixel layer, the insertable B-layer (IBL) [28], was inserted at a mean sensor radius of 3.3 cm. The ID is surrounded by a thin superconducting solenoid providing an axial 2 T magnetic field and by a fine-granularity lead/liquid-argon (LAr) electromagnetic calorimeter covering $|\eta| < 3.2$. A steel/scintillator-tile calorimeter provides coverage for hadronic showers in the central pseudorapidity range ($|\eta| < 1.7$). The endcaps ($1.5 < |\eta| < 3.2$) of the hadronic calorimeter are made of LAr active layers with either copper or tungsten as the absorber material. The forward region ($3.1 < |\eta| < 4.9$) is instrumented with a LAr calorimeter for both the EM and hadronic measurements. A muon spectrometer with an air-core toroidal magnet system surrounds the calorimeters. Three layers of high-precision tracking chambers provide coverage in the range $|\eta| < 2.7$, while dedicated fast chambers allow triggering in the region $|\eta| < 2.4$. The ATLAS trigger system [29] consists of a hardware-based level-1 trigger followed by a software-based high-level trigger (HLT).

4 Data and simulated event samples

The data used in this analysis were collected by the ATLAS detector from pp collisions produced by the LHC at a centre-of-mass-energy of 13 TeV and 25 ns proton bunch spacing over the 2015 and 2016 data-taking periods. The full dataset corresponds to an integrated luminosity of 36.1 fb^{-1} after the application of beam, detector and data-quality requirements. The uncertainty in the combined 2015+2016 integrated luminosity is 2.1%. It is derived, following a methodology similar to that detailed in Ref. [30], from a preliminary calibration of the luminosity scale using $x-y$ beam-separation scans performed in August 2015 and May 2016. Events are required to pass an E_T^{miss} trigger with thresholds of 70 GeV, 100 GeV and 110 GeV at the HLT level for the 2015, early 2016 and late 2016 datasets, respectively. These triggers are fully efficient for events passing the preselection defined in Section 6, which requires the offline reconstructed E_T^{miss} to exceed 200 GeV. There are on average 24 inelastic pp collisions (the interactions other than the hard scatter are referred to as “pile-up”) in the dataset.

Samples of Monte Carlo (MC) simulated events are used to model the signal and background processes in this analysis, except multijet processes, which are estimated from data. SUSY signal samples in which each gluino decays into $b\bar{b}\tilde{\chi}_1^0$, $t\bar{t}\tilde{\chi}_1^0$, or $t\bar{b}\tilde{\chi}_1^-$ were generated with up to two additional partons using **MADGRAPH5_aMC@NLO** [31] v2.2.2 at leading order (LO) with the NNPDF 2.3 [32] parton distribution function (PDF) set. These samples were interfaced to **PYTHIA** v8.186 [33] for the modelling of the parton showering, hadronisation and underlying event.

The dominant background in the signal regions is the production of $t\bar{t}$ pairs with additional high transverse momentum (p_T) jets. For the generation of $t\bar{t}$ and single top quarks in the Wt - and s -channels the PowHEG-Box [34] v2 event generator with the CT10 [35] PDF set in the matrix element calculations was used. Electroweak t -channel single-top-quark events were generated using the PowHEG-Box v1 event generator. This event generator uses the four-flavour scheme for the next-to-leading order (NLO) matrix elements calculations together with the fixed four-flavour PDF set CT10f4. For all processes involving top quarks, top-quark spin correlations are preserved. In the t -channel, top quarks were decayed using MadSpin [36]. The parton shower, fragmentation, and the underlying event were simulated using **PYTHIA** v6.428 [37] with the CTEQ6L1 PDF set [38]. The h_{damp} parameter in PowHEG, which controls the p_T of the first additional emission beyond the Born level and thus regulates the p_T of the recoil emission against the $t\bar{t}$ system, was set to the mass of the top quark ($m_{\text{top}} = 172.5$ GeV). All events with at least one leptonically

decaying W boson are included. Single-top and $t\bar{t}$ events in which all top quarks decay hadronically do not contain sufficient E_T^{miss} to contribute significantly to the background.

Smaller backgrounds in the signal region come from the production of $t\bar{t}$ pairs in association with $W/Z/h$ bosons and possibly additional jets, and production of $t\bar{t}t\bar{t}$, $W/Z+\text{jets}$ and $WW/WZ/\text{ZZ}$ (diboson) events. Other potential sources of background, such as the production of three top quarks or three gauge bosons, are expected to be negligible. The production of $t\bar{t}$ pairs in association with electroweak vector bosons W and Z was modelled by samples generated at LO using `MADGRAPH5_aMC@NLO` v2.2.2 and showered with `PYTHIA` v8.186, while samples to model $t\bar{t}H$ production were generated using `MADGRAPH5_aMC@NLO` v2.2.1 and showered with `HERWIG++` [39] v2.7.1. These samples are described in detail in Ref. [40]. `MADGRAPH5_aMC@NLO` was also used to simulate the $t\bar{t}t\bar{t}$ production and the showering was performed with `PYTHIA` v8.186. The $W/Z+\text{jets}$ processes were simulated using the `SHERPA` v2.2.0 [41] event generator, while `SHERPA` v2.1.1 was used to simulate diboson production processes. Matrix elements for the $W/Z+\text{jets}$ and diboson processes were calculated using `Comix` [42] and `Open-Loops` [43] and merged with the `SHERPA` parton shower [44] using the `ME+PS@NLO` prescription [45]. The `SHERPA` diboson sample cross-section was scaled down to account for its use of $\alpha_{\text{QED}} = 1/129$ rather than $1/132$, corresponding to the use of current Particle Data Group [46] parameters, as input to the G_μ scheme [47]. Samples generated using `MADGRAPH5_aMC@NLO` v2.2.2 were produced with the `NNPDF` 2.3 PDF set and $W/Z+\text{jets}$ samples were generated with the `NNPDF` 3.0 PDF set [48], while all other samples used `CT10` PDFs.

For all samples, except the ones generated using `SHERPA`, the `EvtGEN` v1.2.0 program [49] was used to simulate the properties of the bottom- and charm-hadron decays. All `PYTHIA` v6.428 samples used the `PERUGIA2012` [50] set of tuned parameters (tune) for the underlying event, while `PYTHIA` v8.186 and `HERWIG++` showering were run with the A14 [51] and UEEE5 [52] underlying-event tunes, respectively. In-time and out-of-time pile-up interactions from the same or nearby bunch-crossings were simulated by overlaying additional pp collisions generated by `PYTHIA` v8.186 using the A2 tune [53] and the `MSTW2008LO` parton distribution function set [54] on top of the hard-scattering events. Details of the sample generation and normalisation are summarised in Table 1. Additional samples with different event generators and settings are used to estimate systematic uncertainties in the backgrounds, as described in Section 7.

All simulated event samples were passed through the full ATLAS detector simulation using `GEANT4` [55], with the exception of signal samples in which at least one gluino decays as $\tilde{g} \rightarrow b\bar{b}\tilde{\chi}_1^0$ or $\tilde{g} \rightarrow t\bar{b}\tilde{\chi}_1^-$, which were passed through a fast simulation that uses a parameterisation for the calorimeter response [56] and `GEANT4` for the ID and the muon spectrometer. The simulated events are reconstructed with the same algorithm as that used for data.

The signal samples are normalised using the best cross-section calculations at NLO in the strong coupling constant, adding the resummation of soft gluon emission at next-to-leading-logarithm (NLL) accuracy [57–61]. The nominal cross-section and the uncertainty are taken from an envelope of cross-section predictions using different PDF sets and factorisation and renormalisation scales, as described in Ref. [62]. The cross-section of gluino pair-production in these simplified models is 14 ± 3 fb for a gluino mass of 1.5 TeV, falling to 1.0 ± 0.3 fb for 2 TeV mass gluinos. All background processes are normalised using the best available theoretical calculation for their respective cross-sections. The order of this calculation in perturbative QCD (pQCD) for each process is listed in Table 1. For $t\bar{t}$, the largest background, this corresponds to a cross-section of 831.8 pb.

Table 1: List of event generators used for the different processes. Information is given about the underlying-event tunes, the PDF sets and the pQCD highest-order accuracy used for the normalisation of the different samples.

Process	Event Generator + fragmentation/hadronisation	Tune	PDF set	Cross-section order
SUSY signal	MADGRAPH5_aMC@NLO v2.2.2 + PYTHIA v8.186	A14	NNPDF2.3	NLO+NLL [57–62]
$t\bar{t}$	POWHEG-BOX v2 + PYTHIA v6.428	PERUGIA2012	CT10	NNLO+NNLL [64]
Single top	POWHEG-BOX v1 or v2 + PYTHIA v6.428	PERUGIA2012	CT10	NNLO+NNLL [65–67]
$t\bar{t}W/t\bar{t}Z/4\text{-tops}$	MADGRAPH5_aMC@NLO v2.2.2 + PYTHIA v8.186	A14	NNPDF2.3	NLO [68]
$t\bar{t}H$	MADGRAPH5_aMC@NLO v2.2.1 + HERWIG++ v2.7.1	UEEE5	CT10	NLO [69]
Diboson WW, WZ, ZZ	SHERPA v2.1.1	Default	CT10	NLO [47]
$W/Z+\text{jets}$	SHERPA v2.2.0	Default	NNPDF3.0	NNLO [70]

Finally, contributions from multijet background are estimated from data using a procedure described in Ref. [63], which performs a smearing of the jet response in data events with well-measured E_T^{miss} (so-called “seed events”). The response function is derived in Monte Carlo dijet events and is different for b -tagged and non- b -tagged jets.

5 Event reconstruction

Interaction vertices from the proton–proton collisions are reconstructed from at least two tracks with $p_T > 0.4$ GeV, and are required to be consistent with the beamspot envelope. The primary vertex is identified as the one with the largest sum of squares of the transverse momenta from associated tracks ($\sum |p_{T,\text{track}}|^2$) [71].

Basic selection criteria are applied to define candidates for electrons, muons and jets in the event. An overlap removal procedure is applied to these candidates to prevent double-counting. Further requirements are then made to select the final signal leptons and jets from the remaining candidates. The details of the candidate selections and of the overlap removal procedure are given below.

Candidate jets are reconstructed from three-dimensional topological energy clusters [72] in the calorimeter using the anti- k_t jet algorithm [73, 74] with a radius parameter of 0.4 (small- R jets). Each topological cluster is calibrated to the electromagnetic scale response prior to jet reconstruction. The reconstructed jets are then calibrated to the particle level by the application of a jet energy scale (JES) derived from $\sqrt{s} = 13$ TeV data and simulations [75]. Quality criteria are imposed to reject events that contain at least one jet arising from non-collision sources or detector noise [76]. Further selections are applied to reject jets that originate from pile-up interactions by means of a multivariate algorithm using information about

the tracks matched to each jet [77]. Candidate jets are required to have $p_T > 20$ GeV and $|\eta| < 2.8$. After resolving overlaps with electrons and muons, selected jets are required to satisfy the stricter requirement of $p_T > 30$ GeV.

A jet is tagged as a b -jet candidate by means of a multivariate algorithm using information about the impact parameters of inner detector tracks matched to the jet, the presence of displaced secondary vertices, and the reconstructed flight paths of b - and c -hadrons inside the jet [78, 79]. The b -tagging working point corresponding to an efficiency of 77% to identify b -jets with $p_T > 20$ GeV, as determined from a sample of simulated $t\bar{t}$ events, is found to be optimal for the statistical significance of this search. The corresponding rejection factors against jets originating from c -quarks, τ -leptons and light quarks and gluons in the same sample at this working point are 6, 22 and 134, respectively.

After resolving the overlap with leptons, the candidate small- R jets are re-clustered [80] into large- R jets using the anti- k_t algorithm with a radius parameter of 0.8. The calibration from the input small- R jets propagates directly to the re-clustered jets. These re-clustered jets are then trimmed [80–83] by removing subjets whose p_T falls below 10% of the p_T of the original re-clustered jet. The resulting large- R jets are required to have $p_T > 100$ GeV and $|\eta| < 2.0$. When it is not explicitly stated otherwise, the term “jets” in this paper refers to small- R jets.

Electron candidates are reconstructed from energy clusters in the electromagnetic calorimeter and inner detector tracks and are required to satisfy a set of “loose” quality criteria [84, 85]. They are also required to have $|\eta| < 2.47$. Muon candidates are reconstructed from matching tracks in the inner detector and muon spectrometer. They are required to meet “medium” quality criteria, as described in Ref. [86], and to have $|\eta| < 2.5$. All electron and muon candidates must have $p_T > 20$ GeV.

Leptons are selected from the candidates that survive the overlap removal procedure if they fulfil a requirement on the scalar sum of p_T of additional inner detector tracks in a cone around the lepton track. This isolation requirement is defined to ensure a flat efficiency of around 99% across the whole electron transverse energy and muon transverse momentum ranges. The angular separation between the lepton and the b -jet ensuing from a semileptonic top quark decay narrows as the p_T of the top quark increases. This increased collimation is accounted for by setting the radius of the isolation cone to $\min(0.2, 10 \text{ GeV}/p_T^{\text{lep}})$, where p_T^{lep} is the lepton p_T expressed in GeV. Selected electrons are further required to meet the “tight” quality criteria [84, 85]. Electrons (muons) are matched to the primary vertex by requiring the transverse impact parameter d_0 of the associated ID track to satisfy $|d_0|/\sigma_{d_0} < 5$ (3), where σ_{d_0} is the measured uncertainty of d_0 , and the longitudinal impact parameter z_0 to satisfy $|z_0 \sin \theta| < 0.5$ mm.⁵ In addition, events containing one or more muon candidates with $|d_0| (|z_0|) > 0.2$ mm (1 mm) are rejected to suppress cosmic rays.

Overlaps between candidate objects are removed sequentially. Firstly, electron candidates that lie a distance⁶ $\Delta R < 0.01$ from muon candidates are removed to suppress contributions from muon bremsstrahlung. Overlaps between electron and jet candidates are resolved next, and finally, overlaps between remaining jets and muon candidates are removed.

Overlap removal between electron and jet candidates aims to resolve two sources of ambiguity: it is designed, firstly, to remove jets that are formed primarily from the showering of a prompt electron and, secondly, to remove electrons that are produced in the decay chains of hadrons. Consequently, any non- b -tagged jet whose axis lies $\Delta R < 0.2$ from an electron is discarded. Electrons with $E_T < 50$ GeV are

⁵ Both the transverse and longitudinal impact parameters are defined with respect to the selected primary vertex.

⁶ $\Delta R = \sqrt{(\Delta y)^2 + (\Delta \phi)^2}$ defines the distance in rapidity y and azimuthal angle ϕ .

discarded if they lie $\Delta R < 0.4$ from the axis of any remaining jet and the corresponding jet is kept. For higher- E_T electrons, the latter removal is performed using a threshold of $\Delta R = \min(0.4, 0.04 + 10 \text{ GeV}/E_T)$ to increase the acceptance for events with collimated top quark decays.

The procedure to remove overlaps between muon and jet candidates is designed to remove those muons that are likely to have originated from the decay of hadrons and to retain the overlapping jet. Jets and muons may also appear in close proximity when the jet results from high- p_T muon bremsstrahlung, and in such cases the jet should be removed and the muon retained. Such jets are characterised by having very few matching inner detector tracks. Therefore, if the angular distance ΔR between a muon and a jet is lower than 0.2, the jet is removed if it is not b -tagged and has fewer than three matching inner detector tracks. Like the electrons, muons with p_T below (above) 50 GeV are subsequently discarded if they lie within $\Delta R = 0.4$ ($\Delta R = \min(0.4, 0.04 + 10 \text{ GeV}/p_T)$) of any remaining jet.

The missing transverse momentum (E_T^{miss}) in the event is defined as the magnitude of the negative vector sum (\vec{p}_T^{miss}) of the transverse momenta of all selected and calibrated objects in the event, with an extra term added to account for energy deposits that are not associated with any of these selected objects. This “soft” term is calculated from inner detector tracks matched to the primary vertex to make it more resilient to contamination from pile-up interactions [87, 88].

Corrections derived from data control samples are applied to simulated events to account for differences between data and simulation in the reconstruction efficiencies, momentum scale and resolution of leptons, in the efficiency and fake rate for identifying b -jets, and in the efficiency for rejecting jets originating from pile-up interactions.

6 Event selection

The event selection criteria are defined based on kinematic requirements for the objects defined in Section 5. Other discriminating event-based variables, described in Section 6.1, are used to further reject the background. Two sets of preselection criteria targeting the 0-lepton and the 1-lepton channels are presented in Section 6.2. The modelling of the data in these regions is also discussed in that section. The general analysis strategy and the treatment of background sources is presented in Section 6.3. Finally, the event selection for the cut-and-count and multi-bin analyses are discussed in Sections 6.4 and 6.5, respectively.

6.1 Discriminating variables

The effective mass variable (m_{eff}) is defined as:

$$m_{\text{eff}} = \sum_i p_T^{\text{jet}_i} + \sum_j p_T^{\ell_j} + E_T^{\text{miss}},$$

where the first and second sums are over the selected jets (N_{jet}) and leptons (N_{lepton}), respectively. It typically has a much higher value in pair-produced gluino events than in background events.

In regions with at least one selected lepton, the transverse mass m_T composed of the p_T of the leading selected lepton (ℓ) and E_T^{miss} is defined as:

$$m_T = \sqrt{2 p_T^\ell E_T^{\text{miss}} \{1 - \cos[\Delta\phi(\vec{p}_T^{\text{miss}}, \vec{p}_T^\ell)]\}}.$$

It is used to reduce the $t\bar{t}$ and W +jets background events in which a W boson decays leptonically. Neglecting resolution effects, the m_T distribution for these backgrounds has an expected upper bound corresponding to the W boson mass and typically has higher values for Gtt events. Another useful transverse mass variable is $m_{T,\min}^{b\text{-jets}}$, the minimum transverse mass formed by E_T^{miss} and any of the three highest- p_T b -tagged jets in the event:

$$m_{T,\min}^{b\text{-jets}} = \min_{i \leq 3} \left(\sqrt{2 p_T^{b\text{-jet}_i} E_T^{\text{miss}} \{1 - \cos[\Delta\phi(\vec{p}_T^{\text{miss}}, \vec{p}_T^{b\text{-jet}_i})]\}} \right).$$

The $m_{T,\min}^{b\text{-jets}}$ distribution has an expected upper bound corresponding to the top quark mass for $t\bar{t}$ events with a semileptonic top quark decay, while peaking at higher values for Gbb and Gtt events.

Another powerful variable is the total jet mass variable, defined as:

$$M_J^\Sigma = \sum_{i \leq 4} m_{J,i},$$

where $m_{J,i}$ is the mass of the large-radius re-clustered jet i in the event. The decay products of a hadronically decaying boosted top quark can be reconstructed in a single large-radius re-clustered jet, resulting in a jet with a high mass. This variable typically has larger values for Gtt events than for background events. This is because Gtt events contain as many as four hadronically decaying top quarks while the background is dominated by $t\bar{t}$ events with one or two semileptonic top quark decays.

The requirement of a selected lepton, with the additional requirements on jets, E_T^{miss} and event variables described above, makes the multijet background negligible for the ≥ 1 -lepton signal regions. For the 0-lepton signal regions, the minimum azimuthal angle $\Delta\phi_{\min}^{4j}$ between \vec{p}_T^{miss} and the p_T of the four leading small- R jets in the event, defined as:

$$\Delta\phi_{\min}^{4j} = \min_{i \leq 4} \left(|\phi_{\text{jet}_i} - \phi_{\vec{p}_T^{\text{miss}}} | \right),$$

is required to be greater than 0.4. This requirement suppresses the multijet background, which can produce events with large E_T^{miss} if containing poorly measured jets or neutrinos emitted close to the axis of a jet. A similar variable, denoted $\Delta\phi^{4l}$, is also used in the Gbb signal regions targeting small mass differences between the gluino and the neutralino, allowing the identification of events containing a high- p_T jet coming from initial-state radiation (ISR) and recoiling against the gluino pair. It is defined as the absolute value of the azimuthal angle separating the p_T of the leading jet and \vec{p}_T^{miss} , and is expected to have larger values for the targeted signal than for the background.

6.2 Modelling of the data

Preselection criteria in the 0-lepton and 1-lepton channels require $E_T^{\text{miss}} > 200$ GeV, in addition to the E_T^{miss} trigger requirement, and at least four jets of which at least two must be b -tagged. The 0-lepton (1-lepton) channel requires the event to contain no (at least one) selected lepton.

In this analysis, correction factors need to be extracted to account for shape discrepancies in the m_{eff} spectrum between the data and the expected background for the 1-lepton preselection sample. These factors are defined as the ratio of the number of observed events to the predicted number of background events in a given m_{eff} bin, in a signal-depleted region. This region is defined by applying the 1-lepton

preselection criteria and requiring exactly two b -tagged jets and $m_{T,\min}^{b\text{-jets}} < 140$ GeV. This kinematic reweighting leads to correction factors ranging from 0.7 to 1.1. They are applied to the background prediction and the full size of the correction is taken as an uncertainty for both the background and signal events.

Figures 3 and 4 show the multiplicity of selected jets and b -tagged jets, the distributions of E_T^{miss} , m_{eff} , and M_J^Σ for events passing the 0-lepton or the 1-lepton preselection, respectively. Figure 3 (4) also displays the distribution of $m_{T,\min}^{b\text{-jets}}$ (m_T) in the 0-lepton (1-lepton) channel. The correction described above is applied in the 1-lepton channel. The uncertainty bands include the statistical and experimental systematic uncertainties, as described in Section 7, but not the theoretical uncertainties in the background modelling.

The data and the predicted background are found to agree reasonably well at the preselection level after the kinematic reweighting described above. A discrepancy between data and prediction is observed for the number of b -tagged jets, but it has a negligible impact on the background estimate after the renormalisation of the simulation in dedicated control regions with the same b -tagged jets requirements as the signal regions, as described in Sections 6.4 and 6.5. Example signal models with enhanced cross-sections are overlaid for comparison.

6.3 Analysis strategy and background treatment

In order to enhance the sensitivity to the various signal benchmarks described in Section 2, multiple signal regions (SRs) are defined. The main background in all these regions is the production of a $t\bar{t}$ pair in association with heavy- and light-flavour jets. A normalisation factor for this background is extracted for each individual SR from a data control region (CR) that has comparable background composition and kinematics. This is ensured by keeping the kinematic requirements similar in the two regions. The CRs and SRs are defined to be mutually exclusive. Signal contributions in the CRs are suppressed by inverting or relaxing some requirements on the kinematic variables (e.g. m_T or $m_{T,\min}^{b\text{-jets}}$), leading to a signal contamination in the CRs of 6% at most. The $t\bar{t}$ normalisation is cross-checked in validation regions (VRs) that share similar background composition, i.e. jet and lepton flavours, with the SR. The signal contamination in the VRs is found to be lower than 30% for benchmark signal mass points above the already excluded mass range. The $t\bar{t}$ purity is superior to 73% and 53% in the CRs and VRs, respectively.

The non- $t\bar{t}$ backgrounds mainly consist of single-top, W +jets, Z +jets, $t\bar{t} + W/Z/h$, $t\bar{t}t\bar{t}$ and diboson events. Their normalisation is taken from the simulation normalised using the best available theory prediction. The multijet background is found to be very small or negligible in all regions. It is estimated using a procedure described in Ref. [63], in which the jet response is determined from simulated dijet events. This response function is then used to smear the jet response in low- E_T^{miss} events. The jet response is cross-checked with data where the E_T^{miss} can be unambiguously attributed to the mismeasurement of one of the jets.

Two analysis strategies are followed, and different SR sets are defined for each:

- A **cut-and-count** analysis, using partially overlapping single-bin SRs, optimised to maximise the expected discovery power for benchmark signal models, and allowing for reinterpretation of the results. The SRs are defined to probe the existence of a signal or to assess model-independent upper limits on the number of signal events.

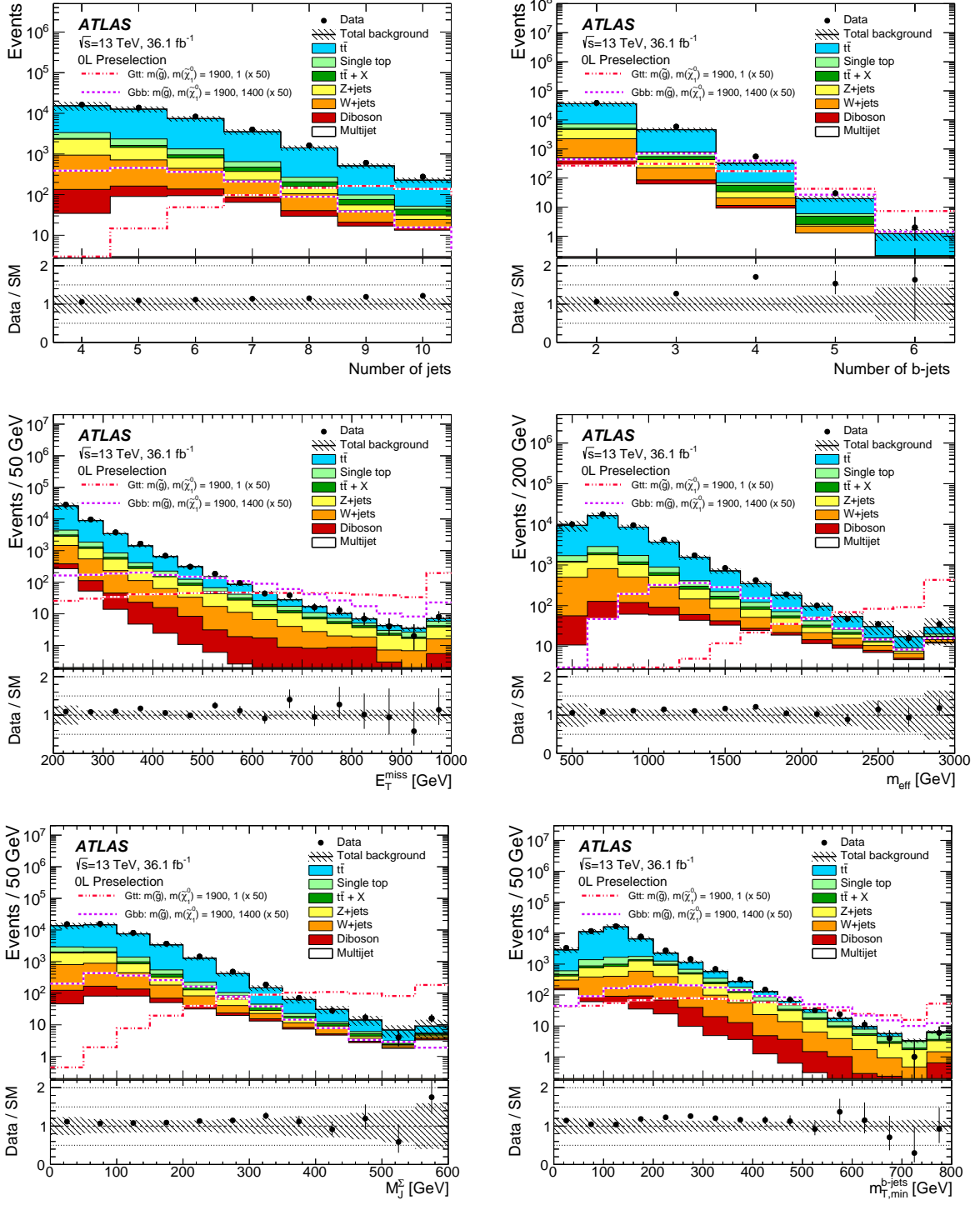


Figure 3: Distributions of (top-left) the number of selected jets (N_{jet}), (top-right) the number of selected b -tagged jets, (centre-left) $E_{\text{T}}^{\text{miss}}$, (centre-right) m_{eff} , (bottom-left) M_j^Σ and (bottom-right) $m_{T,\text{min}}^{b\text{-jets}}$ for events passing the 0-lepton preselection criteria. The statistical and experimental systematic uncertainties (as defined in Section 7) are included in the uncertainty band. The last bin includes overflow events. The lower part of each figure shows the ratio of data to the background prediction. All backgrounds (including $t\bar{t}$) are normalised using the best available theoretical calculation described in Section 4. The background category $t\bar{t} + X$ includes $t\bar{t}W/Z$, $t\bar{t}h$ and $t\bar{t}t\bar{t}$ events. Example signal models with cross-sections enhanced by a factor of 50 are overlaid for comparison.

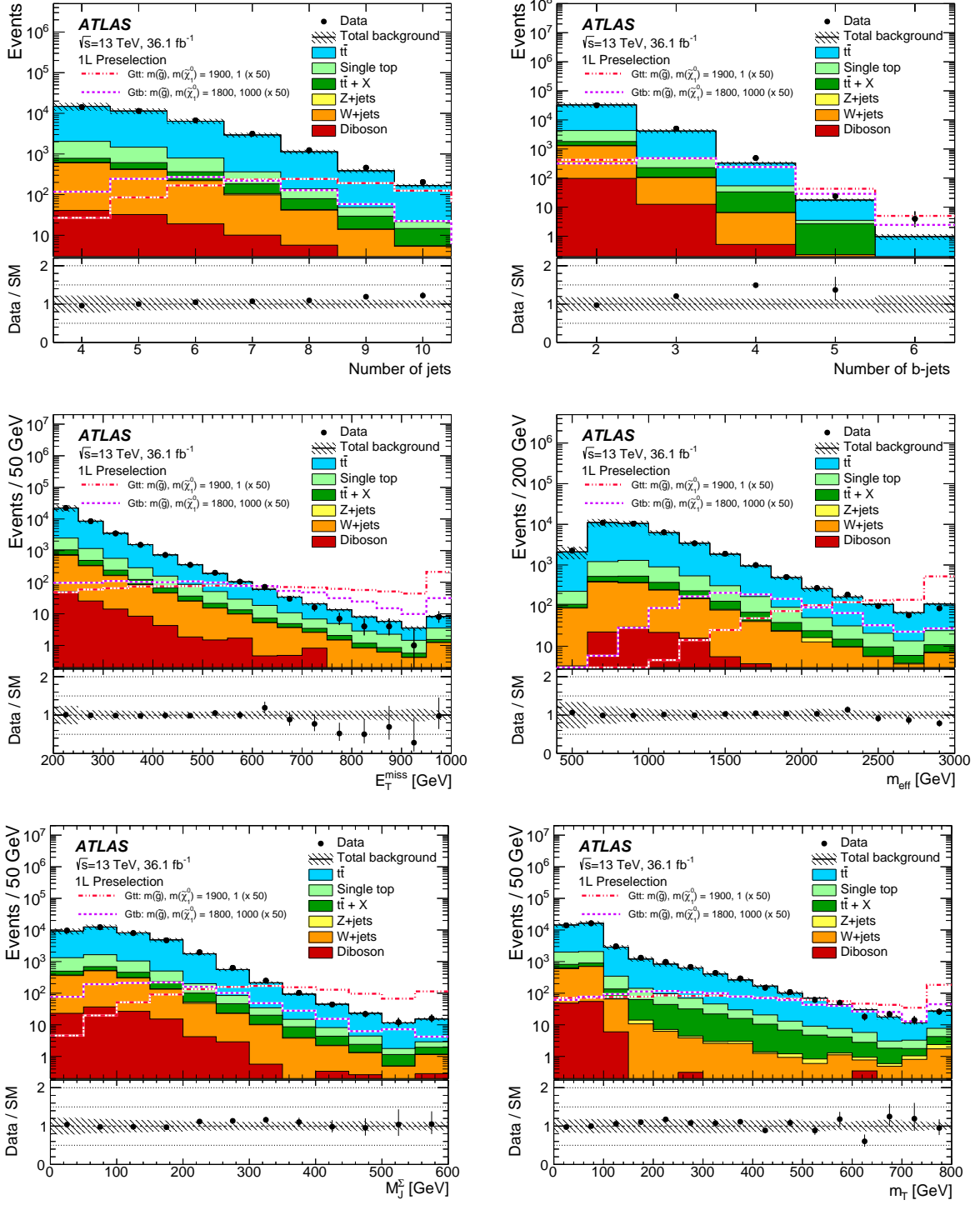


Figure 4: Distributions of (top-left) the number of selected jets (N_{jet}), (top-right) the number of selected b -tagged jets, (centre-left) E_T^{miss} , (centre-right) m_{eff} , (bottom-left) M_J^{Σ} and (bottom-right) m_T for events passing the 1-lepton preselection criteria, after applying the kinematic reweighting to the m_{eff} distribution described in the text. The statistical and experimental systematic uncertainties (as defined in Section 7) are included in the uncertainty band. The last bin includes overflow events. The lower part of each figure shows the ratio of data to the background prediction. All backgrounds (including $t\bar{t}$) are normalised using the best available theoretical calculation described in Section 4. The background category $t\bar{t} + X$ includes $t\bar{t}W/Z$, $t\bar{t}h$ and $t\bar{t}t\bar{t}$ events. Example signal models with cross-sections enhanced by a factor of 50 are overlaid for comparison.

- A **multi-bin** analysis, using a set of non-overlapping SRs and CRs that are combined to strengthen the exclusion limits on the targeted signal benchmarks. This set of regions is used to assess model-dependent interpretations of the various signal models.

6.4 Cut-and-count analysis

The SRs are named in the form SR-X-YL-Z, where X indicates the target model, Y indicates the number of leptons and Z labels the type of region targeted. The cut-and-count regions labelled B (for “boosted”) are optimised for signals with a large mass difference between the gluino and the neutralino ($\Delta m \gtrsim 1.5$ TeV), possibly leading to highly boosted objects in the final state. Conversely, regions C (for “compressed”) primarily focus on signals for which the gluino decay products are softer due to the small Δm ($\Delta m \lesssim 300$ GeV). Regions M (for “moderate”) target intermediate values of Δm . SRs targeting the Gtt model in the 1- and 0-lepton channels are presented in Table 2.

In the 1-lepton channel, these regions differ mainly in their kinematic selections thresholds: m_{eff} , E_T^{miss} and M_J^Σ selections are relaxed when going from region B to C to improve the acceptance for softer signals. The resulting background increase is compensated for by tightening the requirements on the number of (b -tagged) jets or $m_{T,\text{min}}^{b\text{-jets}}$. CRs constraining the $t\bar{t}$ background are defined in the low- m_T region to remove overlaps with the SRs. The requirements on $m_{T,\text{min}}^{b\text{-jets}}$ are removed, and the selections on kinematic variables are relaxed to ensure at least about 10 events in each CR. The requirement of an exclusive jet multiplicity permits the definition of VRs kinematically close to the SRs and mutually exclusive to both the CRs and SRs. VR- m_T validates the background prediction in the high- m_T region. It is kept mutually exclusive with the SR by an inverted selection on M_J^Σ or $m_{T,\text{min}}^{b\text{-jets}}$. VR- $m_{T,\text{min}}^{b\text{-jets}}$ checks the background prediction in the high- $m_{T,\text{min}}^{b\text{-jets}}$ regime, with an upper bound on m_T to keep the region mutually exclusive with the corresponding SR. The other kinematic requirements are kept as close as possible to those of the SRs to ensure that the event kinematics are similar, and allow sufficiently large yields.

The signal regions of the 0-lepton channel follow a similar strategy to the 1-lepton channel. Background composition studies performed on simulated event samples show that semileptonic $t\bar{t}$ events, for which the lepton is outside the acceptance or is a hadronically decaying τ -lepton, dominate in the SRs. Thus, CRs to normalise the $t\bar{t}$ +jets background make use of the 1-lepton channel, requiring the presence of exactly one signal lepton. An inverted selection on m_T is applied to remove overlaps with the 1-lepton SRs. The background prediction is validated in a 0-lepton region, inverting the M_J^Σ selection to remove any overlap with the SRs.

Regions targeting the Gbb model are presented in Table 3. The region definition follows the same pattern as for Gtt-OL regions, in particular for regions B, M and C. For very small values of Δm , the Gbb signal does not lead to a significant amount of E_T^{miss} , except if a hard ISR jet recoils against the gluino pair. Such events are targeted by region VC (for “very compressed”) that identifies an ISR-jet candidate as a non- b -tagged high- p_T leading jet (j_1), with a large azimuthal separation $\Delta\phi^{j_1}$ with respect to \vec{p}_T^{miss} . Similarly, the normalisation factor of the $t\bar{t}$ background is extracted from a 1-lepton CR, to which an inverted selection on m_T is applied to remove the overlaps with Gtt 1-lepton SRs and the corresponding signal contamination. The 0-lepton VRs are constructed in the 0-lepton channel with selections very close to the SR ones. They are mutually exclusive due to an inverted E_T^{miss} selection in the VR.

Table 2: Definitions of the Gtt SRs, CRs and VRs of the cut-and-count analysis. All kinematic variables are expressed in GeV except $\Delta\phi_{\min}^{4j}$, which is in radians. The jet p_T requirement is also applied to b -tagged jets.

Gtt 1-lepton										
Criteria common to all regions: ≥ 1 signal lepton, $p_T^{\text{jet}} > 30 \text{ GeV}$, $N_{b\text{-jets}} \geq 3$										
Targeted kinematics	Type	N_{jet}	m_T	$m_{T,\min}^{b\text{-jets}}$	E_T^{miss}	$m_{\text{eff}}^{\text{incl}}$	M_J^Σ			
Region B (Boosted, Large Δm)	SR	≥ 5	> 150	> 120	> 500	> 2200	> 200			
	CR	$= 5$	< 150	–	> 300	> 1700	> 150			
	VR- m_T	≥ 5	> 150	–	> 300	> 1600	< 200			
	VR- $m_{T,\min}^{b\text{-jets}}$	> 5	< 150	> 120	> 400	> 1400	> 200			
Region M (Moderate Δm)	SR	≥ 6	> 150	> 160	> 450	> 1800	> 200			
	CR	$= 6$	< 150	–	> 400	> 1500	> 100			
	VR- m_T	≥ 6	> 200	–	> 250	> 1200	< 100			
	VR- $m_{T,\min}^{b\text{-jets}}$	> 6	< 150	> 140	> 350	> 1200	> 150			
Region C (Compressed, small Δm)	SR	≥ 7	> 150	> 160	> 350	> 1000	–			
	CR	$= 7$	< 150	–	> 350	> 1000	–			
	VR- m_T	≥ 7	> 150	< 160	> 300	> 1000	–			
	VR- $m_{T,\min}^{b\text{-jets}}$	> 7	< 150	> 160	> 300	> 1000	–			
Gtt 0-lepton										
Criteria common to all regions: $p_T^{\text{jet}} > 30 \text{ GeV}$										
Targeted kinematics	Type	N_{lepton}	$N_{b\text{-jets}}$	N_{jet}	$\Delta\phi_{\min}^{4j}$	m_T	$m_{T,\min}^{b\text{-jets}}$	E_T^{miss}	$m_{\text{eff}}^{\text{incl}}$	M_J^Σ
Region B (Boosted, Large Δm)	SR	$= 0$	≥ 3	≥ 7	> 0.4	–	> 60	> 350	> 2600	> 300
	CR	$= 1$	≥ 3	≥ 6	–	< 150	–	> 275	> 1800	> 300
	VR	$= 0$	≥ 3	≥ 6	> 0.4	–	–	> 250	> 2000	< 300
Region M (Moderate Δm)	SR	$= 0$	≥ 3	≥ 7	> 0.4	–	> 120	> 500	> 1800	> 200
	CR	$= 1$	≥ 3	≥ 6	–	< 150	–	> 400	> 1700	> 200
	VR	$= 0$	≥ 3	≥ 6	> 0.4	–	–	> 450	> 1400	< 200
Region C (Compressed, moderate Δm)	SR	$= 0$	≥ 4	≥ 8	> 0.4	–	> 120	> 250	> 1000	> 100
	CR	$= 1$	≥ 4	≥ 7	–	< 150	–	> 250	> 1000	> 100
	VR	$= 0$	≥ 4	≥ 7	> 0.4	–	–	> 250	> 1000	< 100

Table 3: Definitions of the Gbb SRs, CRs and VRs of the cut-and-count analysis. All kinematic variables are expressed in GeV except $\Delta\phi_{\min}^{4j}$, which is in radians. The jet p_T requirement is applied to the four leading jets, a subset of which are b -tagged jets. The $j_1 \neq b$ requirement specifies that the leading jet is not b -tagged.

Criteria common to all regions: $N_{\text{jet}} \geq 4$, $p_T^{\text{jet}} > 30$ GeV									
Targeted kinematics	Type	N_{lepton}	$N_{b\text{-jets}}$	$\Delta\phi_{\min}^{4j}$	m_T	$m_{T,\min}^{b\text{-jets}}$	E_T^{miss}	m_{eff}	Others
Region B (Boosted, Large Δm)	SR	= 0	≥ 3	> 0.4	—	—	> 400	> 2800	—
	CR	= 1	≥ 3	—	< 150	—	> 400	> 2500	—
	VR	= 0	≥ 3	> 0.4	—	—	> 350	1900–2800	—
Region M (Moderate Δm)	SR	= 0	≥ 4	> 0.4	—	> 90	> 450	> 1600	—
	CR	= 1	≥ 4	—	< 150	—	> 300	> 1600	—
	VR	= 0	≥ 4	> 0.4	—	> 100	250–450	1600–1900	—
Region C (Compressed, small Δm)	SR	= 0	≥ 4	> 0.4	—	> 155	> 450	—	—
	CR	= 1	≥ 4	—	< 150	—	> 375	—	—
	VR	= 0	≥ 4	> 0.4	—	> 125	350–450	—	—
Region VC (Very Compressed, very small Δm)	SR	= 0	≥ 3	> 0.4	—	> 100	> 600	—	$p_T^{j_1} > 400$, $j_1 \neq b$, $\Delta\phi^{ji} > 2.5$
	CR	= 1	≥ 3	—	< 150	—	> 600	—	
	VR	= 0	≥ 3	> 0.4	—	> 100	225–600	—	

6.5 Multi-bin analysis

Figures 3 and 4 show that a good separation between signal and background can be achieved with various kinematic variables. The distribution of N_{jet} and m_{eff} for different signal benchmarks and Δm values is used to build a two-dimensional slicing of the phase space in a set of non-overlapping SRs, CRs and VRs that can be statistically combined. The slicing scheme is presented in Figure 5. The SRs are named in the form SR-YL-Z₁Z₂, where Y indicates the number of leptons, Z₁ labels the jet multiplicity bin and Z₂ labels the m_{eff} bin. For Z₁ and Z₂, the letters “H” stands for “high”, “I” for “intermediate” and “L” for “low”. In the 0-lepton channel, there is also a 0L-ISR region that is a subset of the IL, LL, II and LI regions, and kept mutually exclusive with them as detailed below.

The low- N_{jet} region probes especially Gbb-like models, for which the number of hard jets is lower than in decay topologies containing top quarks. This category of events is thus only considered in the 0-lepton channel. Gtt events are mostly expected in the high- N_{jet} bin. The intermediate jet multiplicity bin is built to be sensitive to decay topologies with a number of top quarks intermediate between Gbb and Gtt, but also to Gbb (with additional jets originating from radiation) and to Gtt (when some jets fall outside the acceptance). The m_{eff} bins are chosen to provide sensitivity to various kinematic regimes: the low- m_{eff} regions are essentially sensitive to soft signals (low Δm), while the high- m_{eff} regions are designed to select highly boosted events.

For each $N_{\text{jet}}-m_{\text{eff}}$ region presented in Figure 5, the selection was optimised over all the other variables to maximise the exclusion power for the Gbb and Gtt models. For each m_{eff} bin, a targeted range of Δm was used in the optimisation procedure.

The high- and intermediate- N_{jet} regions are presented in Tables 4 and 5, respectively. For each m_{eff} region, 0- and 1-lepton channels are used to provide sensitivity to the Gtt model and the decay topologies of the variable branching ratio model which contain at least one top quark. In the intermediate- N_{jet} categories the leading jet is required to be b -tagged or the value of $\Delta\phi^{j_1}$ to be lower than 2.9 in order to ensure they are mutually exclusive with the 0L-ISR regions. Corresponding 0-lepton and 1-lepton SRs share a single CR, hosted in the 1-lepton channel, after the application of an inverted m_{T} selection to remove the overlap

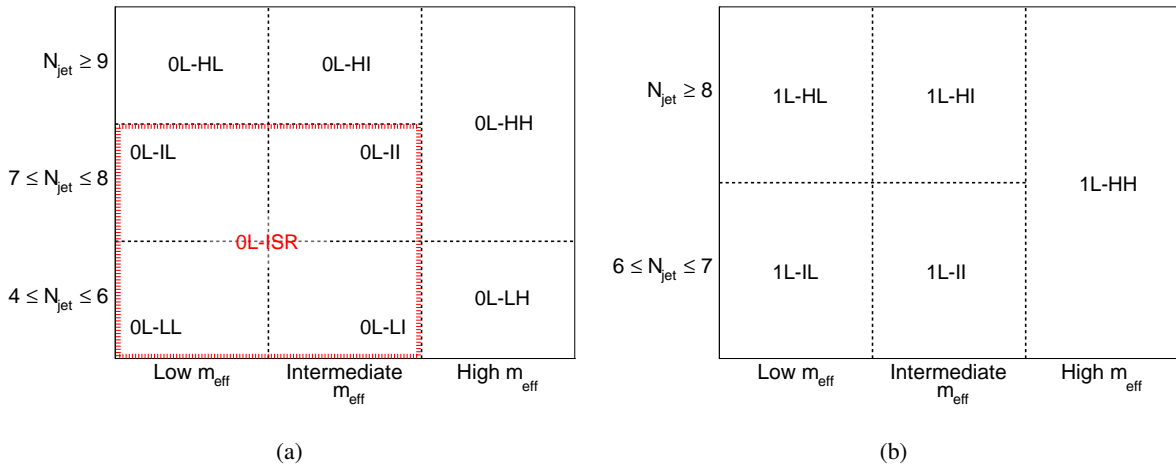


Figure 5: Scheme of the multi-bin analysis for the (a) 0-lepton and (b) 1-lepton regions. The 0L-ISR region is represented with the broad red dashed line in (a).

with the 1-lepton SRs. The other kinematic requirements are kept close to the ones of the SR. One VR is defined for each SR in the corresponding lepton channel. Full independence between the signal and VRs is guaranteed by E_T^{miss} and $m_{T,\text{min}}^{b\text{-jets}}$ requirements.

The low- N_{jet} regions are presented in Table 6. Targeting primarily the Gbb model, the transverse momentum of the fourth jet is required to be larger than 90 GeV in all SRs. In the intermediate and low m_{eff} regions, the leading jet is required to be b -tagged or the value of $\Delta\phi^{11}$ to be lower than 2.9 in order to be mutually exclusive with the OL-ISR regions. The $t\bar{t}$ background dominates in all regions, and is normalised in dedicated 1-lepton regions, defined with a low m_T requirement, as done for the regions of the cut-and-count analysis. VRs are constructed in the 0-lepton channel, closely reproducing the background composition and kinematics of the SR events.

A dedicated set of regions is designed to target very compressed Gbb scenarios in which a hard ISR jet recoils against the gluino pair. The definition of these regions is presented in Table 6.

Table 4: Definition of the high- N_{jet} SRs, CRs and VRs of the multi-bin analysis. All kinematic variables are expressed in GeV except $\Delta\phi_{\min}^{4j}$, which is in radians.

High- N_{jet} regions

Criteria common to all regions: $N_{b\text{-jets}} \geq 3$, $p_T^{\text{jet}} > 30$ GeV

Targeted kinematics	Type	N_{lepton}	$\Delta\phi_{\min}^{4j}$	m_T	N_{jet}	$m_{T,\min}^{b\text{-jets}}$	M_J^Σ	E_T^{miss}	m_{eff}
SR-0L									
High-m_{eff} (HH) (Large Δm)	SR-1L	≥ 1	—	> 150	≥ 6	> 120	> 200	> 400	> 2500
	CR	≥ 1	—	< 150	≥ 6	> 60	> 150	> 500	> 2300
	VR-0L	$= 0$	> 0.4	—	≥ 7	< 100 if $E_T^{\text{miss}} > 300$	—	< 300 if $m_{T,\min}^{b\text{-jets}} > 100$	> 2100
	VR-1L	≥ 1	—	> 150	≥ 6	< 140 if $m_{\text{eff}} > 2300$	—	< 500	> 2100
	SR-0L	$= 0$	> 0.4	—	≥ 9	> 140	> 150	> 300	[1800, 2500]
	SR-1L	≥ 1	—	> 150	≥ 8	> 140	> 150	> 300	[1800, 2300]
Intermediate-m_{eff} (HI) (Intermediate Δm)	CR	≥ 1	—	< 150	≥ 8	> 60	> 150	> 200	[1700, 2100]
	VR-0L	$= 0$	> 0.4	—	≥ 9	< 140 if $E_T^{\text{miss}} > 300$	—	< 300 if $m_{T,\min}^{b\text{-jets}} > 140$	[1650, 2100]
	VR-1L	≥ 1	—	> 150	≥ 8	< 140 if $E_T^{\text{miss}} > 300$	—	< 300 if $m_{T,\min}^{b\text{-jets}} > 140$	[1600, 2100]
	SR-0L	$= 0$	> 0.4	—	≥ 9	> 140	—	> 300	[1900, 1800]
	SR-1L	≥ 1	—	> 150	≥ 8	> 140	—	> 300	[1900, 1800]
	CR	≥ 1	—	< 150	≥ 8	> 130	—	> 250	[1900, 1700]
Low-m_{eff} (HL) (Small Δm)	VR-0L	$= 0$	> 0.4	—	≥ 9	< 140	—	> 300	[1900, 1650]
	VR-1L	≥ 1	—	> 150	≥ 8	< 140	—	> 225	[1900, 1650]

Table 5: Definition of the intermediate- N_{jet} SRs, CRs and VRs of the multi-bin analysis. All kinematic variables are expressed in GeV except $\Delta\phi_{\min}^{4j}$, which is in radians. The $j_1 = b$ requirement specifies that the leading jet is b -tagged.

Intermediate- N_{jet} regions										
Criteria common to all regions: $N_{b\text{-jets}} \geq 3, p_T^{\text{jet}} > 30 \text{ GeV}$										
Targeted kinematics	Type	N_{lepton}	$\Delta\phi_{\min}^{4j}$	m_T	N_{jet}	$j_1 = b$ or $\Delta\phi_{\min}^{4j} \leq 2.9$	$m_{T,\text{min}}^{b\text{-jets}}$	M_f^{Σ}	E_T^{miss}	m_{eff}
Intermediate- m_{eff} (II) (Intermediate Δm)	SR-0L	= 0	> 0.4	–	[7, 8]	✓	> 140	> 150	> 300	[1600, 2500]
	SR-1L	≥ 1	–	> 150	[6, 7]	–	> 140	> 150	> 300	[1600, 2300]
	CR	≥ 1	–	< 150	[6, 7]	✓	> 110	> 150	> 200	[1600, 2100]
	VR-0L	= 0	> 0.4	–	[7, 8]	✓	< 140	–	> 300	[1450, 2000]
	VR-1L	≥ 1	–	> 150	[6, 7]	–	< 140	–	> 225	[1450, 2000]
Low- m_{eff} (IL) (Low Δm)	SR-0L	= 0	> 0.4	–	[7, 8]	✓	> 140	–	> 300	[800, 1600]
	SR-1L	≥ 1	–	> 150	[6, 7]	–	> 140	–	> 300	[800, 1600]
	CR	≥ 1	–	< 150	[6, 7]	✓	> 130	–	> 300	[800, 1600]
	VR-0L	= 0	> 0.4	–	[7, 8]	✓	< 140	–	> 300	[800, 1450]
	VR-1L	≥ 1	–	> 150	[6, 7]	–	< 140	–	> 300	[800, 1450]

Table 6: Definition of the low- N_{jet} and ISR SRs, CRs and VRs of the multi-bin analysis. All kinematic variables are expressed in GeV except $\Delta\phi_{\min}^{4j}$, which is in radians. The $j_1 = b$ ($j_1 \neq b$) requirement specifies that the leading jet is (not) b -tagged.

Low- N_{jet} regions
Criteria common to all regions: $N_{b\text{-jets}} \geq 3, p_T^{\text{jet}} > 30 \text{ GeV}$

Targeted kinematics **Type** N_{lepton} $\Delta\phi_{\min}^{4j}$ m_T N_{jet} $j_1 = b$ or $\Delta\phi^{jj} \leq 2.9$ p_T^{j4} $m_{T,\min}^{b\text{-jets}}$ E_T^{miss} m_{eff}

High- m_{eff} (LH) (Large Δm)	SR	= 0	> 0.4	–	[4, 6]	–	> 90	–	> 300	> 2400
	CR	≥ 1	–	< 150	[4, 5]	–	–	–	> 200	> 2100
	VR	= 0	> 0.4	–	[4, 6]	–	> 90 if $E_T^{\text{miss}} < 300$	–	> 200	[2000, 2400]

Intermediate- m_{eff} (LI) (Intermediate Δm)	SR	= 0	> 0.4	–	[4, 6]	✓	> 90	> 140	> 350	[1400, 2400]
	CR	≥ 1	–	< 150	[4, 5]	✓	> 70	–	> 300	[1400, 2000]
	VR	= 0	> 0.4	–	[4, 6]	✓	> 90	< 140	> 300	[1250, 1800]

Low- m_{eff} (LL) (Low Δm)	SR	= 0	> 0.4	–	[4, 6]	✓	> 90	> 140	> 350	[800, 1400]
	CR	≥ 1	–	< 150	[4, 5]	✓	> 70	–	> 300	[800, 1400]
	VR	= 0	> 0.4	–	[4, 6]	✓	> 90	< 140	> 300	[800, 1250]

ISR regions
Criteria common to all regions: $N_{b\text{-jets}} \geq 3, \Delta\phi^{jj} > 2.9, p_T^j > 400 \text{ GeV}, p_T^{\text{jet}} > 30 \text{ GeV}, j_1 \neq b$

Type	N_{lepton}	$\Delta\phi_{\min}^{4j}$	m_T	N_{jet}	$m_{T,\min}^{b\text{-jets}}$	E_T^{miss}	m_{eff}	
	SR	= 0	> 0.4	–	[4, 8]	> 100	> 600	< 2200
	CR	≥ 1	–	< 150	[4, 7]	–	> 400	< 2000
VR	= 0	> 0.4	–	[4, 8]	> 100	> 250	< 2000	

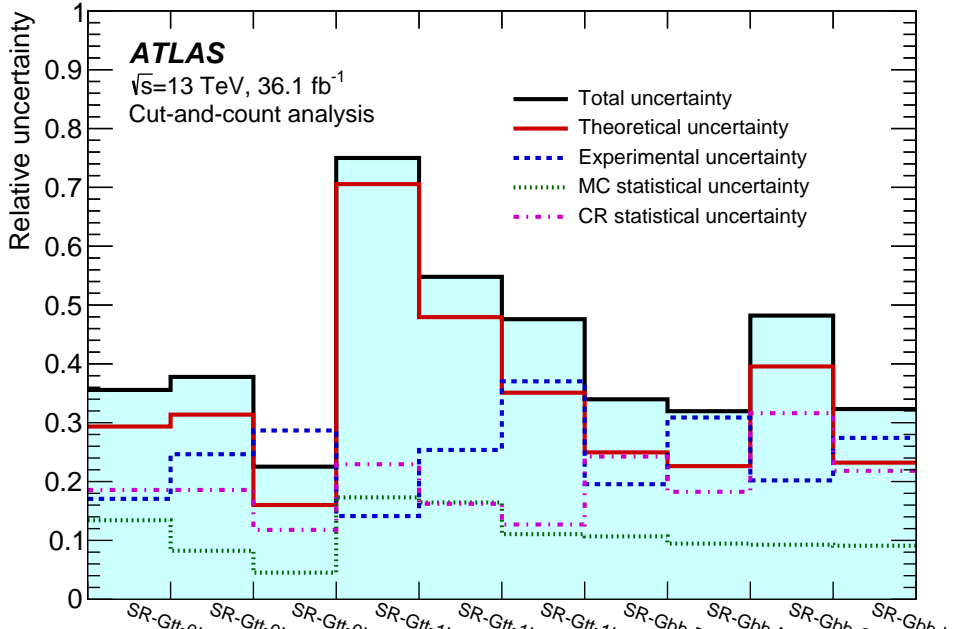
7 Systematic uncertainties

Figures 6(a) and 6(b) summarise the relative systematic uncertainties in the background estimate for the cut-and-count and multi-bin analyses, respectively. These uncertainties arise from the extrapolation of the $t\bar{t}$ normalisation obtained in the CRs to the SRs as well as from the yields of the minor backgrounds in the SRs, which are predicted by the simulation. The total systematic uncertainties range from approximately 20% to 80% in the various SRs.

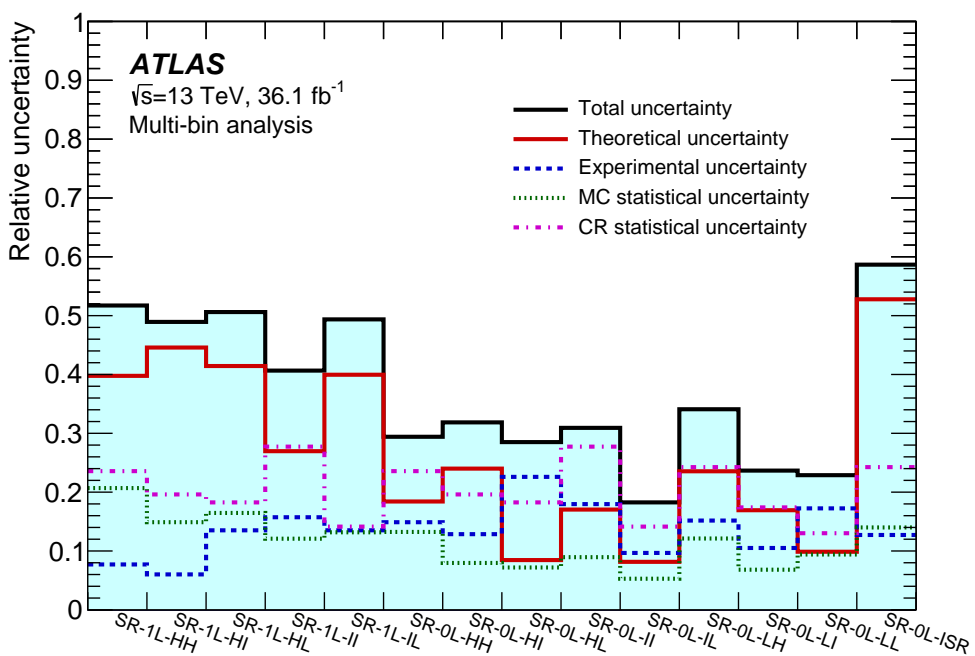
The detector-related systematic uncertainties affect both the background estimate and the signal yield. The largest sources in this analysis relate to the jet energy scale, jet energy resolution (JER) and the b -tagging efficiencies and mistagging rates. The JES uncertainties for the small- R jets are derived from $\sqrt{s} = 13$ TeV data and simulations while the JER uncertainties are extrapolated from 8 TeV data using MC simulations [89]. These uncertainties are also propagated to the re-clustered large- R jets, which use them as inputs. The jet mass scale and resolution uncertainties have a negligible impact on the re-clustered jet mass. The impact of the JES uncertainties on the expected background yields is between 4% and 35%, while JER uncertainties affect the background yields by approximately 0–26% in the various regions. Uncertainties in the measured b -tagging efficiencies and mistagging rates are the subleading sources of experimental uncertainty.

The impact of these uncertainties on the expected background yields is 3–24% depending on the considered region. The uncertainties associated with lepton reconstruction and energy measurements have a negligible impact on the final results. All lepton and jet measurement uncertainties are propagated to the calculation of E_T^{miss} , and additional uncertainties are included in the scale and resolution of the soft term. The overall impact of the E_T^{miss} soft-term uncertainties is also small.

Since the normalisation of the $t\bar{t}$ background is fit to data in the CRs, uncertainties in the modelling of this background only affect the extrapolation from the CRs to the SRs and VRs. Hadronisation and parton showering model uncertainties are estimated using a sample generated with PowHEG and showered by HERWIG++ v2.7.1 with the UEEE5 underlying-event tune. Systematic uncertainties in the modelling of initial- and final-state radiation are explored with PowHEG samples showered with two alternative settings of PYTHIA v6.428. The first of these uses the PERUGIA2012radHi tune [50] and has the renormalisation and factorisation scales set to twice the nominal value, resulting in more radiation in the final state. In addition, it has h_{damp} set to $2m_{\text{top}}$. The second sample, using the PERUGIA2012radLo tune, has $h_{\text{damp}} = m_{\text{top}}$ and the renormalisation and factorisation scales are set to half of their nominal values, resulting in less radiation in the event. In each case, the uncertainty is taken as the change in the expected yield of $t\bar{t}$ background with respect to the nominal sample. The uncertainty due to the choice of event generator is estimated by comparing the expected yields obtained using a $t\bar{t}$ sample generated with MADGRAPH5_aMC@NLO and one that is generated with PowHEG. Both of these samples are showered with HERWIG++ v2.7.1. The total theoretical uncertainty in the inclusive $t\bar{t}$ background is taken as the sum in quadrature of these individual components. An additional uncertainty is assigned to the fraction of $t\bar{t}$ events produced in association with additional heavy-flavour jets (i.e. $t\bar{t}+ \geq 1b$ and $t\bar{t}+ \geq 1c$), a process which suffers from large theoretical uncertainties. Simulation studies show that the heavy-flavour fractions in each set of SR, CR and VR, which have almost identical b -tagged jets requirements, are similar. Therefore, the theoretical uncertainties in this fraction affect these regions in a similar way, and thus largely cancel out in the semi-data-driven $t\bar{t}$ normalisation based on the observed CR yields. The residual uncertainty in the $t\bar{t}$ prediction is taken as the difference between the nominal $t\bar{t}$ prediction and the one obtained after varying the cross-section of $t\bar{t}$ events with additional heavy-flavour jets by 30%, in accordance with the results of the ATLAS measurement of this cross-section at $\sqrt{s} = 8$ TeV [90]. This



(a)



(b)

Figure 6: Relative systematic uncertainty in the background estimate for the (a) cut-and-count and (b) multi-bin analyses. The individual uncertainties can be correlated, such that the total background uncertainty is not necessarily their sum in quadrature.

component typically makes a small contribution (0–8%) to the total impact of the $t\bar{t}$ modelling uncertainties on the background yields, which ranges between 5% and 76% for the various regions. The statistical uncertainty of the CRs used to extract the $t\bar{t}$ normalisation factors, which is included in the systematic uncertainties, ranges from 10% to 30% depending on the SR.

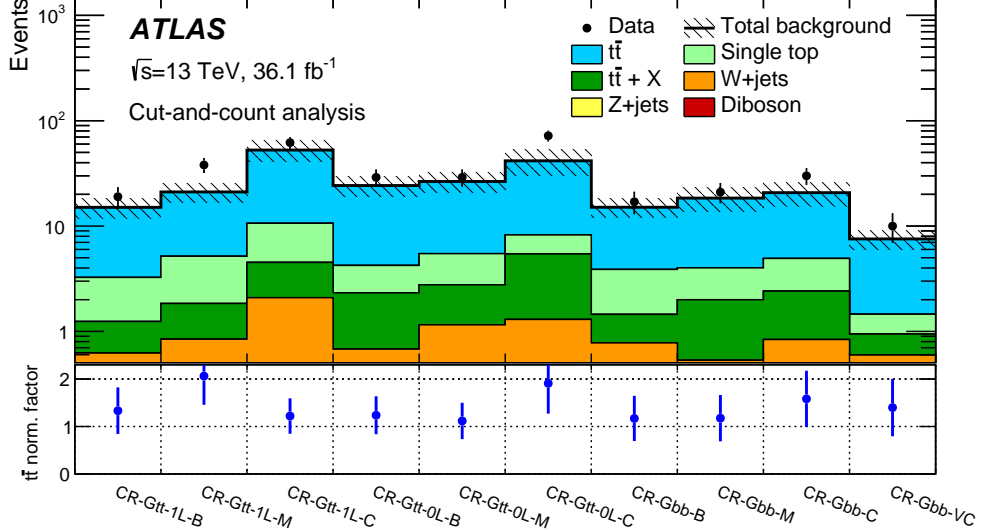
Modelling uncertainties affecting the single-top process arise especially from the interference between the $t\bar{t}$ and Wt processes. This uncertainty is estimated using inclusive $WWbb$ events, generated using `MADGRAPH5_aMC@NLO`, which are compared with the sum of $t\bar{t}$ and Wt processes. Furthermore, as in the $t\bar{t}$ modelling uncertainties, variations of `PYTHIA v6.428` settings increasing or decreasing the amount of radiation are also used. An additional 5% uncertainty is included in the cross-section of single-top processes [91]. Overall, the modelling uncertainties affecting the single-top process lead to changes of approximately 0–11% in the total yields in the various regions. Uncertainties in the $W/Z+jets$ backgrounds are estimated by varying independently the scales for factorisation, renormalisation and resummation by factors of 0.5 and 2. The scale used for the matching between jets originating from the matrix element and the parton shower is also varied. The resulting uncertainties in the total yield range from approximately 0 to 50% in the various regions. A 50% normalisation uncertainty is assigned to $t\bar{t}+W/Z/h$, $t\bar{t}t\bar{t}$ and diboson backgrounds and are found to have no significant impact on the sensitivity of this analysis. Uncertainties arising from variations of the parton distribution functions were found to affect background yields by less than 2%, and therefore these uncertainties are neglected here. Uncertainties due to the limited number of events in the MC background samples are included if above 5%. They reach approximately 20% in regions targeting large mass-splitting.

The uncertainties in the cross-sections of signal processes are determined from an envelope of different cross-section predictions, as described in Section 4. A systematic uncertainty is also assigned to the kinematic correction described in Section 6. The total size of the correction is used as an uncertainty, and is applied to all simulated event samples for the 1-lepton channel.

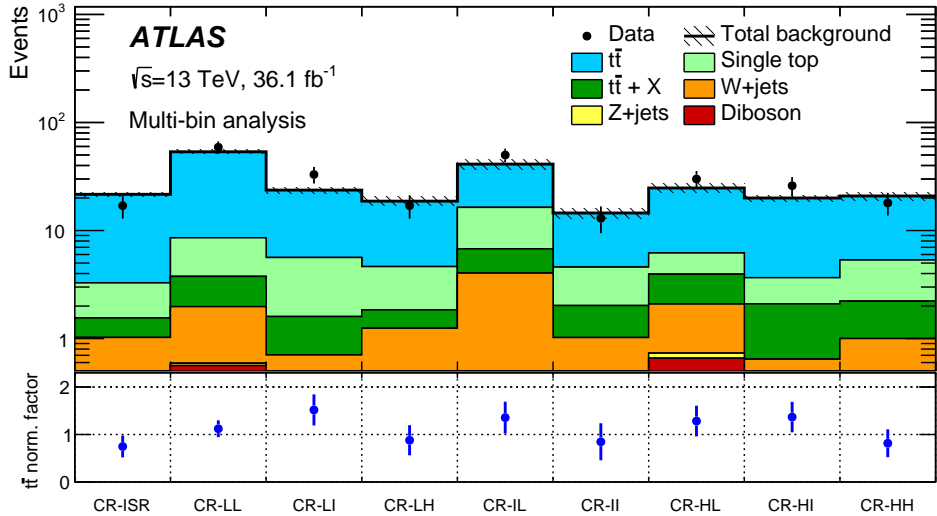
8 Results

The expected SM background is determined separately in each SR with a profile likelihood fit [92] implemented in the `HistFitter` framework [93], referred to as a background-only fit. The fit uses as a constraint the observed event yield in the associated CR to adjust the $t\bar{t}$ normalisation, assuming that no signal contributes to this yield, and applies that normalisation factor to the number of $t\bar{t}$ events predicted by simulation in the SR. The values of the normalisation factors, the expected numbers of background events and the observed data yields in all the CRs are shown in Figures 7(a) and 7(b) for the cut-and-count and multi-bin analyses, respectively.

The inputs to the background-only fit for each SR are the number of events observed in its associated CR and the number of events predicted by simulation in each region for all background processes. The numbers of observed and predicted events in each CR are described by Poisson probability density functions. The systematic uncertainties in the expected values are included in the fit as nuisance parameters. They are constrained by Gaussian distributions with widths corresponding to the sizes of the uncertainties and are treated as correlated, when appropriate, between the various regions. The product of the various probability density functions forms the likelihood, which the fit maximises by adjusting the $t\bar{t}$ normalisation and the nuisance parameters.



(a)



(b)

Figure 7: Pre-fit event yield in control regions and related $t\bar{t}$ normalization factors after the background-only fit for (a) the cut-and-count and (b) the multi-bin analyses. The upper panel shows the observed number of events and the predicted background yield before the fit. The background category $t\bar{t} + X$ includes $t\bar{t}W/Z$, $t\bar{t}H$ and $t\bar{t}t\bar{t}$ events. All of these regions require at least one signal lepton, for which the multijet background is negligible. All uncertainties described in Section 7 are included in the uncertainty band. The $t\bar{t}$ normalisation is obtained from the fit and is displayed in the bottom panel.

Figures 8(a) and 8(b) show the results of the background-only fit to the CRs, extrapolated to the VRs for the cut-and-count and multi-bin analyses, respectively. The number of events predicted by the background-only fit is compared to the data in the upper panel. The pull, defined by the difference between the observed number of events (n_{obs}) and the predicted background yield (n_{pred}) divided by the total uncertainty (σ_{tot}), is shown for each region in the lower panel. No evidence of significant background mismodelling is observed in the VRs.

The event yields in the SRs for the cut-and-count and multi-bin analyses are presented in Figure 9, where the pull is shown for each region in the lower panel. No significant excess is found above the predicted background. The maximum deviation is observed in region SR-0L-HH of the multi-bin analysis with a local significance of 2.3 standard deviations. The background is dominated by $t\bar{t}$ events in all SRs. The subdominant background contributions in the 0-lepton regions are $Z(\rightarrow \nu\nu) + \text{jets}$ and $W(\rightarrow \ell\nu) + \text{jets}$ events, where for $W + \text{jets}$ events the lepton is an unidentified electron or muon or a hadronically decaying τ -lepton. In the 1-lepton SRs, the subdominant backgrounds are single-top, $t\bar{t}W$ and $t\bar{t}Z$.

Table 7 shows the observed number of events and predicted number of background events from the background-only fit in the Gtt 1-lepton, Gtt 0-lepton and Gbb regions for the cut-and-count analysis. The central value of the fitted background is in general larger than the MC-only prediction. This is in part due to an underestimation of the cross-section of $t\bar{t}+ \geq 1b$ and $t\bar{t}+ \geq 1c$ processes in the simulation.

9 Interpretation

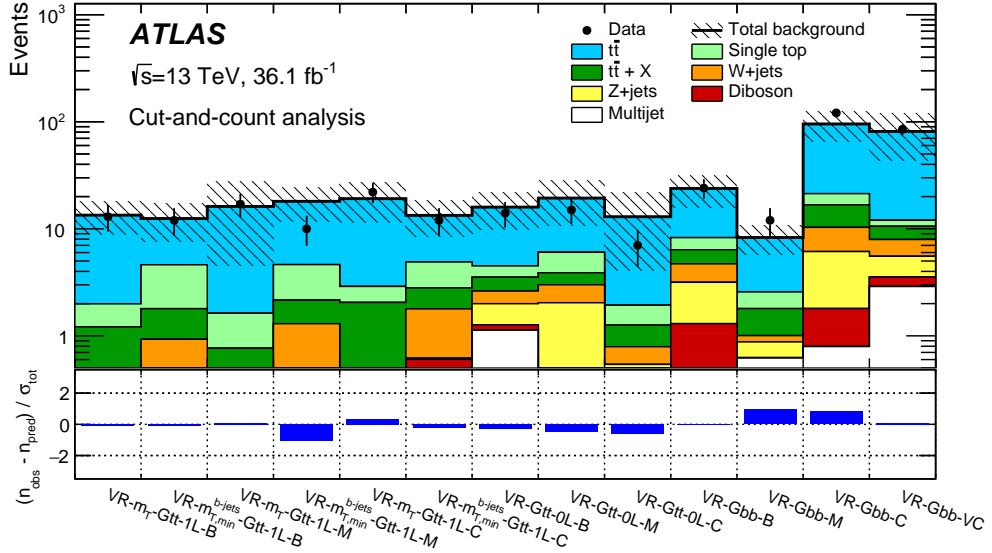
Since no significant excess over the expected background from SM processes is observed, the data are used to derive one-sided upper limits at 95% confidence level (CL). Two levels of interpretation are provided in this paper: model-independent exclusion limits and model-dependent exclusion limits set on the Gbb, Gtt and gluino variable branching ratio models.

9.1 Model-independent exclusion limits

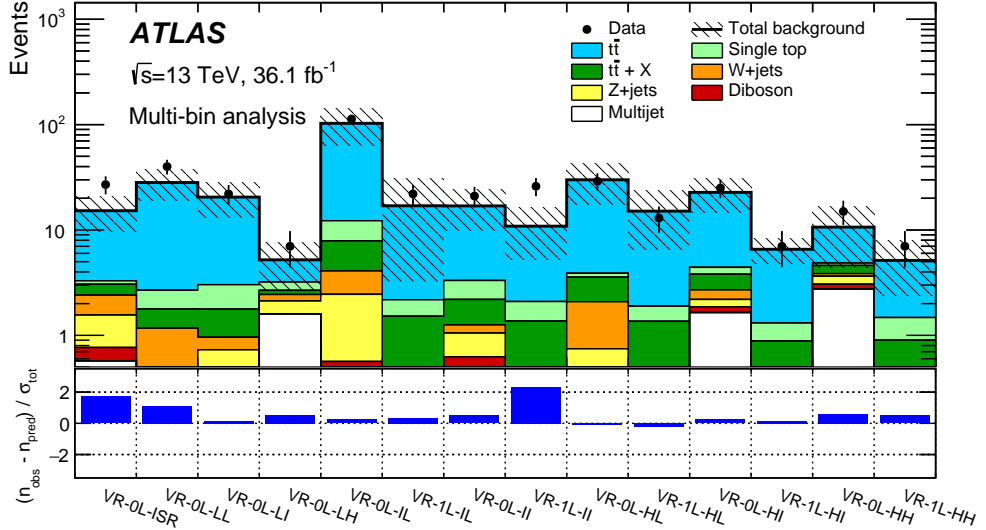
Model-independent limits on the number of beyond-the-SM (BSM) events for each SR are derived with pseudoexperiments using the CL_s prescription [94] and neglecting a possible signal contamination in the CR. Only the single-bin regions from the cut-and-count analysis are used for this purpose, to aid in the reinterpretation of these limits. Limits are obtained with a fit in each SR which proceeds in the same way as the fit used to predict the background, except that the number of events observed in the SR is added as an input to the fit. Also, an additional parameter for the non-SM signal strength, constrained to be non-negative, is fit. Upper limits on the visible BSM cross-section (σ_{vis}^{95}) are obtained by dividing the observed upper limits on the number of BSM events with the integrated luminosity. The results are given in Table 8, where the p_0 -values, which represent the probability of the SM background alone to fluctuate to the observed number of events or higher, are also provided.

9.2 Model-dependent exclusion limits

The results are used to place exclusion limits on various signal models. The results are obtained using the CL_s prescription in the asymptotic approximation [92]. The expected and observed limits were compared to the CL_s calculated from pseudoexperiments and found to be compatible. The signal contamination

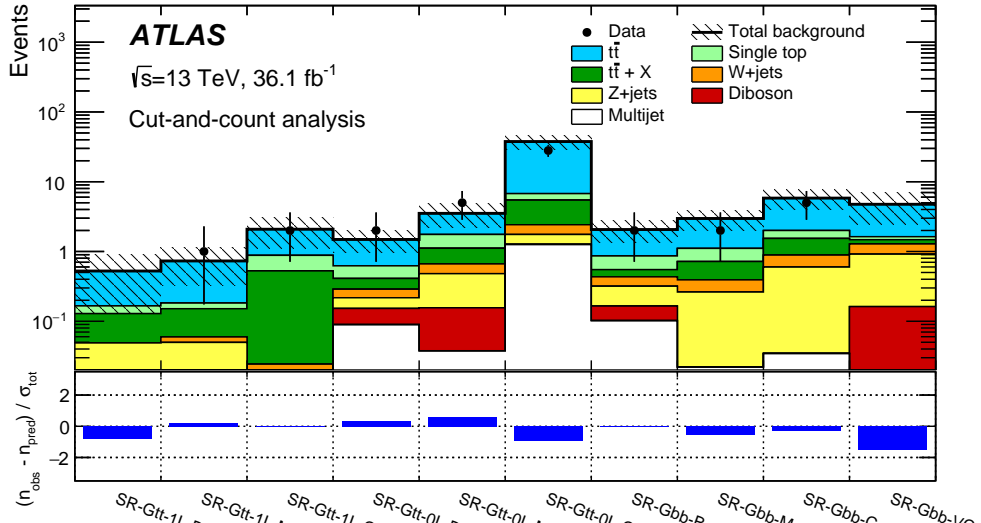


(a)

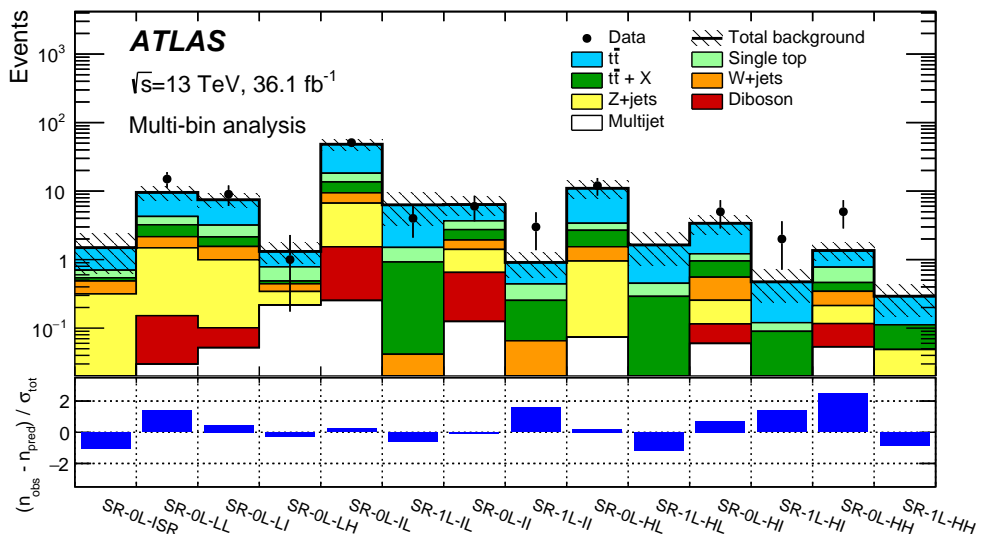


(b)

Figure 8: Results of the background-only fit extrapolated to the VRs of (a) the cut-and-count and (b) the multi-bin analyses. The $t\bar{t}$ normalisation is obtained from the fit to the CRs shown in Figure 7. The upper panel shows the observed number of events and the predicted background yield. All uncertainties defined in Section 7 are included in the uncertainty band. The background category $t\bar{t} + X$ includes $t\bar{t}W/Z$, $t\bar{t}H$ and $t\bar{t}t\bar{t}$ events. The lower panel shows the pulls in each VR.



(a)



(b)

Figure 9: Results of the background-only fit extrapolated to the SRs for (a) the cut-and-count and (b) the multi-bin analyses. The data in the SRs are not included in the fit. The upper panel shows the observed number of events and the predicted background yield. All uncertainties defined in Section 7 are included in the uncertainty band. The background category $t\bar{t} + X$ includes $t\bar{t}W/Z$, $t\bar{t}H$ and $t\bar{t}\bar{t}$ events. The lower panel shows the pulls in each SR.

Table 7: Results of the background-only fit extrapolated to the Gtt 1-lepton, Gtt 0-lepton and Gbb SRs in the cut-and-count analysis, for the total background prediction and breakdown of the main background sources. The uncertainties shown include all systematic uncertainties. The data in the SRs are not included in the fit. The background category $t\bar{t} + X$ includes $t\bar{t}W/Z$, $t\bar{t}H$ and $t\bar{t}t\bar{t}$ events. The row “MC-only background” provides the total background prediction when the $t\bar{t}$ normalisation is obtained from a theoretical calculation [64].

SR-Gtt-1L				
Targeted kinematics	B	M	C	
Observed events	0	1	2	
Fitted background	0.5 ± 0.4	0.7 ± 0.4	2.1 ± 1.0	
$t\bar{t}$	0.4 ± 0.4	0.5 ± 0.4	1.2 ± 0.8	
Single-top	0.04 ± 0.05	0.03 ± 0.06	0.35 ± 0.28	
$t\bar{t} + X$	0.08 ± 0.05	0.09 ± 0.06	0.50 ± 0.28	
Z+jets	0.049 ± 0.023	0.050 ± 0.023	< 0.01	
W+jets	< 0.01	< 0.01	0.024 ± 0.026	
Diboson	< 0.01	< 0.01	< 0.01	
MC-only background	0.43	0.45	1.9	
SR-Gtt-0L				
Targeted kinematics	B	M	C	
Observed events	2	5	28	
Fitted background	1.5 ± 0.5	3.5 ± 1.3	38 ± 8	
$t\bar{t}$	0.9 ± 0.4	1.8 ± 0.7	31 ± 8	
Single-top	0.21 ± 0.14	0.6 ± 0.4	1.3 ± 1.1	
$t\bar{t} + X$	0.12 ± 0.07	0.45 ± 0.25	3.0 ± 1.6	
Z+jets	0.06 ± 0.10	0.3 ± 0.9	0.49 ± 0.31	
W+jets	0.07 ± 0.06	0.18 ± 0.15	0.67 ± 0.22	
Diboson	0.06 ± 0.07	0.12 ± 0.07	< 0.01	
Multijet	0.09 ± 0.11	0.04 ± 0.05	1.3 ± 2.1	
MC-only background	1.3	3.3	23	
SR-Gbb				
Targeted kinematics	B	M	C	VC
Observed events	2	2	5	0
Fitted background	2.1 ± 0.7	3.0 ± 1.0	5.8 ± 1.9	4.7 ± 2.3
$t\bar{t}$	1.2 ± 0.6	1.9 ± 0.7	3.8 ± 1.3	3.1 ± 1.3
Single-top	0.31 ± 0.16	0.39 ± 0.16	0.46 ± 0.20	0.15 ± 0.18
$t\bar{t} + X$	0.12 ± 0.06	0.33 ± 0.19	0.6 ± 0.4	0.19 ± 0.11
Z+jets	0.15 ± 0.34	0.2 ± 0.6	0.6 ± 1.3	0.8 ± 1.9
W+jets	0.12 ± 0.09	0.13 ± 0.12	0.29 ± 0.19	0.37 ± 0.30
Diboson	0.06 ± 0.04	< 0.01	< 0.01	0.15 ± 0.08
Multijet	0.10 ± 0.12	0.022 ± 0.025	0.03 ± 0.04	0.016 ± 0.020
MC-only background	1.9	2.7	4.4	3.9

Table 8: The p_0 -values and Z (the number of equivalent Gaussian standard deviations), the 95% CL upper limits on the visible cross-section (σ_{vis}^{95}), and the observed and expected 95% CL upper limits on the number of BSM events (S_{obs}^{95} and S_{exp}^{95}). The maximum allowed p_0 -value is truncated at 0.5.

Signal channel	p_0 (Z)	σ_{vis}^{95} [fb]	S_{obs}^{95}	S_{exp}^{95}
SR-Gtt-1L-B	0.50 (0.00)	0.08	3.0	$3.0^{+1.0}_{-0.0}$
SR-Gtt-1L-M	0.34 (0.42)	0.11	3.9	$3.6^{+1.1}_{-0.4}$
SR-Gtt-1L-C	0.50 (0.00)	0.13	4.8	$4.7^{+1.8}_{-0.9}$
SR-Gtt-0L-B	0.32 (0.48)	0.13	4.8	$4.1^{+1.7}_{-0.6}$
SR-Gtt-0L-M	0.25 (0.69)	0.21	7.5	$6.0^{+2.3}_{-1.4}$
SR-Gtt-0L-C	0.50 (0.00)	0.39	14.0	$17.8^{+6.6}_{-4.5}$
SR-Gbb-B	0.50 (0.00)	0.13	4.6	$4.6^{+1.7}_{-1.0}$
SR-Gbb-M	0.50 (0.00)	0.12	4.4	$5.0^{+1.9}_{-1.1}$
SR-Gbb-C	0.50 (0.00)	0.18	6.6	$6.9^{+2.7}_{-1.8}$
SR-Gbb-VC	0.50 (0.00)	0.08	3.0	$4.6^{+2.0}_{-1.3}$

in the CRs and the experimental systematic uncertainties in the signal are taken into account for this calculation. All the regions of the multi-bin analysis are statistically combined to set model-dependent upper limits on the Gbb, Gtt and variable branching ratio models.

The 95% CL observed and expected exclusion limits for the Gtt and Gbb models are shown in the LSP and gluino mass plane in Figures 10(a) and 10(b), respectively. The $\pm 1\sigma_{\text{theory}}^{\text{SUSY}}$ lines around the observed limits are obtained by changing the SUSY cross-section by one standard deviation ($\pm 1\sigma$), as described in Section 4. The yellow band around the expected limit shows the $\pm 1\sigma$ uncertainty, including all statistical and systematic uncertainties except the theoretical uncertainties in the SUSY cross-section. Compared to the previous results [19], the gluino mass sensitivities of the current search (assuming massless LSPs) have improved by 300 GeV and 450 GeV for the Gbb and Gtt models, respectively. Gluinos with masses below 1.97 (1.92) TeV are excluded at 95% CL for neutralino masses lower than 300 GeV in the Gtt (Gbb) model. The observed limit for the Gtt model at high gluino mass is weaker than the expected limits due to the mild excesses observed in the signal regions SR-0L-HH and SR-1L-HI of the multi-bin fit analysis. The best exclusion limit on the LSP mass is approximately 1.19 (1.20) TeV, which is reached for a gluino mass of approximately 1.40 (1.68) TeV for Gbb and Gtt models, respectively.

Limits are also set in the signal model described in Section 2 for which the branching ratios of the gluinos to $t\bar{b}\tilde{\chi}_1^-$ (with $\tilde{\chi}_1^- \rightarrow f\bar{f}\tilde{\chi}_1^0$), $t\bar{t}\tilde{\chi}_1^0$, and $b\bar{b}\tilde{\chi}_1^0$ are allowed to vary, with a unitarity constraint imposed on the sum of the three branching ratios. The expected and observed exclusions are shown in Figure 11(a) for a fixed neutralino mass hypothesis ($m_{\tilde{\chi}_1^0} = 1$ GeV) and various gluino masses. The results are presented in the $B(\tilde{g} \rightarrow t\bar{t}\tilde{\chi}_1^0)$ vs. $B(\tilde{g} \rightarrow b\bar{b}\tilde{\chi}_1^0)$ plane, where the branching ratio for $\tilde{g} \rightarrow t\bar{b}\tilde{\chi}_1^-$ is equal to $1 - (B(\tilde{g} \rightarrow t\bar{t}\tilde{\chi}_1^0) + B(\tilde{g} \rightarrow b\bar{b}\tilde{\chi}_1^0))$. The exclusion limits are weaker in the lower left corner, where the branching ratio for $\tilde{g} \rightarrow t\bar{b}\tilde{\chi}_1^-$ is substantial, which is expected since these decays were not included in the optimisation procedure. Due to the mild excess observed in some regions of the multi-bin analysis and despite an expected sensitivity across the whole plane for a massless neutralino hypothesis,

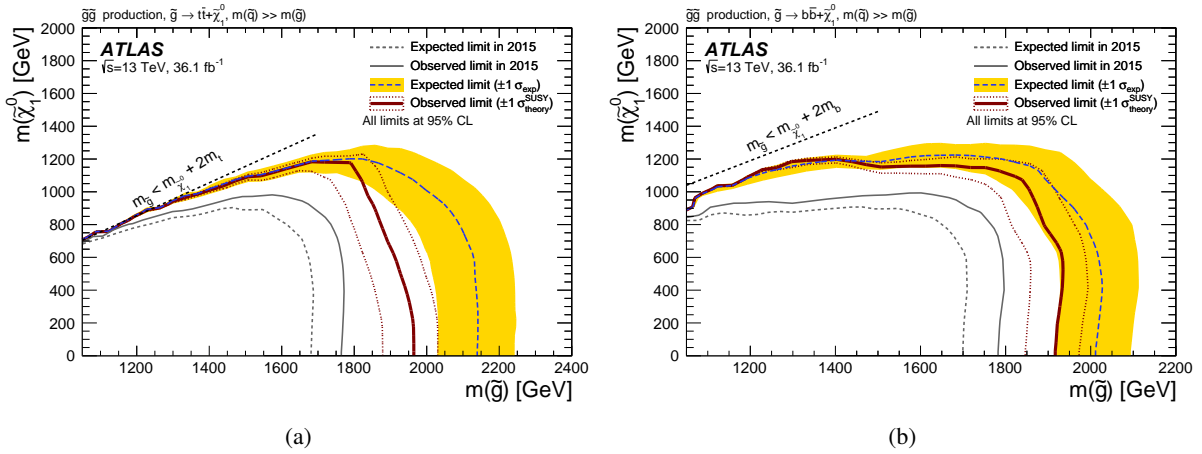


Figure 10: Exclusion limits in the $\tilde{\chi}_1^0$ and \tilde{g} mass plane for the (a) Gtt and (b) Gbb models obtained in the context of the multi-bin analysis. The dashed and solid bold lines show the 95% CL expected and observed limits, respectively. The shaded bands around the expected limits show the impact of the experimental and background uncertainties. The dotted lines show the impact on the observed limit of the variation of the nominal signal cross-section by $\pm 1\sigma$ of its theoretical uncertainty. The 95% CL expected and observed limits from the ATLAS search based on 2015 data [19] are also shown.

the 95% CL limit for a 1.8 TeV gluino is of $B(\tilde{g} \rightarrow t\bar{t}\tilde{\chi}_1^0) \geq 30\%$ ($B(\tilde{g} \rightarrow b\bar{b}\tilde{\chi}_1^0) \geq 40\%$) when assuming $B(\tilde{g} \rightarrow b\bar{b}\tilde{\chi}_1^0) = 0$ ($B(\tilde{g} \rightarrow t\bar{t}\tilde{\chi}_1^0) = 0$). None of the points in the plane are excluded for gluino masses larger than 2.0 TeV.

Similar results are presented in Figure 11(b) assuming a gluino mass of 1.9 TeV and scanning various neutralino masses (1, 600 and 1000 GeV). For neutralino masses between 1 and 600 GeV, most of the branching ratio plane is expected to be excluded at 95% CL. The observed limit is nevertheless worse due to the mild excess observed in the SRs. Thus, for instance, for a massless neutralino hypothesis, only the region with $B(\tilde{g} \rightarrow b\bar{b}\tilde{\chi}_1^0) > 90\%$ is excluded for all values of $B(\tilde{g} \rightarrow t\bar{t}\tilde{\chi}_1^0)$.

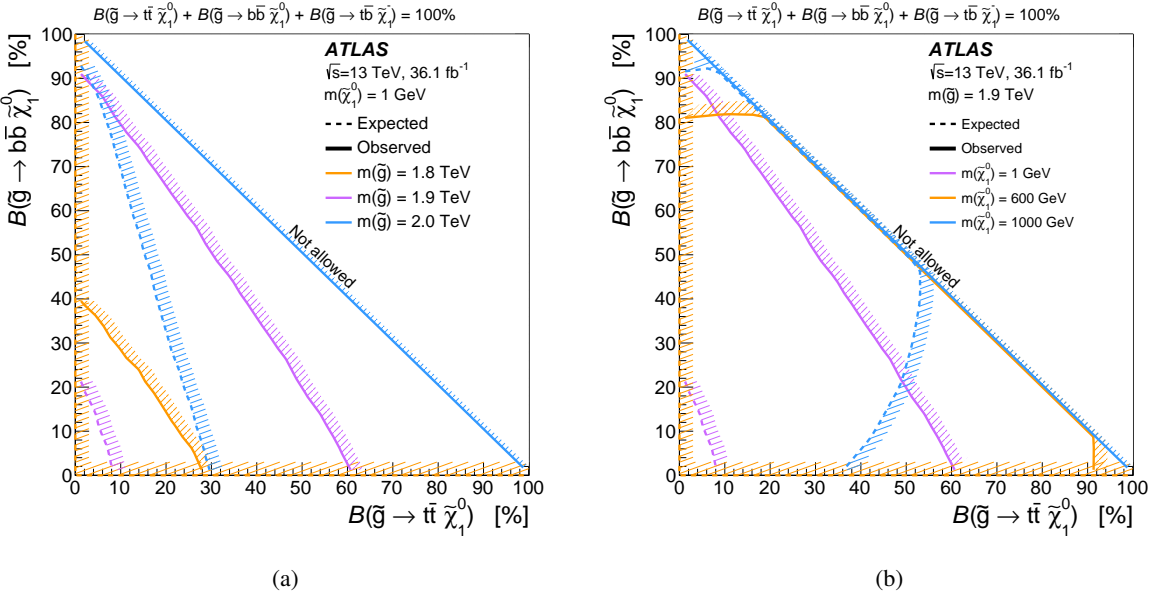


Figure 11: Exclusion limits in the $\tilde{g} \rightarrow t\bar{t}\tilde{\chi}_1^0$ and $\tilde{g} \rightarrow b\bar{b}\tilde{\chi}_1^0$ branching ratio plane assuming (a) a neutralino mass of 1 GeV and various gluino masses (1.8, 1.9 and 2.0 TeV) and (b) a gluino mass of 1.9 TeV and three neutralino masses (1, 600 and 1000 GeV). In (a), the expected limit for a gluino mass of 1.8 TeV follows the plot axes, meaning that the whole plane is expected to be excluded at 95% CL. The same is true in (b) for a neutralino mass of 600 GeV. The dashed and solid bold lines show the 95% CL expected and observed limits, respectively. The hashing indicates which side of the line is excluded. The upper right half of the plane is forbidden by the requirement that the sum of branching ratios does not exceed 100%.

10 Conclusion

A search for pair-produced gluinos decaying via bottom or top squarks is presented. LHC proton–proton collision data from the full 2015 and 2016 data-taking periods are analysed, corresponding to an integrated luminosity of 36.1 fb^{-1} collected at $\sqrt{s} = 13 \text{ TeV}$ by the ATLAS detector. The search uses multiple signal regions designed for different scenarios of gluino and LSP masses. The signal regions require several high- p_T jets, of which at least three must be b -tagged, large E_T^{miss} and either zero or at least one charged lepton. Two strategies are employed: one in which the signal regions are optimised for discovery, and another one in which several non-overlapping signal regions are fitted simultaneously to achieve optimal exclusion limits for benchmark signals. For all signal regions, the background is generally dominated by $t\bar{t}$ +jets, which is normalised in dedicated control regions. No excess is found above the predicted background in any of the signal regions. Model-independent limits are set on the visible cross-section for new physics processes. Exclusion limits are set on gluino and LSP masses in two simplified models where the gluino decays exclusively as $\tilde{g} \rightarrow b\bar{b}\tilde{\chi}_1^0$ or $\tilde{g} \rightarrow t\bar{t}\tilde{\chi}_1^0$. For LSP masses below approximately 300 GeV, gluino masses of less than 1.97 TeV and 1.92 TeV are excluded at the 95% CL for the $\tilde{g} \rightarrow t\bar{t}\tilde{\chi}_1^0$ and $\tilde{g} \rightarrow b\bar{b}\tilde{\chi}_1^0$ models, respectively. These results improve upon the exclusion limits obtained with the 2015 dataset alone. The results are also interpreted in a model with variable gluino branching ratios to $\tilde{g} \rightarrow b\bar{b}\tilde{\chi}_1^0$, $\tilde{g} \rightarrow t\bar{b}\tilde{\chi}_1^-$ and $\tilde{g} \rightarrow t\bar{t}\tilde{\chi}_1^0$. For example, a mass point with $m_{\tilde{g}} = 1.9 \text{ TeV}$ and $m_{\tilde{\chi}_1^0} = 1 \text{ GeV}$ is excluded at the 95% CL only if $B(\tilde{g} \rightarrow t\bar{b}\tilde{\chi}_1^-) < 10\%$.

Acknowledgements

We thank CERN for the very successful operation of the LHC, as well as the support staff from our institutions without whom ATLAS could not be operated efficiently.

We acknowledge the support of ANPCyT, Argentina; YerPhI, Armenia; ARC, Australia; BMWFW and FWF, Austria; ANAS, Azerbaijan; SSTC, Belarus; CNPq and FAPESP, Brazil; NSERC, NRC and CFI, Canada; CERN; CONICYT, Chile; CAS, MOST and NSFC, China; COLCIENCIAS, Colombia; MSMT CR, MPO CR and VSC CR, Czech Republic; DNRF and DNSRC, Denmark; IN2P3-CNRS, CEA-DRF/IRFU, France; SRNSFG, Georgia; BMBF, HGF, and MPG, Germany; GSRT, Greece; RGC, Hong Kong SAR, China; ISF, I-CORE and Benoziyo Center, Israel; INFN, Italy; MEXT and JSPS, Japan; CNRST, Morocco; NWO, Netherlands; RCN, Norway; MNiSW and NCN, Poland; FCT, Portugal; MNE/IFA, Romania; MES of Russia and NRC KI, Russian Federation; JINR; MESTD, Serbia; MSSR, Slovakia; ARRS and MIZŠ, Slovenia; DST/NRF, South Africa; MINECO, Spain; SRC and Wallenberg Foundation, Sweden; SERI, SNSF and Cantons of Bern and Geneva, Switzerland; MOST, Taiwan; TAEK, Turkey; STFC, United Kingdom; DOE and NSF, United States of America. In addition, individual groups and members have received support from BCKDF, the Canada Council, CANARIE, CRC, Compute Canada, FQRNT, and the Ontario Innovation Trust, Canada; EPLANET, ERC, ERDF, FP7, Horizon 2020 and Marie Skłodowska-Curie Actions, European Union; Investissements d’Avenir Labex and Idex, ANR, Région Auvergne and Fondation Partager le Savoir, France; DFG and AvH Foundation, Germany; Herakleitos, Thales and Aristeia programmes co-financed by EU-ESF and the Greek NSRF; BSF, GIF and Minerva, Israel; BRF, Norway; CERCA Programme Generalitat de Catalunya, Generalitat Valenciana, Spain; the Royal Society and Leverhulme Trust, United Kingdom.

The crucial computing support from all WLCG partners is acknowledged gratefully, in particular from CERN, the ATLAS Tier-1 facilities at TRIUMF (Canada), NDGF (Denmark, Norway, Sweden), CC-IN2P3 (France), KIT/GridKA (Germany), INFN-CNAF (Italy), NL-T1 (Netherlands), PIC (Spain), ASGC (Taiwan), RAL (UK) and BNL (USA), the Tier-2 facilities worldwide and large non-WLCG resource providers. Major contributors of computing resources are listed in Ref. [95].

References

- [1] Yu. A. Golfand and E. P. Likhtman, *Extension of the Algebra of Poincare Group Generators and Violation of p Invariance*, JETP Lett. **13** (1971) 323, [*Pisma Zh. Eksp. Teor. Fiz.* 13 (1971) 452].
- [2] D. V. Volkov and V. P. Akulov, *Is the Neutrino a Goldstone Particle?*, Phys. Lett. B **46** (1973) 109.
- [3] J. Wess and B. Zumino, *Supergauge Transformations in Four-Dimensions*, Nucl. Phys. B **70** (1974) 39.
- [4] J. Wess and B. Zumino, *Supergauge Invariant Extension of Quantum Electrodynamics*, Nucl. Phys. B **78** (1974) 1.
- [5] S. Ferrara and B. Zumino, *Supergauge Invariant Yang-Mills Theories*, Nucl. Phys. B **79** (1974) 413.
- [6] A. Salam and J. A. Strathdee, *Supersymmetry and Nonabelian Gauges*, Phys. Lett. B **51** (1974) 353.
- [7] G. R. Farrar and P. Fayet, *Phenomenology of the Production, Decay, and Detection of New Hadronic States Associated with Supersymmetry*, Phys. Lett. B **76** (1978) 575.
- [8] N. Sakai, *Naturalness in Supersymmetric Guts*, Z. Phys. C **11** (1981) 153.

- [9] S. Dimopoulos, S. Raby and F. Wilczek, *Supersymmetry and the Scale of Unification*, *Phys. Rev. D* **24** (1981) 1681.
- [10] L. E. Ibanez and G. G. Ross, *Low-Energy Predictions in Supersymmetric Grand Unified Theories*, *Phys. Lett. B* **105** (1981) 439.
- [11] S. Dimopoulos and H. Georgi, *Softly Broken Supersymmetry and SU(5)*, *Nucl. Phys. B* **193** (1981) 150.
- [12] K. Inoue, A. Kakuto, H. Komatsu and S. Takeshita, *Aspects of Grand Unified Models with Softly Broken Supersymmetry*, *Prog. Theor. Phys.* **68** (1982) 927, [Erratum: *Prog. Theor. Phys.* 70,330(1983)].
- [13] J. R. Ellis and S. Rudaz, *Search for Supersymmetry in Toponium Decays*, *Phys. Lett. B* **128** (1983) 248.
- [14] R. Barbieri and G. F. Giudice, *Upper Bounds on Supersymmetric Particle Masses*, *Nucl. Phys. B* **306** (1988) 63.
- [15] ATLAS Collaboration, *The ATLAS Experiment at the CERN Large Hadron Collider*, *JINST* **3** (2008) S08003.
- [16] J. Alwall, M.-P. Le, M. Lisanti and J. G. Wacker, *Searching for Directly Decaying Gluinos at the Tevatron*, *Phys. Lett. B* **666** (2008) 34, arXiv: [0803.0019 \[hep-ph\]](#).
- [17] J. Alwall, P. Schuster and N. Toro, *Simplified Models for a First Characterization of New Physics at the LHC*, *Phys. Rev. D* **79** (2009) 075020, arXiv: [0810.3921 \[hep-ph\]](#).
- [18] D. Alves et al., *Simplified Models for LHC New Physics Searches*, *J. Phys. G* **39** (2012) 105005, arXiv: [1105.2838 \[hep-ph\]](#).
- [19] ATLAS Collaboration, *Search for pair production of gluinos decaying via stop and sbottom in events with b-jets and large missing transverse momentum in pp collisions at $\sqrt{s} = 13$ TeV with the ATLAS detector*, *Phys. Rev. D* **94** (2016) 032003, arXiv: [1605.09318 \[hep-ex\]](#).
- [20] ATLAS Collaboration, *Search for supersymmetry at $\sqrt{s} = 13$ TeV in final states with jets and two same-sign leptons or three leptons with the ATLAS detector*, *Eur. Phys. J. C* **76** (2016) 259, arXiv: [1602.09058 \[hep-ex\]](#).
- [21] ATLAS Collaboration, *Search for supersymmetry in final states with two same-sign or three leptons and jets using 36 fb^{-1} of $\sqrt{s} = 13$ TeV pp collision data with the ATLAS detector*, *JHEP* **09** (2017) 084, arXiv: [1706.03731 \[hep-ex\]](#).
- [22] CMS Collaboration, *Search for physics beyond the standard model in events with two leptons of same sign, missing transverse momentum, and jets in proton–proton collisions at $\sqrt{s} = 13$ TeV*, *Eur. Phys. J. C* **77** (2017) 578, arXiv: [1704.07323 \[hep-ex\]](#).
- [23] CMS Collaboration, *Search for Supersymmetry in pp Collisions at $\sqrt{s} = 13$ TeV in the Single-Lepton Final State Using the Sum of Masses of Large-Radius Jets*, *Phys. Rev. Lett.* **119** (2017) 151802, arXiv: [1705.04673 \[hep-ex\]](#).
- [24] CMS Collaboration, *Search for supersymmetry in multijet events with missing transverse momentum in proton-proton collisions at 13 TeV*, *Phys. Rev. D* **96** (2017) 032003, arXiv: [1704.07781 \[hep-ex\]](#).
- [25] CMS Collaboration, *Search for new phenomena with the M_{T2} variable in the all-hadronic final state produced in proton–proton collisions at $\sqrt{s} = 13$ TeV*, *Eur. Phys. J. C* **77** (2017) 710, arXiv: [1705.04650 \[hep-ex\]](#).

- [26] ATLAS Collaboration, *Search for strong production of supersymmetric particles in final states with missing transverse momentum and at least three b-jets at $\sqrt{s} = 8$ TeV proton-proton collisions with the ATLAS detector*, JHEP **10** (2014) 24, arXiv: [1407.0600 \[hep-ex\]](#).
- [27] CMS Collaboration, *Inclusive search for supersymmetry using razor variables in pp collisions at $\sqrt{s} = 13$ TeV*, Phys. Rev. D **95** (2017) 012003, arXiv: [1609.07658 \[hep-ex\]](#).
- [28] ATLAS Collaboration, *ATLAS Insertable B-Layer Technical Design Report*, ATLAS-TDR-19, 2010, URL: <https://cds.cern.ch/record/1291633>, ATLAS Insertable B-Layer Technical Design Report Addendum, ATLAS-TDR-19-ADD-1, 2012, URL: <https://cds.cern.ch/record/1451888>.
- [29] ATLAS Collaboration, *Performance of the ATLAS Trigger System in 2015*, Eur. Phys. J. C **77** (2017) 317, arXiv: [1611.09661 \[hep-ex\]](#).
- [30] ATLAS Collaboration, *Luminosity determination in pp collisions at $\sqrt{s} = 8$ TeV using the ATLAS detector at the LHC*, Eur. Phys. J. C **76** (2016) 653, arXiv: [1608.03953 \[hep-ex\]](#).
- [31] J. Alwall, R. Frederix, S. Frixione, V. Hirschi, F. Maltoni et al., *The automated computation of tree-level and next-to-leading order differential cross sections, and their matching to parton shower simulations*, JHEP **07** (2014) 079, arXiv: [1405.0301 \[hep-ph\]](#).
- [32] R. D. Ball et al., *Parton distributions with LHC data*, Nucl. Phys. B **867** (2013) 244, arXiv: [1207.1303 \[hep-ph\]](#).
- [33] T. Sjöstrand, S. Mrenna and P. Z. Skands, *A Brief Introduction to PYTHIA 8.1*, Comput. Phys. Commun. **178** (2008) 852, arXiv: [0710.3820 \[hep-ph\]](#).
- [34] S. Alioli, P. Nason, C. Oleari and E. Re, *A general framework for implementing NLO calculations in shower Monte Carlo programs: the POWHEG BOX*, JHEP **06** (2010) 043, arXiv: [1002.2581 \[hep-ph\]](#).
- [35] H.-L. Lai, M. Guzzi, J. Huston, Z. Li, P. M. Nadolsky et al., *New parton distributions for collider physics*, Phys. Rev. D **82** (2010) 074024, arXiv: [1007.2241 \[hep-ph\]](#).
- [36] P. Artoisenet, R. Frederix, O. Mattelaer and R. Rietkerk, *Automatic spin-entangled decays of heavy resonances in Monte Carlo simulations*, JHEP **03** (2013) 015, arXiv: [1212.3460 \[hep-ph\]](#).
- [37] T. Sjöstrand, S. Mrenna and P. Z. Skands, *PYTHIA 6.4 Physics and Manual*, JHEP **05** (2006) 026, arXiv: [hep-ph/0603175](#).
- [38] J. Pumplin et al., *New generation of parton distributions with uncertainties from global QCD analysis*, JHEP **07** (2002) 012, arXiv: [hep-ph/0201195](#).
- [39] M. Bahr et al., *Herwig++ Physics and Manual*, Eur. Phys. J. C **58** (2008) 639, arXiv: [0803.0883 \[hep-ph\]](#).
- [40] ATLAS Collaboration, *Modelling of the $t\bar{t}H$ and $t\bar{t}V(V = W, Z)$ processes for $\sqrt{s} = 13$ TeV ATLAS analyses*, ATL-PHYS-PUB-2016-005, URL: <https://cds.cern.ch/record/2120826>.
- [41] T. Gleisberg, S. Höche, F. Krauss, M. Schönherr, S. Schumann et al., *Event generation with SHERPA 1.1*, JHEP **02** (2009) 007, arXiv: [0811.4622 \[hep-ph\]](#).
- [42] T. Gleisberg and S. Höche, *Comix, a new matrix element generator*, JHEP **12** (2008) 039, arXiv: [0808.3674 \[hep-ph\]](#).
- [43] F. Cascioli, P. Maierhofer and S. Pozzorini, *Scattering Amplitudes with Open Loops*, Phys. Rev. Lett. **108** (2012) 111601, arXiv: [1111.5206 \[hep-ph\]](#).

- [44] S. Schumann and F. Krauss, *A Parton shower algorithm based on Catani-Seymour dipole factorisation*, JHEP **03** (2008) 038, arXiv: [0709.1027 \[hep-ph\]](#).
- [45] S. Höche, F. Krauss, M. Schönherr and F. Siegert, *QCD matrix elements + parton showers: The NLO case*, JHEP **04** (2013) 027, arXiv: [1207.5030 \[hep-ph\]](#).
- [46] C. Patrignani et al. (Particle Data Group), *Review of Particle Physics*, Chin. Phys. C **40** (2016) 100001.
- [47] ATLAS Collaboration, *Multi-boson simulation for 13 TeV ATLAS analyses*, ATL-PHYS-PUB-2016-002, URL: <https://cds.cern.ch/record/2119986>.
- [48] R. D. Ball et al., *Parton distributions for the LHC Run II*, JHEP **04** (2015) 040, arXiv: [1410.8849 \[hep-ph\]](#).
- [49] D. J. Lange, *The EvtGen particle decay simulation package*, Nucl. Instrum. Meth. A **462** (2001) 152.
- [50] P. Z. Skands, *Tuning Monte Carlo Generators: The Perugia Tunes*, Phys. Rev. D **82** (2010) 074018, arXiv: [1005.3457 \[hep-ph\]](#).
- [51] ATLAS Collaboration, *ATLAS Pythia 8 tunes to 7 TeV data*, ATL-PHYS-PUB-2014-021, URL: <https://cds.cern.ch/record/1966419>.
- [52] S. Gieseke, C. Rohr and A. Siódmiak, *Colour reconnections in Herwig++*, Eur. Phys. J. C **72** (2012) 2225, arXiv: [1206.0041 \[hep-ph\]](#).
- [53] ATLAS Collaboration, *Summary of ATLAS Pythia 8 tunes*, ATL-PHYS-PUB-2012-003, 2012, URL: <https://cds.cern.ch/record/1474107>.
- [54] A. D. Martin, W. J. Stirling, R. S. Thorne and G. Watt, *Parton distributions for the LHC*, Eur. Phys. J. C **63** (2009) 189, arXiv: [0901.0002 \[hep-ph\]](#).
- [55] S. Agostinelli et al., *GEANT4: A simulation toolkit*, Nucl. Instrum. Meth. A **506** (2003) 250.
- [56] ATLAS Collaboration, *The simulation principle and performance of the ATLAS fast calorimeter simulation FastCaloSim*, ATL-PHYS-PUB-2010-013, 2010, URL: <https://cds.cern.ch/record/1300517>.
- [57] W. Beenakker, R. Hopker, M. Spira and P. Zerwas, *Squark and gluino production at hadron colliders*, Nucl. Phys. B **492** (1997) 51, arXiv: [hep-ph/9610490](#).
- [58] A. Kulesza and L. Motyka, *Threshold resummation for squark-antisquark and gluino-pair production at the LHC*, Phys. Rev. Lett. **102** (2009) 111802, arXiv: [0807.2405 \[hep-ph\]](#).
- [59] A. Kulesza and L. Motyka, *Soft gluon resummation for the production of gluino-gluino and squark-antisquark pairs at the LHC*, Phys. Rev. D **80** (2009) 095004, arXiv: [0905.4749 \[hep-ph\]](#).
- [60] W. Beenakker, S. Brensing, M. Kramer, A. Kulesza, E. Laenen et al., *Soft-gluon resummation for squark and gluino hadroproduction*, JHEP **12** (2009) 041, arXiv: [0909.4418 \[hep-ph\]](#).
- [61] W. Beenakker, S. Brensing, M. Kramer, A. Kulesza, E. Laenen et al., *Squark and gluino hadroproduction*, Int. J. Mod. Phys. A **26** (2011) 2637, arXiv: [1105.1110 \[hep-ph\]](#).
- [62] C. Borschensky et al., *Squark and gluino production cross sections in pp collisions at $\sqrt{s} = 13, 14, 33$ and 100 TeV*, Eur. Phys. J. C **74** (2014) 3174, arXiv: [1407.5066 \[hep-ph\]](#).
- [63] ATLAS Collaboration, *Search for squarks and gluinos with the ATLAS detector in final states with jets and missing transverse momentum using 4.7 fb^{-1} of $\sqrt{s} = 7 \text{ TeV}$ proton-proton collision data*, Phys. Rev. D **87** (2013) 012008, arXiv: [1208.0949 \[hep-ex\]](#).
- [64] M. Czakon and A. Mitov, *Top++: A Program for the Calculation of the Top-Pair Cross-Section at Hadron Colliders*, Comput. Phys. Commun. **185** (2014) 2930, arXiv: [1112.5675 \[hep-ph\]](#).

- [65] N. Kidonakis, *NNLL resummation for s-channel single top quark production*, Phys. Rev. D **81** (2010) 054028, arXiv: [1001.5034 \[hep-ph\]](#).
- [66] N. Kidonakis, *Two-loop soft anomalous dimensions for single top quark associated production with a W^- or H^-* , Phys. Rev. D **82** (2010) 054018, arXiv: [1005.4451 \[hep-ph\]](#).
- [67] N. Kidonakis, *Next-to-next-to-leading-order collinear and soft gluon corrections for t-channel single top quark production*, Phys. Rev. D **83** (2011) 091503, arXiv: [1103.2792 \[hep-ph\]](#).
- [68] D. de Florian et al., *Handbook of LHC Higgs Cross Sections: 4. Deciphering the Nature of the Higgs Sector*, (2016), arXiv: [1610.07922 \[hep-ph\]](#).
- [69] J. R. Andersen et al., *Handbook of LHC Higgs Cross Sections: 3. Higgs Properties*, (2013), arXiv: [1307.1347 \[hep-ph\]](#).
- [70] S. Catani, L. Cieri, G. Ferrera, D. de Florian and M. Grazzini, *Vector boson production at hadron colliders: a fully exclusive QCD calculation at NNLO*, Phys. Rev. Lett. **103** (2009) 082001, arXiv: [0903.2120 \[hep-ph\]](#).
- [71] ATLAS Collaboration, *Vertex Reconstruction Performance of the ATLAS Detector at $\sqrt{s} = 13$ TeV*, ATL-PHYS-PUB-2015-026, URL: <https://cds.cern.ch/record/2037717>.
- [72] ATLAS Collaboration, *Topological cell clustering in the ATLAS calorimeters and its performance in LHC Run 1*, Eur. Phys. J. C **77** (2017) 490, arXiv: [1603.02934 \[hep-ex\]](#).
- [73] M. Cacciari, G. P. Salam and G. Soyez, *The anti- k_t jet clustering algorithm*, JHEP **04** (2008) 063, arXiv: [0802.1189 \[hep-ph\]](#).
- [74] M. Cacciari, G. P. Salam and G. Soyez, *FastJet User Manual*, Eur. Phys. J. C **72** (2012) 1896, arXiv: [1111.6097 \[hep-ph\]](#).
- [75] ATLAS Collaboration, *Jet energy scale measurements and their systematic uncertainties in proton-proton collisions at $\sqrt{s} = 13$ TeV with the ATLAS detector*, Submitted to Phys. Rev. D (2017), arXiv: [1703.09665 \[hep-ex\]](#).
- [76] ATLAS Collaboration, *Selection of jets produced in 13 TeV proton–proton collisions with the ATLAS detector*, ATLAS-CONF-2015-029, 2015, URL: <https://cds.cern.ch/record/2037702>.
- [77] ATLAS Collaboration, *Performance of pile-up mitigation techniques for jets in pp collisions at $\sqrt{s} = 8$ TeV using the ATLAS detector*, Eur. Phys. J. C **76** (2016) 581, arXiv: [1510.03823 \[hep-ex\]](#).
- [78] ATLAS Collaboration, *Performance of b-jet identification in the ATLAS experiment*, JINST **11** (2016) P04008, arXiv: [1512.01094 \[hep-ex\]](#).
- [79] ATLAS Collaboration, *Optimisation of the ATLAS b-tagging performance for the 2016 LHC Run*, ATL-PHYS-PUB-2016-012, URL: <https://cds.cern.ch/record/2160731>.
- [80] B. Nachman, P. Nef, A. Schwartzman, M. Swiatlowski and C. Wanotayaroj, *Jets from Jets: Reclustering as a tool for large radius jet reconstruction and grooming at the LHC*, JHEP **02** (2015) 075, arXiv: [1407.2922 \[hep-ph\]](#).
- [81] D. Krohn, J. Thaler and L.-T. Wang, *Jet Trimming*, JHEP **02** (2010) 084, arXiv: [0912.1342 \[hep-ph\]](#).
- [82] ATLAS Collaboration, *Performance of jet substructure techniques for large-R jets in proton–proton collisions at $\sqrt{s} = 7$ TeV using the ATLAS detector*, JHEP **09** (2013) 076, arXiv: [1306.4945 \[hep-ex\]](#).

- [83] ATLAS Collaboration, *Performance of Top Quark and W Boson Tagging in Run 2 with ATLAS*, ATLAS-CONF-2017-064, 2017, URL: <https://cds.cern.ch/record/2281054>.
- [84] ATLAS Collaboration, *Electron and photon energy calibration with the ATLAS detector using LHC Run 1 data*, *Eur. Phys. J. C* **74** (2014) 3071, arXiv: [1407.5063 \[hep-ex\]](https://arxiv.org/abs/1407.5063).
- [85] ATLAS Collaboration, *Electron efficiency measurements with the ATLAS detector using the 2015 LHC proton–proton collision data*, ATLAS-CONF-2016-024, 2016, URL: <https://cds.cern.ch/record/2157687>.
- [86] ATLAS Collaboration, *Muon reconstruction performance of the ATLAS detector in proton–proton collision data at $\sqrt{s} = 13$ TeV*, *Eur. Phys. J. C* **76** (2016) 292, arXiv: [1603.05598 \[hep-ex\]](https://arxiv.org/abs/1603.05598).
- [87] ATLAS Collaboration, *Performance of missing transverse momentum reconstruction with the ATLAS detector in the first proton–proton collisions at $\sqrt{s} = 13$ TeV*, ATL-PHYS-PUB-2015-027, URL: <https://cds.cern.ch/record/2037904>.
- [88] ATLAS Collaboration, *Expected performance of missing transverse momentum reconstruction for the ATLAS detector at $\sqrt{s} = 13$ TeV*, ATL-PHYS-PUB-2015-023, URL: <https://cds.cern.ch/record/2037700>.
- [89] ATLAS Collaboration, *Jet Calibration and Systematic Uncertainties for Jets Reconstructed in the ATLAS Detector at $\sqrt{s} = 13$ TeV*, ATL-PHYS-PUB-2015-015, URL: <https://cds.cern.ch/record/2037613>.
- [90] ATLAS Collaboration, *Measurements of fiducial cross-sections for $t\bar{t}$ production with one or two additional b -jets in pp collisions at $\sqrt{s} = 8$ TeV using the ATLAS detector*, *Eur. Phys. J. C* **76** (2016) 11, arXiv: [1508.06868 \[hep-ex\]](https://arxiv.org/abs/1508.06868).
- [91] P. Kant et al., *HatHor for single top-quark production: Updated predictions and uncertainty estimates for single top-quark production in hadronic collisions*, *Comput. Phys. Commun.* **191** (2015) 74, arXiv: [1406.4403 \[hep-ph\]](https://arxiv.org/abs/1406.4403).
- [92] G. Cowan, K. Cranmer, E. Gross and O. Vitells, *Asymptotic formulae for likelihood-based tests of new physics*, *Eur. Phys. J. C* **71** (2011) 1554, arXiv: [1007.1727 \[physics.data-an\]](https://arxiv.org/abs/1007.1727), Erratum: *Eur. Phys. J. C* **73** (2013) 2501.
- [93] M. Baak, G. Besjes, D. Côte, A. Koutsman, J. Lorenz et al., *HistFitter software framework for statistical data analysis*, *Eur. Phys. J. C* **75** (2015) 153, arXiv: [1410.1280 \[hep-ex\]](https://arxiv.org/abs/1410.1280).
- [94] A. L. Read, *Presentation of Search Results: The CL(s) Technique*, *J. Phys. G* **28** (2002) 2693.
- [95] ATLAS Collaboration, *ATLAS Computing Acknowledgements 2016–2017*, ATL-GEN-PUB-2016-002, URL: <https://cds.cern.ch/record/2202407>.

The ATLAS Collaboration

M. Aaboud^{34d}, G. Aad⁹⁹, B. Abbott¹²⁴, O. Abdinov^{13,*}, B. Abelsoos¹²⁸, S.H. Abidi¹⁶⁵, O.S. AbouZeid¹⁴³, N.L. Abraham¹⁵³, H. Abramowicz¹⁵⁹, H. Abreu¹⁵⁸, R. Abreu¹²⁷, Y. Abulaiti^{43a,43b}, B.S. Acharya^{64a,64b,o}, S. Adachi¹⁶¹, L. Adamczyk^{81a}, J. Adelman¹¹⁹, M. Adersberger¹¹², T. Adye¹⁴¹, A.A. Affolder¹⁴³, T. Agatonovic-Jovin¹⁶, C. Agheorghiesei^{27c}, J.A. Aguilar-Saavedra^{136f,136a}, F. Ahmadov^{77,ag}, G. Aielli^{71a,71b}, S. Akatsuka⁸³, H. Akerstedt^{43a,43b}, T.P.A. Åkesson⁹⁴, E. Akilli⁵², A.V. Akimov¹⁰⁸, G.L. Alberghi^{23b,23a}, J. Albert¹⁷⁴, P. Albicocco⁴⁹, M.J. Alconada Verzini⁸⁶, S. Alderweireldt¹¹⁷, M. Aleksa³⁵, I.N. Aleksandrov⁷⁷, C. Alexa^{27b}, G. Alexander¹⁵⁹, T. Alexopoulos¹⁰, M. Alhoob¹²⁴, B. Ali¹³⁸, G. Alimonti^{66a}, J. Alison³⁶, S.P. Alkire³⁸, B.M.M. Allbrooke¹⁵³, B.W. Allen¹²⁷, P.P. Allport²¹, A. Aloisio^{67a,67b}, A. Alonso³⁹, F. Alonso⁸⁶, C. Alpigiani¹⁴⁵, A.A. Alshehri⁵⁵, M.I. Alstaty⁹⁹, B. Alvarez Gonzalez³⁵, D. Álvarez Piqueras¹⁷², M.G. Alvaggi^{67a,67b}, B.T. Amadio¹⁸, Y. Amaral Coutinho^{78b}, C. Amelung²⁶, D. Amidei¹⁰³, S.P. Amor Dos Santos^{136a,136c}, A. Amorim^{136a}, S. Amoroso³⁵, G. Amundsen²⁶, C. Anastopoulos¹⁴⁶, L.S. Ancu⁵², N. Andari²¹, T. Andeen¹¹, C.F. Anders^{59b}, J.K. Anders⁸⁸, K.J. Anderson³⁶, A. Andreazza^{66a,66b}, V. Andrei^{59a}, S. Angelidakis⁹, I. Angelozzi¹¹⁸, A. Angerami³⁸, A.V. Anisenkov^{120b,120a}, N. Anjos¹⁴, A. Annovi^{69a}, C. Antel^{59a}, M. Antonelli⁴⁹, A. Antonov^{110,*}, D.J.A. Antrim¹⁶⁹, F. Anulli^{70a}, M. Aoki⁷⁹, L. Aperio Bella³⁵, G. Arabidze¹⁰⁴, Y. Arai⁷⁹, J.P. Araque^{136a}, V. Araujo Ferraz^{78b}, A.T.H. Arce⁴⁷, R.E. Ardell⁹¹, F.A. Arduh⁸⁶, J-F. Arguin¹⁰⁷, S. Argyropoulos⁷⁵, M. Arik^{12c}, A.J. Armbruster³⁵, L.J. Armitage⁹⁰, O. Arnaez¹⁶⁵, H. Arnold⁵⁰, M. Arratia³¹, O. Arslan²⁴, A. Artamonov^{109,*}, G. Artoni¹³¹, S. Artz⁹⁷, S. Asai¹⁶¹, N. Asbah⁴⁴, A. Ashkenazi¹⁵⁹, L. Asquith¹⁵³, K. Assamagan²⁹, R. Astalos^{28a}, M. Atkinson¹⁷¹, N.B. Atlay¹⁴⁸, K. Augsten¹³⁸, G. Avolio³⁵, B. Axen¹⁸, M.K. Ayoub¹²⁸, G. Azuelos^{107,au}, A.E. Baas^{59a}, M.J. Baca²¹, H. Bachacou¹⁴², K. Bachas^{65a,65b}, M. Backes¹³¹, M. Backhaus³⁵, P. Bagnaia^{70a,70b}, M. Bahmani⁸², H. Bahrasemani¹⁴⁹, J.T. Baines¹⁴¹, M. Bajic³⁹, O.K. Baker¹⁸¹, E.M. Baldin^{120b,120a}, P. Balek¹⁷⁸, F. Balli¹⁴², W.K. Balunas¹³³, E. Banas⁸², A. Bandyopadhyay²⁴, S. Banerjee^{179,1}, A.A.E. Bannoura¹⁸⁰, L. Barak³⁵, E.L. Barberio¹⁰², D. Barberis^{53b,53a}, M. Barbero⁹⁹, T. Barillari¹¹³, M-S. Barisits³⁵, J. Barkeloo¹²⁷, T. Barklow¹⁵⁰, N. Barlow³¹, S.L. Barnes^{58c}, B.M. Barnett¹⁴¹, R.M. Barnett¹⁸, Z. Barnovska-Blenessy^{58a}, A. Baroncelli^{72a}, G. Barone²⁶, A.J. Barr¹³¹, L. Barranco Navarro¹⁷², F. Barreiro⁹⁶, J. Barreiro Guimarães da Costa^{15a}, R. Bartoldus¹⁵⁰, A.E. Barton⁸⁷, P. Bartos^{28a}, A. Basalaev¹³⁴, A. Bassalat¹²⁸, R.L. Bates⁵⁵, S.J. Batista¹⁶⁵, J.R. Batley³¹, M. Battaglia¹⁴³, M. Bauce^{70a,70b}, F. Bauer¹⁴², H.S. Bawa^{150,m}, J.B. Beacham¹²², M.D. Beattie⁸⁷, T. Beau¹³², P.H. Beauchemin¹⁶⁸, P. Bechtle²⁴, H.C. Beck⁵¹, H.P. Beck^{20,r}, K. Becker¹³¹, M. Becker⁹⁷, M. Beckingham¹⁷⁶, C. Becot¹²¹, A. Beddall^{12d}, A.J. Beddall^{12a}, V.A. Bednyakov⁷⁷, M. Bedognetti¹¹⁸, C.P. Bee¹⁵², T.A. Beermann³⁵, M. Begalli^{78b}, M. Begel²⁹, J.K. Behr⁴⁴, A.S. Bell⁹², G. Bella¹⁵⁹, L. Bellagamba^{23b}, A. Bellerive³³, M. Bellomo¹⁵⁸, K. Belotskiy¹¹⁰, O. Beltramello³⁵, N.L. Belyaev¹¹⁰, O. Benary^{159,*}, D. Benchekroun^{34a}, M. Bender¹¹², K. Bendtz^{43a,43b}, N. Benekos¹⁰, Y. Benhammou¹⁵⁹, E. Benhar Noccioli¹⁸¹, J. Benitez⁷⁵, D.P. Benjamin⁴⁷, M. Benoit⁵², J.R. Bensinger²⁶, S. Bentvelsen¹¹⁸, L. Beresford¹³¹, M. Beretta⁴⁹, D. Berge¹¹⁸, E. Bergeaas Kuutmann¹⁷⁰, N. Berger⁵, J. Beringer¹⁸, S. Berlendis⁵⁶, N.R. Bernard¹⁰⁰, G. Bernardi¹³², C. Bernius¹⁵⁰, F.U. Bernlochner²⁴, T. Berry⁹¹, P. Berta¹³⁹, C. Bertella^{15a}, G. Bertoli^{43a,43b}, F. Bertolucci^{69a,69b}, I.A. Bertram⁸⁷, C. Bertsche⁴⁴, D. Bertsche¹²⁴, G.J. Besjes³⁹, O. Bessidskaia Bylund^{43a,43b}, M. Bessner⁴⁴, N. Besson¹⁴², C. Betancourt⁵⁰, A. Bethani⁹⁸, S. Bethke¹¹³, A.J. Bevan⁹⁰, J. Beyer¹¹³, R.M.B. Bianchi¹³⁵, O. Biebel¹¹², D. Biedermann¹⁹, R. Bielski⁹⁸, K. Bierwagen⁹⁷, N.V. Biesuz^{69a,69b}, M. Biglietti^{72a}, T.R.V. Billoud¹⁰⁷, H. Bilokon⁴⁹, M. Bindi⁵¹, A. Bingul^{12d}, C. Bini^{70a,70b}, S. Biondi^{23b,23a}, T. Bisanz⁵¹, C. Bittrich⁴⁶, D.M. Bjergaard⁴⁷, C.W. Black¹⁵⁴, J.E. Black¹⁵⁰, K.M. Black²⁵, R.E. Blair⁶, T. Blazek^{28a}, I. Bloch⁴⁴, C. Blocker²⁶, A. Blue⁵⁵, W. Blum^{97,*}, U. Blumenschein⁹⁰, Dr. Blunier^{144a}, G.J. Bobbink¹¹⁸,

V.S. Bobrovnikov^{120b,120a}, S.S. Bocchetta⁹⁴, A. Bocci⁴⁷, C. Bock¹¹², M. Boehler⁵⁰, D. Boerner¹⁸⁰,
 D. Bogavac¹¹², A.G. Bogdanchikov^{120b,120a}, C. Bohm^{43a}, V. Boisvert⁹¹, P. Bokan^{170,x}, T. Bold^{81a},
 A.S. Boldyrev¹¹¹, A.E. Bolz^{59b}, M. Bomben¹³², M. Bona⁹⁰, M. Boonekamp¹⁴², A. Borisov¹⁴⁰,
 G. Borissov⁸⁷, J. Bortfeldt³⁵, D. Bortoletto¹³¹, V. Bortolotto^{61a,61b,61c}, D. Boscherini^{23b}, M. Bosman¹⁴,
 J.D. Bossio Sola³⁰, J. Boudreau¹³⁵, J. Bouffard², E.V. Bouhova-Thacker⁸⁷, D. Boumediene³⁷,
 C. Bourdarios¹²⁸, S.K. Boutle⁵⁵, A. Boveia¹²², J. Boyd³⁵, I.R. Boyko⁷⁷, J. Bracinik²¹, A. Brandt⁸,
 G. Brandt⁵¹, O. Brandt^{59a}, U. Bratzler¹⁶², B. Brau¹⁰⁰, J.E. Brau¹²⁷, W.D. Breaden Madden⁵⁵,
 K. Brendlinger⁴⁴, A.J. Brennan¹⁰², L. Brenner¹¹⁸, R. Brenner¹⁷⁰, S. Bressler¹⁷⁸, D.L. Briglin²¹,
 T.M. Bristow⁴⁸, D. Britton⁵⁵, D. Britzger⁴⁴, I. Brock²⁴, R. Brock¹⁰⁴, G. Brooijmans³⁸, T. Brooks⁹¹,
 W.K. Brooks^{144b}, J. Brosamer¹⁸, E. Brost¹¹⁹, J.H. Broughton²¹, P.A. Bruckman de Renstrom⁸²,
 D. Bruncko^{28b}, A. Bruni^{23b}, G. Bruni^{23b}, L.S. Bruni¹¹⁸, B.H. Brunt³¹, M. Bruschi^{23b}, N. Bruscino²⁴,
 P. Bryant³⁶, L. Bryngemark⁴⁴, T. Buanes¹⁷, Q. Buat¹⁴⁹, P. Buchholz¹⁴⁸, A.G. Buckley⁵⁵, I.A. Budagov⁷⁷,
 F. Buehrer⁵⁰, M.K. Bugge¹³⁰, O. Bulekov¹¹⁰, D. Bullock⁸, T.J. Burch¹¹⁹, S. Burdin⁸⁸, C.D. Burgard⁵⁰,
 A.M. Burger⁵, B. Burghgrave¹¹⁹, K. Burka⁸², S. Burke¹⁴¹, I. Burmeister⁴⁵, J.T.P. Burr¹³¹, E. Busato³⁷,
 D. Büscher⁵⁰, V. Büscher⁹⁷, P. Bussey⁵⁵, J.M. Butler²⁵, C.M. Buttar⁵⁵, J.M. Butterworth⁹², P. Buttì³⁵,
 W. Buttinger²⁹, A. Buzatu^{15b}, A.R. Buzykaev^{120b,120a}, S. Cabrera Urbán¹⁷², D. Caforio¹³⁸,
 V.M.M. Cairo^{40b,40a}, O. Cakir^{4a}, N. Calace⁵², P. Calafiura¹⁸, A. Calandri⁹⁹, G. Calderini¹³²,
 P. Calfayan⁶³, G. Callea^{40b,40a}, L.P. Caloba^{78b}, S. Calvente Lopez⁹⁶, D. Calvet³⁷, S. Calvet³⁷,
 T.P. Calvet⁹⁹, R. Camacho Toro³⁶, S. Camarda³⁵, P. Camarri^{71a,71b}, D. Cameron¹³⁰,
 R. Caminal Armadans¹⁷¹, C. Camincher⁵⁶, S. Campana³⁵, M. Campanelli⁹², A. Camplani^{66a,66b},
 A. Campoverde¹⁴⁸, V. Canale^{67a,67b}, M. Cano Bret^{58c}, J. Cantero¹²⁵, T. Cao¹⁵⁹,
 M.D.M. Capeans Garrido³⁵, I. Caprini^{27b}, M. Caprini^{27b}, M. Capua^{40b,40a}, R.M. Carbone³⁸,
 R. Cardarelli^{71a}, F.C. Cardillo⁵⁰, I. Carli¹³⁹, T. Carli³⁵, G. Carlino^{67a}, B.T. Carlson¹³⁵,
 L. Carminati^{66a,66b}, R.M.D. Carney^{43a,43b}, S. Caron¹¹⁷, E. Carquin^{144b}, S. Carrá^{66a,66b},
 G.D. Carrillo-Montoya³⁵, J. Carvalho^{136a}, D. Casadei²¹, M.P. Casado^{14,g}, M. Casolino¹⁴,
 D.W. Casper¹⁶⁹, R. Castelijn¹¹⁸, V. Castillo Gimenez¹⁷², N.F. Castro^{136a}, A. Catinaccio³⁵,
 J.R. Catmore¹³⁰, A. Cattai³⁵, J. Caudron²⁴, V. Cavalieri¹⁷¹, E. Cavallaro¹⁴, D. Cavalli^{66a},
 M. Cavalli-Sforza¹⁴, V. Cavasinni^{69a,69b}, E. Celebi^{12b}, F. Ceradini^{72a,72b}, L. Cerdà Alberich¹⁷²,
 A.S. Cerqueira^{78a}, A. Cerri¹⁵³, L. Cerrito^{71a,71b}, F. Cerutti¹⁸, A. Cervelli²⁰, S.A. Cetin^{12b}, A. Chafaq^{34a},
 D Chakraborty¹¹⁹, S.K. Chan⁵⁷, W.S. Chan¹¹⁸, Y.L. Chan^{61a}, P. Chang¹⁷¹, J.D. Chapman³¹,
 D.G. Charlton²¹, C.C. Chau¹⁶⁵, C.A. Chavez Barajas¹⁵³, S. Che¹²², S. Cheatham^{64a,64c},
 A. Chegwidden¹⁰⁴, S. Chekanov⁶, S.V. Chekulaev^{166a}, G.A. Chelkov^{77,at}, M.A. Chelstowska³⁵,
 C.H. Chen⁷⁶, H. Chen²⁹, J. Chen^{58a}, S. Chen¹⁶¹, S.J. Chen^{15c}, X. Chen^{15b,as}, Y. Chen⁸⁰, H.C. Cheng¹⁰³,
 H.J. Cheng^{15d}, A. Cheplakov⁷⁷, E. Cheremushkina¹⁴⁰, R. Cherkaoui El Moursli^{34e}, E. Cheu⁷,
 K. Cheung⁶², L. Chevalier¹⁴², V. Chiarella⁴⁹, G. Chiarelli^{69a}, G. Chiodini^{65a}, A.S. Chisholm³⁵,
 A. Chitan^{27b}, Y.H. Chiu¹⁷⁴, M.V. Chizhov⁷⁷, K. Choi⁶³, A.R. Chomont³⁷, S. Chouridou¹⁶⁰,
 V. Christodoulou⁹², D. Chromek-Burckhart³⁵, M.C. Chu^{61a}, J. Chudoba¹³⁷, A.J. Chuinard¹⁰¹,
 J.J. Chwastowski⁸², L. Chytka¹²⁶, A.K. Ciftci^{4a}, D. Cinca⁴⁵, V. Cindro⁸⁹, I.A. Cioara²⁴, C. Cioce^{23b,23a},
 A. Ciocio¹⁸, F. Cirotto^{67a,67b}, Z.H. Citron¹⁷⁸, M. Citterio^{66a}, M. Ciubancan^{27b}, A. Clark⁵², B.L. Clark⁵⁷,
 M.R. Clark³⁸, P.J. Clark⁴⁸, R.N. Clarke¹⁸, C. Clement^{43a,43b}, Y. Coadou⁹⁹, M. Cobal^{64a,64c},
 A. Coccaro⁵², J. Cochran⁷⁶, L. Colasurdo¹¹⁷, B. Cole³⁸, A.P. Colijn¹¹⁸, J. Collot⁵⁶, T. Colombo¹⁶⁹,
 P. Conde Muiño^{136a,136b}, E. Coniavitis⁵⁰, S.H. Connell^{32b}, I.A. Connolly⁹⁸, S. Constantinescu^{27b},
 G. Conti³⁵, F. Conventi^{67a,av}, M. Cooke¹⁸, A.M. Cooper-Sarkar¹³¹, F. Cormier¹⁷³, K.J.R. Cormier¹⁶⁵,
 M. Corradi^{70a,70b}, F. Corriveau^{101,ae}, A. Cortes-Gonzalez³⁵, G. Cortiana¹¹³, G. Costa^{66a}, M.J. Costa¹⁷²,
 D. Costanzo¹⁴⁶, G. Cottin³¹, G. Cowan⁹¹, B.E. Cox⁹⁸, K. Cranmer¹²¹, S.J. Crawley⁵⁵, R.A. Creager¹³³,
 G. Cree³³, S. Crépé-Renaudin⁵⁶, F. Crescioli¹³², W.A. Cribbs^{43a,43b}, M. Cristinziani²⁴, V. Croft¹¹⁷,
 G. Crosetti^{40b,40a}, A. Cueto⁹⁶, T. Cuhadar Donszelmann¹⁴⁶, A.R. Cukierman¹⁵⁰, J. Cummings¹⁸¹,

M. Curatolo⁴⁹, J. Cúth⁹⁷, P. Czodrowski³⁵, M.J. Da Cunha Sargedas De Sousa^{136a,136b}, C. Da Via⁹⁸,
 W. Dabrowski^{81a}, T. Dado^{28a,x}, T. Dai¹⁰³, O. Dale¹⁷, F. Dallaire¹⁰⁷, C. Dallapiccola¹⁰⁰, M. Dam³⁹,
 G. D'amen^{23b,23a}, J.R. Dandoy¹³³, M.F. Daneri³⁰, N.P. Dang^{179,1}, A.C. Daniells²¹, N.D Dann⁹⁸,
 M. Danninger¹⁷³, M. Dano Hoffmann¹⁴², V. Dao¹⁵², G. Darbo^{53b}, S. Darmora⁸, J. Dassoulas³,
 A. Dattagupta¹²⁷, T. Daubney⁴⁴, S. D'Auria⁵⁵, W. Davey²⁴, C. David⁴⁴, T. Davidek¹³⁹, D.R. Davis⁴⁷,
 P. Davison⁹², E. Dawe¹⁰², I. Dawson¹⁴⁶, K. De⁸, R. De Asmundis^{67a}, A. De Benedetti¹²⁴,
 S. De Castro^{23b,23a}, S. De Cecco¹³², N. De Groot¹¹⁷, P. de Jong¹¹⁸, H. De la Torre¹⁰⁴, F. De Lorenzi⁷⁶,
 A. De Maria^{51,t}, D. De Pedis^{70a}, A. De Salvo^{70a}, U. De Sanctis^{71a,71b}, A. De Santo¹⁵³,
 K. De Vasconcelos Corga⁹⁹, J.B. De Vie De Regie¹²⁸, W.J. Dearnaley⁸⁷, R. Debbe²⁹,
 C. Debenedetti¹⁴³, D.V. Dedovich⁷⁷, N. Dehghanian³, I. Deigaard¹¹⁸, M. Del Gaudio^{40b,40a},
 J. Del Peso⁹⁶, D. Delgove¹²⁸, F. Deliot¹⁴², C.M. Delitzsch⁵², M. Della Pietra^{67a,67b}, D. Della Volpe⁵²,
 A. Dell'Acqua³⁵, L. Dell'Asta²⁵, M. Dell'Orso^{69a,69b}, M. Delmastro⁵, C. Delporte¹²⁸, P.A. Delsart⁵⁶,
 D.A. DeMarco¹⁶⁵, S. Demers¹⁸¹, M. Demichev⁷⁷, A. Demilly¹³², S.P. Denisov¹⁴⁰, D. Denysiuk¹⁴²,
 L. D'Eramo¹³², D. Derendarz⁸², J.E. Derkaoui^{34d}, F. Derue¹³², P. Dervan⁸⁸, K. Desch²⁴, C. Deterre⁴⁴,
 K. Dette⁴⁵, M.R. Devesa³⁰, P.O. Deviveiros³⁵, A. Dewhurst¹⁴¹, S. Dhaliwal²⁶, F.A. Di Bello⁵²,
 A. Di Ciaccio^{71a,71b}, L. Di Ciaccio⁵, W.K. Di Clemente¹³³, C. Di Donato^{67a,67b}, A. Di Girolamo³⁵,
 B. Di Girolamo³⁵, B. Di Micco^{72a,72b}, R. Di Nardo³⁵, K.F. Di Petrillo⁵⁷, A. Di Simone⁵⁰, R. Di Sipio¹⁶⁵,
 D. Di Valentino³³, C. Diaconu⁹⁹, M. Diamond¹⁶⁵, F.A. Dias³⁹, M.A. Diaz^{144a}, E.B. Diehl¹⁰³,
 J. Dietrich¹⁹, S. Díez Cornell⁴⁴, A. Dimitrievska¹⁶, J. Dingfelder²⁴, P. Dita^{27b}, S. Dita^{27b}, F. Dittus³⁵,
 F. Djama⁹⁹, T. Djobava^{157b}, J.I. Djuvsland^{59a}, M.A.B. Do Vale^{78c}, D. Dobos³⁵, M. Dobre^{27b},
 C. Doglioni⁹⁴, J. Dolejsi¹³⁹, Z. Dolezal¹³⁹, M. Donadelli^{78d}, S. Donati^{69a,69b}, P. Dondero^{68a,68b},
 J. Donini³⁷, M. D'Onofrio⁸⁸, J. Dopke¹⁴¹, A. Doria^{67a}, M.T. Dova⁸⁶, A.T. Doyle⁵⁵, E. Drechsler⁵¹,
 M. Dris¹⁰, Y. Du^{58b}, J. Duarte-Campderros¹⁵⁹, A. Dubreuil⁵², E. Duchovni¹⁷⁸, G. Duckeck¹¹²,
 A. Ducourthial¹³², O.A. Ducu^{107,w}, D. Duda¹¹⁸, A. Dudarev³⁵, A.C. Dudder⁹⁷, E.M. Duffield¹⁸,
 L. Duflot¹²⁸, M. Dührssen³⁵, M. Dumancic¹⁷⁸, A.E. Dumitriu^{27b,e}, A.K. Duncan⁵⁵, M. Dunford^{59a},
 H. Duran Yildiz^{4a}, M. Düren⁵⁴, A. Durglishvili^{157b}, D. Duschinger⁴⁶, B. Dutta⁴⁴, D. Duvnjak¹,
 M. Dyndal⁴⁴, B.S. Dziedzic⁸², C. Eckardt⁴⁴, K.M. Ecker¹¹³, R.C. Edgar¹⁰³, T. Eifert³⁵, G. Eigen¹⁷,
 K. Einsweiler¹⁸, T. Ekelof¹⁷⁰, M. El Kacimi^{34c}, R. El Kosseifi⁹⁹, V. Ellajosyula⁹⁹, M. Ellert¹⁷⁰, S. Elles⁵,
 F. Ellinghaus¹⁸⁰, A.A. Elliot¹⁷⁴, N. Ellis³⁵, J. Elmsheuser²⁹, M. Elsing³⁵, D. Emeliyanov¹⁴¹, Y. Enari¹⁶¹,
 O.C. Endner⁹⁷, J.S. Ennis¹⁷⁶, J. Erdmann⁴⁵, A. Ereditato²⁰, M. Ernst²⁹, S. Errede¹⁷¹, M. Escalier¹²⁸,
 C. Escobar¹⁷², B. Esposito⁴⁹, O. Estrada Pastor¹⁷², A.I. Etienvre¹⁴², E. Etzion¹⁵⁹, H. Evans⁶³,
 A. Ezhilov¹³⁴, M. Ezzi^{34e}, F. Fabbri^{23b,23a}, L. Fabbri^{23b,23a}, V. Fabiani¹¹⁷, G. Facini⁹²,
 R.M. Fakhrutdinov¹⁴⁰, S. Falciano^{70a}, R.J. Falla⁹², J. Faltova³⁵, Y. Fang^{15a}, M. Fanti^{66a,66b}, A. Farbin⁸,
 A. Farilla^{72a}, C. Farina¹³⁵, E.M. Farina^{68a,68b}, T. Farooque¹⁰⁴, S. Farrell¹⁸, S.M. Farrington¹⁷⁶,
 P. Farthouat³⁵, F. Fassi^{34e}, P. Fassnacht³⁵, D. Fassouliotis⁹, M. Faucci Giannelli⁹¹, A. Favareto^{53b,53a},
 W.J. Fawcett¹³¹, L. Fayard¹²⁸, O.L. Fedin^{134,q}, W. Fedorko¹⁷³, S. Feigl¹³⁰, L. Feligioni⁹⁹, C. Feng^{58b},
 E.J. Feng³⁵, H. Feng¹⁰³, M.J. Fenton⁵⁵, A.B. Fenyuk¹⁴⁰, L. Feremenga⁸, P. Fernandez Martinez¹⁷²,
 S. Fernandez Perez¹⁴, J. Ferrando⁴⁴, A. Ferrari¹⁷⁰, P. Ferrari¹¹⁸, R. Ferrari^{68a}, D.E. Ferreira de Lima^{59b},
 A. Ferrer¹⁷², D. Ferrere⁵², C. Ferretti¹⁰³, F. Fiedler⁹⁷, M. Filipuzzi⁴⁴, A. Filipčič⁸⁹, F. Filthaut¹¹⁷,
 M. Fincke-Keeler¹⁷⁴, K.D. Finelli¹⁵⁴, M.C.N. Fiolhais^{136a,136c,b}, L. Fiorini¹⁷², A. Fischer², C. Fischer¹⁴,
 J. Fischer¹⁸⁰, W.C. Fisher¹⁰⁴, N. Flaschel⁴⁴, I. Fleck¹⁴⁸, P. Fleischmann¹⁰³, R.R.M. Fletcher¹³³,
 T. Flick¹⁸⁰, B.M. Flierl¹¹², L.R. Flores Castillo^{61a}, M.J. Flowerdew¹¹³, G.T. Forcolin⁹⁸, A. Formica¹⁴²,
 F.A. Förster¹⁴, A.C. Forti⁹⁸, A.G. Foster²¹, D. Fournier¹²⁸, H. Fox⁸⁷, S. Fracchia¹⁴⁶, P. Francavilla¹³²,
 M. Franchini^{23b,23a}, S. Franchino^{59a}, D. Francis³⁵, L. Franconi¹³⁰, M. Franklin⁵⁷, M. Frate¹⁶⁹,
 M. Fraternali^{68a,68b}, D. Freeborn⁹², S.M. Fressard-Batraneanu³⁵, B. Freund¹⁰⁷, D. Froidevaux³⁵,
 J.A. Frost¹³¹, C. Fukunaga¹⁶², T. Fusayasu¹¹⁴, J. Fuster¹⁷², C. Gabaldon⁵⁶, O. Gabizon¹⁵⁸,
 A. Gabrielli^{23b,23a}, A. Gabrielli¹⁸, G.P. Gach^{81a}, S. Gadatsch³⁵, S. Gadomski⁵², G. Gagliardi^{53b,53a},

L.G. Gagnon¹⁰⁷, C. Galea¹¹⁷, B. Galhardo^{136a,136c}, E.J. Gallas¹³¹, B.J. Gallop¹⁴¹, P. Gallus¹³⁸,
 G. Galster³⁹, K.K. Gan¹²², S. Ganguly³⁷, Y. Gao⁸⁸, Y.S. Gao^{150,m}, C. García¹⁷², J.E. García Navarro¹⁷²,
 J.A. García Pascual^{15a}, M. Garcia-Sciveres¹⁸, R.W. Gardner³⁶, N. Garelli¹⁵⁰, V. Garonne¹³⁰,
 A. Gascon Bravo⁴⁴, K. Gasnikova⁴⁴, C. Gatti⁴⁹, A. Gaudiello^{53b,53a}, G. Gaudio^{68a}, I.L. Gavrilenko¹⁰⁸,
 C. Gay¹⁷³, G. Gaycken²⁴, E.N. Gazis¹⁰, C.N.P. Gee¹⁴¹, J. Geisen⁵¹, M. Geisen⁹⁷, M.P. Geisler^{59a},
 K. Gellerstedt^{43a,43b}, C. Gemme^{53b}, M.H. Genest⁵⁶, C. Geng¹⁰³, S. Gentile^{70a,70b}, C. Gentsos¹⁶⁰,
 S. George⁹¹, D. Gerbaudo¹⁴, A. Gershon¹⁵⁹, G. Gessner⁴⁵, S. Ghasemi¹⁴⁸, M. Ghneimat²⁴,
 B. Giacobbe^{23b}, S. Giagu^{70a,70b}, N. Giangiocomi^{23b,23a}, P. Giannetti^{69a}, S.M. Gibson⁹¹, M. Gignac¹⁷³,
 M. Gilchriese¹⁸, D. Gillberg³³, G. Gilles¹⁸⁰, D.M. Gingrich^{3,au}, N. Giokaris^{9,*}, M.P. Giordani^{64a,64c},
 F.M. Giorgi^{23b}, P.F. Giraud¹⁴², P. Giromini⁵⁷, G. Giugliarelli^{64a,64c}, D. Giugni^{66a}, F. Giulì¹³¹,
 C. Giuliani¹¹³, M. Giulini^{59b}, B.K. Gjelsten¹³⁰, S. Gkaitatzis¹⁶⁰, I. Gkialas^{9,k}, E.L. Gkougkousis¹⁴³,
 P. Gkountoumis¹⁰, L.K. Gladilin¹¹¹, C. Glasman⁹⁶, J. Glatzer¹⁴, P.C.F. Glaysher⁴⁴, A. Glazov⁴⁴,
 M. Goblirsch-Kolb²⁶, J. Godlewski⁸², S. Goldfarb¹⁰², T. Golling⁵², D. Golubkov¹⁴⁰,
 A. Gomes^{136a,136b,136d}, R. Goncalves Gama^{78b}, J. Goncalves Pinto Firmino Da Costa¹⁴², R. Gonçalo^{136a},
 G. Gonella⁵⁰, L. Gonella²¹, A. Gongadze⁷⁷, S. González de la Hoz¹⁷², S. Gonzalez-Sevilla⁵²,
 L. Goossens³⁵, P.A. Gorbounov¹⁰⁹, H.A. Gordon²⁹, I. Gorelov¹¹⁶, B. Gorini³⁵, E. Gorini^{65a,65b},
 A. Gorišek⁸⁹, A.T. Goshaw⁴⁷, C. Gössling⁴⁵, M.I. Gostkin⁷⁷, C.A. Gottardo²⁴, C.R. Goudet¹²⁸,
 D. Goujdami^{34c}, A.G. Goussiou¹⁴⁵, N. Govender^{32b,c}, E. Gozani¹⁵⁸, L. Graber⁵¹, I. Grabowska-Bold^{81a},
 P.O.J. Gradin¹⁷⁰, J. Gramling¹⁶⁹, E. Gramstad¹³⁰, S. Grancagnolo¹⁹, V. Gratchev¹³⁴, P.M. Gravila^{27f},
 C. Gray⁵⁵, H.M. Gray¹⁸, Z.D. Greenwood^{93,aj}, C. Grefe²⁴, K. Gregersen⁹², I.M. Gregor⁴⁴, P. Grenier¹⁵⁰,
 K. Grevtsov⁵, J. Griffiths⁸, A.A. Grillo¹⁴³, K. Grimm⁸⁷, S. Grinstein^{14,y}, Ph. Gris³⁷, J.-F. Grivaz¹²⁸,
 S. Groh⁹⁷, E. Gross¹⁷⁸, J. Grosse-Knetter⁵¹, G.C. Grossi⁹³, Z.J. Grout⁹², A. Grummer¹¹⁶, L. Guan¹⁰³,
 W. Guan¹⁷⁹, J. Guenther⁷⁴, F. Guescini^{166a}, D. Guest¹⁶⁹, O. Gueta¹⁵⁹, B. Gui¹²², E. Guido^{53b,53a},
 T. Guillemin⁵, S. Guindon², U. Gul⁵⁵, C. Gumpert³⁵, J. Guo^{58c}, W. Guo¹⁰³, Y. Guo^{58a,s}, R. Gupta⁴¹,
 S. Gupta¹³¹, G. Gustavino^{70a,70b}, P. Gutierrez¹²⁴, N.G. Gutierrez Ortiz⁹², C. Gutschow⁹², C. Guyot¹⁴²,
 M.P. Guzik^{81a}, C. Gwenlan¹³¹, C.B. Gwilliam⁸⁸, A. Haas¹²¹, C. Haber¹⁸, H.K. Hadavand⁸,
 N. Haddad^{34e}, A. Hadef⁹⁹, S. Hageböck²⁴, M. Hagihara¹⁶⁷, H. Hakobyan^{182,*}, M. Haleem⁴⁴, J. Haley¹²⁵,
 G. Halladjian¹⁰⁴, G.D. Hallewell⁹⁹, K. Hamacher¹⁸⁰, P. Hamal¹²⁶, K. Hamano¹⁷⁴, A. Hamilton^{32a},
 G.N. Hamity¹⁴⁶, P.G. Hamnett⁴⁴, L. Han^{58a}, S. Han^{15d}, K. Hanagaki^{79,v}, K. Hanawa¹⁶¹, M. Hance¹⁴³,
 B. Haney¹³³, P. Hanke^{59a}, J.B. Hansen³⁹, J.D. Hansen³⁹, M.C. Hansen²⁴, P.H. Hansen³⁹, K. Hara¹⁶⁷,
 A.S. Hard¹⁷⁹, T. Harenberg¹⁸⁰, F. Hariri¹²⁸, S. Harkusha¹⁰⁵, R.D. Harrington⁴⁸, P.F. Harrison¹⁷⁶,
 N.M. Hartmann¹¹², M. Hasegawa⁸⁰, Y. Hasegawa¹⁴⁷, A. Hasib⁴⁸, S. Hassani¹⁴², S. Haug²⁰,
 R. Hauser¹⁰⁴, L. Hauswald⁴⁶, L.B. Havener³⁸, M. Havranek¹³⁸, C.M. Hawkes²¹, R.J. Hawkings³⁵,
 D. Hayakawa¹⁶³, D. Hayden¹⁰⁴, C.P. Hays¹³¹, J.M. Hays⁹⁰, H.S. Hayward⁸⁸, S.J. Haywood¹⁴¹,
 S.J. Head²¹, T. Heck⁹⁷, V. Hedberg⁹⁴, L. Heelan⁸, S. Heer²⁴, K.K. Heidegger⁵⁰, S. Heim⁴⁴, T. Heim¹⁸,
 B. Heinemann^{44,ap}, J.J. Heinrich¹¹², L. Heinrich¹²¹, C. Heinz⁵⁴, J. Hejbal¹³⁷, L. Helary³⁵, A. Held¹⁷³,
 S. Hellman^{43a,43b}, C. Helsens³⁵, R.C.W. Henderson⁸⁷, Y. Heng¹⁷⁹, S. Henkelmann¹⁷³,
 A.M. Henriques Correia³⁵, S. Henrot-Versille¹²⁸, G.H. Herbert¹⁹, H. Herde²⁶, V. Herget¹⁷⁵,
 Y. Hernández Jiménez^{32c}, H. Herr⁹⁷, G. Herten⁵⁰, R. Hertenberger¹¹², L. Hervas³⁵, T.C. Herwig¹³³,
 G.G. Hesketh⁹², N.P. Hessey^{166a}, J.W. Hetherly⁴¹, S. Higashino⁷⁹, E. Higón-Rodriguez¹⁷²,
 K. Hildebrand³⁶, E. Hill¹⁷⁴, J.C. Hill³¹, K.H. Hiller⁴⁴, S.J. Hillier²¹, M. Hils⁴⁶, I. Hinchliffe¹⁸,
 M. Hirose⁵⁰, D. Hirschbuehl¹⁸⁰, B. Hiti⁸⁹, O. Hladík¹³⁷, X. Hoad⁴⁸, J. Hobbs¹⁵², N. Hod^{166a},
 M.C. Hodgkinson¹⁴⁶, P. Hodgson¹⁴⁶, A. Hoecker³⁵, M.R. Hoeferkamp¹¹⁶, F. Hoenig¹¹², D. Hohn²⁴,
 T.R. Holmes³⁶, M. Homann⁴⁵, S. Honda¹⁶⁷, T. Honda⁷⁹, T.M. Hong¹³⁵, B.H. Hooberman¹⁷¹,
 W.H. Hopkins¹²⁷, Y. Horii¹¹⁵, A.J. Horton¹⁴⁹, J.-Y. Hostachy⁵⁶, S. Hou¹⁵⁵, A. Hoummada^{34a},
 J. Howarth⁹⁸, J. Hoya⁸⁶, M. Hrabovsky¹²⁶, J. Hrdinka³⁵, I. Hristova¹⁹, J. Hrivnac¹²⁸, A. Hrynevich¹⁰⁶,
 T. Hrynn'ova⁵, P.J. Hsu⁶², S.-C. Hsu¹⁴⁵, Q. Hu^{58a}, S. Hu^{58c}, Y. Huang^{15a}, Z. Hubacek¹³⁸, F. Hubaut⁹⁹,

F. Huegging²⁴, T.B. Huffman¹³¹, E.W. Hughes³⁸, G. Hughes⁸⁷, M. Huhtinen³⁵, P. Huo¹⁵²,
 N. Huseynov^{77,ag}, J. Huston¹⁰⁴, J. Huth⁵⁷, G. Iacobucci⁵², G. Iakovidis²⁹, I. Ibragimov¹⁴⁸,
 L. Iconomidou-Fayard¹²⁸, Z. Idrissi^{34e}, P. Iengo³⁵, O. Igonkina^{118,ab}, T. Iizawa¹⁷⁷, Y. Ikegami⁷⁹,
 M. Ikeno⁷⁹, Y. Ilchenko¹¹, D. Iliadis¹⁶⁰, N. Ilic¹⁵⁰, G. Introzzi^{68a,68b}, P. Ioannou^{9,*}, M. Iodice^{72a},
 K. Iordanidou³⁸, V. Ippolito⁵⁷, M.F. Isacson¹⁷⁰, N. Ishijima¹²⁹, M. Ishino¹⁶¹, M. Ishitsuka¹⁶³,
 C. Issever¹³¹, S. Isti^{12c}, F. Ito¹⁶⁷, J.M. Iturbe Ponce^{61a}, R. Iuppa^{73a,73b}, H. Iwasaki⁷⁹, J.M. Izen⁴²,
 V. Izzo^{67a}, S. Jabbar³, P. Jackson¹, R.M. Jacobs²⁴, V. Jain², K.B. Jakobi⁹⁷, K. Jakobs⁵⁰, S. Jakobsen⁷⁴,
 T. Jakoubek¹³⁷, D.O. Jamin¹²⁵, D.K. Jana⁹³, R. Jansky⁵², J. Janssen²⁴, M. Janus⁵¹, P.A. Janus^{81a},
 G. Jarlskog⁹⁴, N. Javadov^{77,ag}, T. Javurek⁵⁰, M. Javurkova⁵⁰, F. Jeanneau¹⁴², L. Jeanty¹⁸,
 J. Jejelava^{157a,ah}, A. Jelinskas¹⁷⁶, P. Jenni^{50,d}, C. Jeske¹⁷⁶, S. Jézéquel⁵, H. Ji¹⁷⁹, J. Jia¹⁵², H. Jiang⁷⁶,
 Y. Jiang^{58a}, Z. Jiang¹⁵⁰, S. Jiggins⁹², J. Jimenez Pena¹⁷², S. Jin^{15a}, A. Jinaru^{27b}, O. Jinnouchi¹⁶³,
 H. Jivan^{32c}, P. Johansson¹⁴⁶, K.A. Johns⁷, C.A. Johnson⁶³, W.J. Johnson¹⁴⁵, K. Jon-And^{43a,43b},
 R.W.L. Jones⁸⁷, S.D. Jones¹⁵³, S. Jones⁷, T.J. Jones⁸⁸, J. Jongmanns^{59a}, P.M. Jorge^{136a,136b},
 J. Jovicevic^{166a}, X. Ju¹⁷⁹, A. Juste Rozas^{14,y}, A. Kaczmarska⁸², M. Kado¹²⁸, H. Kagan¹²², M. Kagan¹⁵⁰,
 S.J. Kahn⁹⁹, T. Kaji¹⁷⁷, E. Kajomovitz⁴⁷, C.W. Kalderon⁹⁴, A. Kaluza⁹⁷, S. Kama⁴¹,
 A. Kamenshchikov¹⁴⁰, N. Kanaya¹⁶¹, L. Kanjir⁸⁹, V.A. Kantserov¹¹⁰, J. Kanzaki⁷⁹, B. Kaplan¹²¹,
 L.S. Kaplan¹⁷⁹, D. Kar^{32c}, K. Karakostas¹⁰, N. Karastathis¹⁰, M.J. Kareem⁵¹, E. Karentzos¹⁰,
 S.N. Karpov⁷⁷, Z.M. Karpova⁷⁷, K. Karthik¹²¹, V. Kartvelishvili⁸⁷, A.N. Karyukhin¹⁴⁰, K. Kasahara¹⁶⁷,
 L. Kashif¹⁷⁹, R.D. Kass¹²², A. Kastanas¹⁵¹, Y. Kataoka¹⁶¹, C. Kato¹⁶¹, A. Katre⁵², J. Katzy⁴⁴,
 K. Kawade⁸⁰, K. Kawagoe⁸⁵, T. Kawamoto¹⁶¹, G. Kawamura⁵¹, E.F. Kay⁸⁸, V.F. Kazanin^{120b,120a},
 R. Keeler¹⁷⁴, R. Kehoe⁴¹, J.S. Keller³³, J.J. Kempster⁹¹, J. Kendrick²¹, H. Keoshkerian¹⁶⁵, O. Kepka¹³⁷,
 S. Kersten¹⁸⁰, B.P. Kerševan⁸⁹, R.A. Keyes¹⁰¹, M. Khader¹⁷¹, F. Khalil-Zada¹³, A. Khanov¹²⁵,
 A.G. Kharlamov^{120b,120a}, T. Kharlamova^{120b,120a}, A. Khodinov¹⁶⁴, T.J. Khoo⁵², V. Khovanskiy^{109,*},
 E. Khramov⁷⁷, J. Khubua^{157b}, S. Kido⁸⁰, C.R. Kilby⁹¹, H.Y. Kim⁸, S.H. Kim¹⁶⁷, Y.K. Kim³⁶,
 N. Kimura¹⁶⁰, O.M. Kind¹⁹, B.T. King⁸⁸, D. Kirchmeier⁴⁶, J. Kirk¹⁴¹, A.E. Kiryunin¹¹³,
 T. Kishimoto¹⁶¹, D. Kisielewska^{81a}, V. Kitali⁴⁴, K. Kiuchi¹⁶⁷, O. Kivernyk⁵, E. Kladiva^{28b},
 T. Klapdor-Kleingrothaus⁵⁰, M.H. Klein¹⁰³, M. Klein⁸⁸, U. Klein⁸⁸, K. Kleinknecht⁹⁷, P. Klimek¹¹⁹,
 A. Klimentov²⁹, R. Klingenberg^{45,*}, T. Klingl²⁴, T. Klioutchnikova³⁵, P. Kluit¹¹⁸, S. Kluth¹¹³,
 E. Kneringer⁷⁴, E.B.F.G. Knoops⁹⁹, A. Knue¹¹³, A. Kobayashi¹⁶¹, D. Kobayashi¹⁶³, T. Kobayashi¹⁶¹,
 M. Kobel⁴⁶, M. Kocian¹⁵⁰, P. Kodys¹³⁹, T. Koffas³³, E. Koffeman¹¹⁸, M.K. Köhler¹⁷⁸, N.M. Köhler¹¹³,
 T. Koi¹⁵⁰, M. Kolb^{59b}, I. Koletsou⁵, A.A. Komar^{108,*}, Y. Komori¹⁶¹, T. Kondo⁷⁹, N. Kondrashova^{58c},
 K. Köneke⁵⁰, A.C. König¹¹⁷, T. Kono^{79,ao}, R. Konoplich^{121,ak}, N. Konstantinidis⁹², R. Kopeliansky⁶³,
 S. Koperny^{81a}, A.K. Kopp⁵⁰, K. Korcyl⁸², K. Kordas¹⁶⁰, A. Korn⁹², A.A. Korol^{120b,120a,an}, I. Korolkov¹⁴,
 E.V. Korolkova¹⁴⁶, O. Kortner¹¹³, S. Kortner¹¹³, T. Kosek¹³⁹, V.V. Kostyukhin²⁴, A. Kotwal⁴⁷,
 A. Koulouris¹⁰, A. Kourkoumeli-Charalampidi^{68a,68b}, C. Kourkoumelis⁹, E. Kourlitis¹⁴⁶,
 V. Kouskoura²⁹, A.B. Kowalewska⁸², R. Kowalewski¹⁷⁴, T.Z. Kowalski^{81a}, C. Kozakai¹⁶¹,
 W. Kozanecki¹⁴², A.S. Kozhin¹⁴⁰, V.A. Kramarenko¹¹¹, G. Kramberger⁸⁹, D. Krasnopevtsev¹¹⁰,
 M.W. Krasny¹³², A. Krasznahorkay³⁵, D. Krauss¹¹³, J.A. Kremer^{81a}, J. Kretschmar⁸⁸, K. Kreutzfeldt⁵⁴,
 P. Krieger¹⁶⁵, K. Krizka³⁶, K. Kroeninger⁴⁵, H. Kroha¹¹³, J. Kroll¹³⁷, J. Kroll¹³³, J. Kroseberg²⁴,
 J. Krstic¹⁶, U. Kruchonak⁷⁷, H. Krüger²⁴, N. Krumnack⁷⁶, M.C. Kruse⁴⁷, T. Kubota¹⁰², H. Kucuk⁹²,
 S. Kuday^{4b}, J.T. Kuechler¹⁸⁰, S. Kuehn³⁵, A. Kugel^{59a}, F. Kuger¹⁷⁵, T. Kuhl⁴⁴, V. Kukhtin⁷⁷, R. Kukla⁹⁹,
 Y. Kulchitsky¹⁰⁵, S. Kuleshov^{144b}, Y.P. Kulinich¹⁷¹, M. Kuna^{70a,70b}, T. Kunigo⁸³, A. Kupco¹³⁷,
 T. Kupfer⁴⁵, O. Kuprash¹⁵⁹, H. Kurashige⁸⁰, L.L. Kurchaninov^{166a}, Y.A. Kurochkin¹⁰⁵, M.G. Kurth^{15d},
 V. Kus¹³⁷, E.S. Kuwertz¹⁷⁴, M. Kuze¹⁶³, J. Kvita¹²⁶, T. Kwan¹⁷⁴, D. Kyriazopoulos¹⁴⁶, A. La Rosa¹¹³,
 J.L. La Rosa Navarro^{78d}, L. La Rotonda^{40b,40a}, F. La Ruffa^{40b,40a}, C. Lacasta¹⁷², F. Lacava^{70a,70b},
 J. Lacey⁴⁴, H. Lacker¹⁹, D. Lacour¹³², E. Ladygin⁷⁷, R. Lafaye⁵, B. Laforge¹³², S. Lai⁵¹, S. Lammers⁶³,
 W. Lampl⁷, E. Lançon²⁹, U. Landgraf⁵⁰, M.P.J. Landon⁹⁰, M.C. Lanfermann⁵², V.S. Lang^{59a},

J.C. Lange¹⁴, R.J. Langenberg³⁵, A.J. Lankford¹⁶⁹, F. Lanni²⁹, K. Lantzsch²⁴, A. Lanza^{68a},
 A. Lapertosa^{53b,53a}, S. Laplace¹³², J.F. Laporte¹⁴², T. Lari^{66a}, F. Lasagni Manghi^{23b,23a}, M. Lassnig³⁵,
 P. Laurelli⁴⁹, W. Lavrijzen¹⁸, A.T. Law¹⁴³, P. Laycock⁸⁸, T. Lazovich⁵⁷, M. Lazzaroni^{66a,66b}, B. Le¹⁰²,
 O. Le Dertz¹³², E. Le Guirriec⁹⁹, E.P. Le Quillec¹⁴², M. LeBlanc¹⁷⁴, T. LeCompte⁶,
 F. Ledroit-Guillon⁵⁶, C.A. Lee²⁹, G.R. Lee^{141,i}, L. Lee⁵⁷, S.C. Lee¹⁵⁵, B. Lefebvre¹⁰¹, G. Lefebvre¹³²,
 M. Lefebvre¹⁷⁴, F. Legger¹¹², C. Leggett¹⁸, G. Lehmann Miotto³⁵, X. Lei⁷, W.A. Leight⁴⁴,
 M.A.L. Leite^{78d}, R. Leitner¹³⁹, D. Lellouch¹⁷⁸, B. Lemmer⁵¹, K.J.C. Leney⁹², T. Lenz²⁴, B. Lenzi³⁵,
 R. Leone⁷, S. Leone^{69a}, C. Leonidopoulos⁴⁸, G. Lerner¹⁵³, C. Leroy¹⁰⁷, A.A.J. Lesage¹⁴², C.G. Lester³¹,
 M. Levchenko¹³⁴, J. Levêque⁵, D. Levin¹⁰³, L.J. Levinson¹⁷⁸, M. Levy²¹, D. Lewis⁹⁰, B. Li^{58a,s},
 C-Q. Li^{58a}, H. Li¹⁵², L. Li^{58c}, Q. Li^{15d}, S. Li⁴⁷, X. Li^{58c}, Y. Li¹⁴⁸, Z. Liang^{15a}, B. Liberti^{71a},
 A. Liblong¹⁶⁵, K. Lie^{61c}, J. Liebal²⁴, W. Liebig¹⁷, A. Limosani¹⁵⁴, S.C. Lin¹⁵⁶, T.H. Lin⁹⁷, R.A. Linck⁶³,
 B.E. Lindquist¹⁵², A.L. Lionti⁵², E. Lipeles¹³³, A. Lipniacka¹⁷, M. Lisovyi^{59b}, T.M. Liss^{171,ar},
 A. Lister¹⁷³, A.M. Litke¹⁴³, B. Liu^{155,ad}, H.B. Liu²⁹, H. Liu¹⁰³, J.B. Liu^{58a}, J.K.K. Liu¹³¹, J. Liu^{58b},
 K. Liu⁹⁹, L. Liu¹⁷¹, M. Liu^{58a}, Y.L. Liu^{58a}, Y.W. Liu^{58a}, M. Livan^{68a,68b}, A. Lleres⁵⁶,
 J. Llorente Merino^{15a}, S.L. Lloyd⁹⁰, C.Y. Lo^{61b}, F. Lo Sterzo¹⁵⁵, E.M. Lobodzinska⁴⁴, P. Loch⁷,
 F.K. Loebinger⁹⁸, A. Loesle⁵⁰, K.M. Loew²⁶, A. Loginov^{181,*}, T. Lohse¹⁹, K. Lohwasser¹⁴⁶,
 M. Lokajicek¹³⁷, B.A. Long²⁵, J.D. Long¹⁷¹, R.E. Long⁸⁷, L. Longo^{65a,65b}, K.A.Looper¹²²,
 J.A. Lopez^{144b}, D. Lopez Mateos⁵⁷, I. Lopez Paz¹⁴, A. Lopez Solis¹³², J. Lorenz¹¹²,
 N. Lorenzo Martinez⁵, M. Losada²², P.J. Lösel¹¹², X. Lou^{15a}, A. Lounis¹²⁸, J. Love⁶, P.A. Love⁸⁷,
 H. Lu^{61a}, N. Lu¹⁰³, Y.J. Lu⁶², H.J. Lubatti¹⁴⁵, C. Luci^{70a,70b}, A. Lucotte⁵⁶, C. Luedtke⁵⁰, F. Luehring⁶³,
 W. Lukas⁷⁴, L. Luminari^{70a}, O. Lundberg^{43a,43b}, B. Lund-Jensen¹⁵¹, M.S. Lutz¹⁰⁰, P.M. Luzi¹³²,
 D. Lynn²⁹, R. Lysak¹³⁷, E. Lytken⁹⁴, F. Lyu^{15a}, V. Lyubushkin⁷⁷, H. Ma²⁹, L.L. Ma^{58b}, Y. Ma^{58b},
 G. Maccarrone⁴⁹, A. Macchioli¹¹³, C.M. Macdonald¹⁴⁶, J. Machado Miguens^{133,136b}, D. Madaffari¹⁷²,
 R. Madar³⁷, W.F. Mader⁴⁶, A. Madsen⁴⁴, J. Maeda⁸⁰, S. Maeland¹⁷, T. Maeno²⁹, A.S. Maevskiy¹¹¹,
 V. Magerl⁵⁰, J. Mahlstedt¹¹⁸, C. Maiani¹²⁸, C. Maidantchik^{78b}, A.A. Maier¹¹³, T. Maier¹¹²,
 A. Maio^{136a,136b,136d}, O. Majersky^{28a}, S. Majewski¹²⁷, Y. Makida⁷⁹, N. Makovec¹²⁸, B. Malaescu¹³²,
 Pa. Malecki⁸², V.P. Maleev¹³⁴, F. Malek⁵⁶, U. Mallik⁷⁵, D. Malon⁶, C. Malone³¹, S. Maltezos¹⁰,
 S. Malyukov³⁵, J. Mamuzic¹⁷², G. Mancini⁴⁹, I. Mandic⁸⁹, J. Maneira^{136a,136b},
 L. Manhaes de Andrade Filho^{78a}, J. Manjarres Ramos⁴⁶, K.H. Mankinen⁹⁴, A. Mann¹¹², A. Manousos³⁵,
 B. Mansoulie¹⁴², J.D. Mansour^{15a}, R. Mantifel¹⁰¹, M. Mantoani⁵¹, S. Manzoni^{66a,66b}, L. Mapelli³⁵,
 G. Marceca³⁰, L. March⁵², L. Marchese¹³¹, G. Marchiori¹³², M. Marcisovsky¹³⁷, M. Marjanovic³⁷,
 D.E. Marley¹⁰³, F. Marroquim^{78b}, S.P. Marsden⁹⁸, Z. Marshall¹⁸, M.U.F Martensson¹⁷⁰,
 S. Marti-Garcia¹⁷², C.B. Martin¹²², T.A. Martin¹⁷⁶, V.J. Martin⁴⁸, B. Martin dit Latour¹⁷,
 M. Martinez^{14,y}, V.I. Martinez Outschoorn¹⁷¹, S. Martin-Haugh¹⁴¹, V.S. Martoiu^{27b}, A.C. Martyniuk⁹²,
 A. Marzin³⁵, L. Masetti⁹⁷, T. Mashimo¹⁶¹, R. Mashinistov¹⁰⁸, J. Masik⁹⁸, A.L. Maslennikov^{120b,120a},
 L. Massa^{71a,71b}, P. Mastrandrea⁵, A. Mastroberardino^{40b,40a}, T. Masubuchi¹⁶¹, P. Mättig¹⁸⁰, J. Maurer^{27b},
 B. Maček⁸⁹, S.J. Maxfield⁸⁸, D.A. Maximov^{120b,120a}, R. Mazini¹⁵⁵, I. Maznas¹⁶⁰, S.M. Mazza^{66a,66b},
 N.C. Mc Fadden¹¹⁶, G. Mc Goldrick¹⁶⁵, S.P. Mc Kee¹⁰³, A. McCarn¹⁰³, R.L. McCarthy¹⁵²,
 T.G. McCarthy¹¹³, L.I. McClymont⁹², E.F. McDonald¹⁰², J.A. McFayden⁹², G. Mchedlidze⁵¹,
 S.J. McMahon¹⁴¹, P.C. McNamara¹⁰², R.A. McPherson^{174,ae}, S. Meehan¹⁴⁵, T. Megy⁵⁰, S. Mehlhase¹¹²,
 A. Mehta⁸⁸, T. Meideck⁵⁶, B. Meirose⁴², D. Melini^{172,h}, B.R. Mellado Garcia^{32c}, J.D. Mellenthin⁵¹,
 M. Melo^{28a}, F. Meloni²⁰, A. Melzer²⁴, S.B. Menary⁹⁸, L. Meng⁸⁸, X.T. Meng¹⁰³, A. Mengarelli^{23b,23a},
 S. Menke¹¹³, E. Meoni^{40b,40a}, S. Mergelmeyer¹⁹, P. Mermod⁵², L. Merola^{67a,67b}, C. Meroni^{66a},
 F.S. Merritt³⁶, A. Messina^{70a,70b}, J. Metcalfe⁶, A.S. Mete¹⁶⁹, C. Meyer¹³³, J. Meyer¹¹⁸, J-P. Meyer¹⁴²,
 H. Meyer Zu Theenhausen^{59a}, F. Miano¹⁵³, R.P. Middleton¹⁴¹, S. Miglioranzo^{53b,53a}, L. Mijović⁴⁸,
 G. Mikenberg¹⁷⁸, M. Mikestikova¹³⁷, M. Mikuž⁸⁹, M. Milesi¹⁰², A. Milic¹⁶⁵, D.W. Miller³⁶, C. Mills⁴⁸,
 A. Milov¹⁷⁸, D.A. Milstead^{43a,43b}, A.A. Minaenko¹⁴⁰, Y. Minami¹⁶¹, I.A. Minashvili^{157b}, A.I. Mincer¹²¹,

B. Mindur^{81a}, M. Mineev⁷⁷, Y. Minegishi¹⁶¹, Y. Ming¹⁷⁹, L.M. Mir¹⁴, K.P. Mistry¹³³, T. Mitani¹⁷⁷,
 J. Mitrevski¹¹², V.A. Mitsou¹⁷², A. Miucci²⁰, P.S. Miyagawa¹⁴⁶, A. Mizukami⁷⁹, J.U. Mjörnmark⁹⁴,
 T. Mkrtchyan¹⁸², M. Mlynarikova¹³⁹, T. Moa^{43a,43b}, K. Mochizuki¹⁰⁷, P. Mogg⁵⁰, S. Mohapatra³⁸,
 S. Molander^{43a,43b}, R. Moles-Valls²⁴, R. Monden⁸³, M.C. Mondragon¹⁰⁴, K. Mönig⁴⁴, J. Monk³⁹,
 E. Monnier⁹⁹, A. Montalbano¹⁵², J. Montejo Berlingen³⁵, F. Monticelli⁸⁶, S. Monzani^{66a}, R.W. Moore³,
 N. Morange¹²⁸, D. Moreno²², M. Moreno Llácer³⁵, P. Morettini^{53b}, S. Morgenstern³⁵, D. Mori¹⁴⁹,
 T. Mori¹⁶¹, M. Morii⁵⁷, M. Morinaga¹⁶¹, V. Morisbak¹³⁰, A.K. Morley³⁵, G. Mornacchi³⁵, J.D. Morris⁹⁰,
 L. Morvaj¹⁵², P. Moschovakos¹⁰, M. Mosidze^{157b}, H.J. Moss¹⁴⁶, J. Moss^{150,n}, K. Motohashi¹⁶³,
 R. Mount¹⁵⁰, E. Mountricha²⁹, E.J.W. Moyse¹⁰⁰, S. Muanza⁹⁹, F. Mueller¹¹³, J. Mueller¹³⁵,
 R.S.P. Mueller¹¹², D. Muenstermann⁸⁷, P. Mullen⁵⁵, G.A. Mullier²⁰, F.J. Munoz Sanchez⁹⁸,
 W.J. Murray^{176,141}, H. Musheghyan³⁵, M. Muškinja⁸⁹, A.G. Myagkov^{140,al}, M. Myska¹³⁸,
 B.P. Nachman¹⁸, O. Nackenhorst⁵², K. Nagai¹³¹, R. Nagai^{79,ao}, K. Nagano⁷⁹, Y. Nagasaka⁶⁰,
 K. Nagata¹⁶⁷, M. Nagel⁵⁰, E. Nagy⁹⁹, A.M. Nairz³⁵, Y. Nakahama¹¹⁵, K. Nakamura⁷⁹, T. Nakamura¹⁶¹,
 I. Nakano¹²³, R.F. Naranjo Garcia⁴⁴, R. Narayan¹¹, D.I. Narrias Villar^{59a}, I. Naryshkin¹³⁴,
 T. Naumann⁴⁴, G. Navarro²², R. Nayyar⁷, H.A. Neal¹⁰³, P.Y. Nechaeva¹⁰⁸, T.J. Neep¹⁴², A. Negri^{68a,68b},
 M. Negrini^{23b}, S. Nektarijevic¹¹⁷, C. Nellist¹²⁸, A. Nelson¹⁶⁹, M.E. Nelson¹³¹, S. Nemecek¹³⁷,
 P. Nemethy¹²¹, M. Nessi^{35,f}, M.S. Neubauer¹⁷¹, M. Neumann¹⁸⁰, P.R. Newman²¹, T.Y. Ng^{61c},
 T. Nguyen Manh¹⁰⁷, R.B. Nickerson¹³¹, R. Nicolaïdou¹⁴², J. Nielsen¹⁴³, V. Nikolaenko^{140,al},
 I. Nikolic-Audit¹³², K. Nikolopoulos²¹, J.K. Nilsen¹³⁰, P. Nilsson²⁹, Y. Ninomiya¹⁶¹, A. Nisati^{70a},
 N. Nishu^{15b}, R. Nisius¹¹³, I. Nitsche⁴⁵, T. Nitta¹⁷⁷, T. Nobe¹⁶¹, Y. Noguchi⁸³, M. Nomachi¹²⁹,
 I. Nomidis³³, M.A. Nomura²⁹, T. Nooney⁹⁰, M. Nordberg³⁵, N. Norjoharuddeen¹³¹, O. Novgorodova⁴⁶,
 M. Nozaki⁷⁹, L. Nozka¹²⁶, K. Ntekas¹⁶⁹, E. Nurse⁹², F. Nuti¹⁰², F.G. Oakham^{33,au}, H. Oberlack¹¹³,
 T. Obermann²⁴, J. Ocariz¹³², A. Ochi⁸⁰, I. Ochoa³⁸, J.P. Ochoa-Ricoux^{144a}, K. O'Connor²⁶, S. Oda⁸⁵,
 S. Odaka⁷⁹, A. Oh⁹⁸, S.H. Oh⁴⁷, C.C. Ohm¹⁸, H. Ohman¹⁷⁰, H. Oide^{53b,53a}, H. Okawa¹⁶⁷,
 Y. Okumura¹⁶¹, T. Okuyama⁷⁹, A. Olariu^{27b}, L.F. Oleiro Seabra^{136a}, S.A. Olivares Pino⁴⁸,
 D. Oliveira Damazio²⁹, A. Olszewski⁸², J. Olszowska⁸², D.C. O'Neil¹⁴⁹, A. Onofre^{136a,136e},
 K. Onogi¹¹⁵, P.U.E. Onyisi¹¹, H. Oppen¹³⁰, M.J. Oreglia³⁶, Y. Oren¹⁵⁹, D. Orestano^{72a,72b},
 N. Orlando^{61b}, A.A. O'Rourke⁴⁴, R.S. Orr¹⁶⁵, B. Osculati^{53b,53a,*}, V. O'Shea⁵⁵, R. Ospanov^{58a},
 G. Otero y Garzon³⁰, H. Otono⁸⁵, M. Ouchrif^{34d}, F. Ould-Saada¹³⁰, A. Ouraou¹⁴², K.P. Oussoren¹¹⁸,
 Q. Ouyang^{15a}, M. Owen⁵⁵, R.E. Owen²¹, V.E. Ozcan^{12c}, N. Ozturk⁸, K. Pachal¹⁴⁹, A. Pacheco Pages¹⁴,
 L. Pacheco Rodriguez¹⁴², C. Padilla Aranda¹⁴, S. Pagan Griso¹⁸, M. Paganini¹⁸¹, F. Paige²⁹,
 G. Palacino⁶³, S. Palazzo^{40b,40a}, S. Palestini³⁵, M. Palka^{81b}, D. Pallin³⁷, E.St. Panagiotopoulou¹⁰,
 I. Panagoulias¹⁰, C.E. Pandini¹³², J.G. Panduro Vazquez⁹¹, P. Pani³⁵, S. Panitkin²⁹, D. Pantea^{27b},
 L. Paolozzi⁵², T.D. Papadopoulou¹⁰, K. Papageorgiou^{9,k}, A. Paramonov⁶, D. Paredes Hernandez¹⁸¹,
 A.J. Parker⁸⁷, K.A. Parker⁴⁴, M.A. Parker³¹, F. Parodi^{53b,53a}, J.A. Parsons³⁸, U. Parzefall⁵⁰,
 V.R. Pascuzzi¹⁶⁵, J.M.P. Pasner¹⁴³, E. Pasqualucci^{70a}, S. Passaggio^{53b}, F. Pastore⁹¹, S. Pataraia⁹⁷,
 J.R. Pater⁹⁸, T. Pauly³⁵, B. Pearson¹¹³, S. Pedraza Lopez¹⁷², R. Pedro^{136a,136b}, S.V. Peleganchuk^{120b,120a},
 O. Penc¹³⁷, C. Peng^{15d}, H. Peng^{58a}, J. Penwell⁶³, B.S. Peralva^{78a}, M.M. Perego¹⁴², D.V. Perepelitsa²⁹,
 F. Peri¹⁹, L. Perini^{66a,66b}, H. Pernegger³⁵, S. Perrella^{67a,67b}, R. Peschke⁴⁴, V.D. Peshekhanov^{77,*},
 K. Peters⁴⁴, R.F.Y. Peters⁹⁸, B.A. Petersen³⁵, T.C. Petersen³⁹, E. Petit⁵⁶, A. Petridis¹, C. Petridou¹⁶⁰,
 P. Petroff¹²⁸, E. Petrolo^{70a}, M. Petrov¹³¹, F. Petrucci^{72a,72b}, N.E. Pettersson¹⁰⁰, A. Peyaud¹⁴²,
 R. Pezoa^{144b}, F.H. Phillips¹⁰⁴, P.W. Phillips¹⁴¹, G. Piacquadio¹⁵², E. Pianori¹⁷⁶, A. Picazio¹⁰⁰,
 E. Piccaro⁹⁰, M.A. Pickering¹³¹, R. Piegai³⁰, J.E. Pilcher³⁶, A.D. Pilkington⁹⁸, A.W.J. Pin⁹⁸,
 M. Pinamonti^{71a,71b}, J.L. Pinfold³, H. Pirumov⁴⁴, M. Pitt¹⁷⁸, L. Plazak^{28a}, M-A. Pleier²⁹, V. Pleskot⁹⁷,
 E. Plotnikova⁷⁷, D. Pluth⁷⁶, P. Podberezk^{120b,120a}, R. Poettgen^{43a,43b}, R. Poggi^{68a,68b}, L. Poggioli¹²⁸,
 D. Pohl²⁴, G. Polesello^{68a}, A. Poley⁴⁴, A. Policicchio^{40b,40a}, R. Polifka³⁵, A. Polini^{23b}, C.S. Pollard⁵⁵,
 V. Polychronakos²⁹, K. Pommès³⁵, D. Ponomarenko¹¹⁰, L. Pontecorvo^{70a}, G.A. Popeneciu^{27d},

A. Poppleton³⁵, S. Pospisil¹³⁸, K. Potamianos¹⁸, I.N. Potrap⁷⁷, C.J. Potter³¹, G. Poulard³⁵, T. Poulsen⁹⁴,
 J. Poveda³⁵, M.E. Pozo Astigarraga³⁵, P. Pralavorio⁹⁹, A. Pranko¹⁸, S. Prell⁷⁶, D. Price⁹⁸,
 M. Primavera^{65a}, S. Prince¹⁰¹, N. Proklova¹¹⁰, K. Prokofiev^{61c}, F. Prokoshin^{144b}, S. Protopopescu²⁹,
 J. Proudfoot⁶, M. Przybycien^{81a}, A. Puri¹⁷¹, P. Puzo¹²⁸, J. Qian¹⁰³, G. Qin⁵⁵, Y. Qin⁹⁸, A. Quadt⁵¹,
 M. Queitsch-Maitland⁴⁴, D. Quilty⁵⁵, S. Raddum¹³⁰, V. Radeka²⁹, V. Radescu¹³¹,
 S.K. Radhakrishnan¹⁵², P. Radloff¹²⁷, P. Rados¹⁰², F. Ragusa^{66a,66b}, G. Rahal⁹⁵, J.A. Raine⁹⁸,
 S. Rajagopalan²⁹, C. Rangel-Smith¹⁷⁰, T. Rashid¹²⁸, S. Raspopov⁵, M.G. Ratti^{66a,66b}, D.M. Rauch⁴⁴,
 F. Rauscher¹¹², S. Rave⁹⁷, I. Ravinovich¹⁷⁸, J.H. Rawling⁹⁸, M. Raymond³⁵, A.L. Read¹³⁰,
 N.P. Readjoff⁵⁶, M. Reale^{65a,65b}, D.M. Rebuzzi^{68a,68b}, A. Redelbach¹⁷⁵, G. Redlinger²⁹, R. Reece¹⁴³,
 R.G. Reed^{32c}, K. Reeves⁴², L. Rehnisch¹⁹, J. Reichert¹³³, A. Reiss⁹⁷, C. Rembser³⁵, H. Ren^{15d},
 M. Rescigno^{70a}, S. Resconi^{66a}, E.D. Resseguei¹³³, S. Rettie¹⁷³, E. Reynolds²¹, O.L. Rezanova^{120b,120a},
 P. Reznicek¹³⁹, R. Rezvani¹⁰⁷, R. Richter¹¹³, S. Richter⁹², E. Richter-Was^{81b}, O. Ricken²⁴, M. Ridel¹³²,
 P. Rieck¹¹³, C.J. Riegel¹⁸⁰, J. Rieger⁵¹, O. Rifki¹²⁴, M. Rijssenbeek¹⁵², A. Rimoldi^{68a,68b}, M. Rimoldi²⁰,
 L. Rinaldi^{23b}, G. Ripellino¹⁵¹, B. Ristic³⁵, E. Ritsch³⁵, I. Riu¹⁴, F. Rizatdinova¹²⁵, E. Rizvi⁹⁰, C. Rizzi¹⁴,
 R.T. Roberts⁹⁸, S.H. Robertson^{101,ae}, A. Robichaud-Veronneau¹⁰¹, D. Robinson³¹, J.E.M. Robinson⁴⁴,
 A. Robson⁵⁵, E. Rocco⁹⁷, C. Roda^{69a,69b}, Y. Rodina^{99,z}, S. Rodriguez Bosca¹⁷², A. Rodriguez Perez¹⁴,
 D. Rodriguez Rodriguez¹⁷², S. Roe³⁵, C.S. Rogan⁵⁷, O. Røhne¹³⁰, J. Roloff⁵⁷, A. Romanouk¹¹⁰,
 M. Romano^{23b,23a}, S.M. Romano Saez³⁷, E. Romero Adam¹⁷², N. Rompotis⁸⁸, M. Ronzani⁵⁰,
 L. Roos¹³², S. Rosati^{70a}, K. Rosbach⁵⁰, P. Rose¹⁴³, N-A. Rosien⁵¹, E. Rossi^{67a,67b}, L.P. Rossi^{53b},
 J.H.N. Rosten³¹, R. Rosten¹⁴⁵, M. Rotaru^{27b}, J. Rothberg¹⁴⁵, D. Rousseau¹²⁸, A. Rozanov⁹⁹,
 Y. Rozen¹⁵⁸, X. Ruan^{32c}, F. Rubbo¹⁵⁰, F. Rühr⁵⁰, A. Ruiz-Martinez³³, Z. Rurikova⁵⁰,
 N.A. Rusakovich⁷⁷, H.L. Russell¹⁰¹, J.P. Rutherford⁷, N. Ruthmann³⁵, Y.F. Ryabov¹³⁴, M. Rybar¹⁷¹,
 G. Rybkin¹²⁸, S. Ryu⁶, A. Ryzhov¹⁴⁰, G.F. Rzehorz⁵¹, A.F. Saavedra¹⁵⁴, G. Sabato¹¹⁸, S. Sacerdoti³⁰,
 H.F-W. Sadrozinski¹⁴³, R. Sadykov⁷⁷, F. Safai Tehrani^{70a}, P. Saha¹¹⁹, M. Sahinsoy^{59a}, M. Saimpert⁴⁴,
 M. Saito¹⁶¹, T. Saito¹⁶¹, H. Sakamoto¹⁶¹, Y. Sakurai¹⁷⁷, G. Salamanna^{72a,72b}, J.E. Salazar Loyola^{144b},
 D. Salek¹¹⁸, P.H. Sales De Bruin¹⁷⁰, D. Salihagic¹¹³, A. Salnikov¹⁵⁰, J. Salt¹⁷², D. Salvatore^{40b,40a},
 F. Salvatore¹⁵³, A. Salvucci^{61a,61b,61c}, A. Salzburger³⁵, D. Sammel⁵⁰, D. Sampsonidis¹⁶⁰,
 D. Sampsonidou¹⁶⁰, J. Sánchez¹⁷², V. Sanchez Martinez¹⁷², A. Sanchez Pineda^{64a,64c}, H. Sandaker¹³⁰,
 R.L. Sandbach⁹⁰, C.O. Sander⁴⁴, M. Sandhoff¹⁸⁰, C. Sandoval²², D.P.C. Sankey¹⁴¹, M. Sannino^{53b,53a},
 Y. Sano¹¹⁵, A. Sansoni⁴⁹, C. Santoni³⁷, H. Santos^{136a}, I. Santoyo Castillo¹⁵³, A. Sapronov⁷⁷,
 J.G. Saraiva^{136a,136d}, B. Sarrazin²⁴, O. Sasaki⁷⁹, K. Sato¹⁶⁷, E. Sauvan⁵, G. Savage⁹¹, P. Savard^{165,au},
 N. Savic¹¹³, C. Sawyer¹⁴¹, L. Sawyer^{93,aj}, J. Saxon³⁶, C. Sbarra^{23b}, A. Sbrizzi^{23b,23a}, T. Scanlon⁹²,
 D.A. Scannicchio¹⁶⁹, M. Scarella¹⁵⁴, J. Schaarschmidt¹⁴⁵, P. Schacht¹¹³, B.M. Schachtner¹¹²,
 D. Schaefer³⁵, L. Schaefer¹³³, R. Schaefer⁴⁴, J. Schaeffer⁹⁷, S. Schaepe²⁴, S. Schaetzl^{59b}, U. Schäfer⁹⁷,
 A.C. Schaffter¹²⁸, D. Schaille¹¹², R.D. Schamberger¹⁵², V.A. Schegelsky¹³⁴, D. Scheirich¹³⁹,
 M. Schernau¹⁶⁹, C. Schiavi^{53b,53a}, S. Schier¹⁴³, L.K. Schildgen²⁴, C. Schillo⁵⁰, M. Schioppa^{40b,40a},
 S. Schlenker³⁵, K.R. Schmidt-Sommerfeld¹¹³, K. Schmieden³⁵, C. Schmitt⁹⁷, S. Schmitt⁴⁴, S. Schmitz⁹⁷,
 U. Schnoor⁵⁰, L. Schoeffel¹⁴², A. Schoening^{59b}, B.D. Schoenrock¹⁰⁴, E. Schopf²⁴, M. Schott⁹⁷,
 J.F.P. Schouwenberg¹¹⁷, J. Schovancova³⁵, S. Schramm⁵², N. Schuh⁹⁷, A. Schulte⁹⁷, M.J. Schultens²⁴,
 H-C. Schultz-Coulon^{59a}, H. Schulz¹⁹, M. Schumacher⁵⁰, B.A. Schumm¹⁴³, Ph. Schune¹⁴²,
 A. Schwartzman¹⁵⁰, T.A. Schwarz¹⁰³, H. Schweiger⁹⁸, Ph. Schwemling¹⁴², R. Schwienhorst¹⁰⁴,
 A. Sciandra²⁴, G. Sciolla²⁶, M. Scornajenghi^{40b,40a}, F. Scuri^{69a}, F. Scutti¹⁰², J. Searcy¹⁰³, P. Seema²⁴,
 S.C. Seidel¹¹⁶, A. Seiden¹⁴³, J.M. Seixas^{78b}, G. Sekhniaidze^{67a}, K. Sekhon¹⁰³, S.J. Sekula⁴¹,
 N. Semprini-Cesari^{23b,23a}, S. Senkin³⁷, C. Serfon¹³⁰, L. Serin¹²⁸, L. Serkin^{64a,64b}, M. Sessa^{72a,72b},
 R. Seuster¹⁷⁴, H. Severini¹²⁴, F. Sforza³⁵, A. Sfyrla⁵², E. Shabalina⁵¹, N.W. Shaikh^{43a,43b}, L.Y. Shan^{15a},
 R. Shang¹⁷¹, J.T. Shank²⁵, M. Shapiro¹⁸, P.B. Shatalov¹⁰⁹, K. Shaw^{64a,64b}, S.M. Shaw⁹⁸,
 A. Shcherbakova^{43a,43b}, C.Y. Shehu¹⁵³, Y. Shen¹²⁴, N. Sherafati³³, P. Sherwood⁹², L. Shi^{155,aq},

S. Shimizu⁸⁰, C.O. Shimmin¹⁸¹, M. Shimojima¹¹⁴, I.P.J. Shipsey¹³¹, S. Shirabe⁸⁵, M. Shiyakova⁷⁷,
 J. Shlomi¹⁷⁸, A. Shmeleva¹⁰⁸, D. Shoaleh Saadi¹⁰⁷, M.J. Shochet³⁶, S. Shojaii^{66a}, D.R. Shope¹²⁴,
 S. Shrestha¹²², E. Shulga¹¹⁰, M.A. Shupe⁷, P. Sicho¹³⁷, A.M. Sickles¹⁷¹, P.E. Sidebo¹⁵¹,
 E. Sideras Haddad^{32c}, O. Sidiropoulou¹⁷⁵, A. Sidoti^{23b,23a}, F. Siegert⁴⁶, Dj. Sijacki¹⁶, J. Silva^{136a,136d},
 S.B. Silverstein^{43a}, V. Simak¹³⁸, L. Simic¹⁶, S. Simion¹²⁸, E. Simioni⁹⁷, B. Simmons⁹², M. Simon⁹⁷,
 P. Sinervo¹⁶⁵, N.B. Sinev¹²⁷, M. Sioli^{23b,23a}, G. Siragusa¹⁷⁵, I. Siral¹⁰³, S.Yu. Sivoklokov¹¹¹,
 J. Sjölin^{43a,43b}, M.B. Skinner⁸⁷, P. Skubic¹²⁴, M. Slater²¹, T. Slavicek¹³⁸, M. Slawinska⁸², K. Sliwa¹⁶⁸,
 R. Slovak¹³⁹, V. Smakhtin¹⁷⁸, B.H. Smart⁵, J. Smiesko^{28a}, N. Smirnov¹¹⁰, S.Yu. Smirnov¹¹⁰,
 Y. Smirnov¹¹⁰, L.N. Smirnova¹¹¹, O. Smirnova⁹⁴, J.W. Smith⁵¹, M.N.K. Smith³⁸, R.W. Smith³⁸,
 M. Smizanska⁸⁷, K. Smolek¹³⁸, A.A. Snesarev¹⁰⁸, I.M. Snyder¹²⁷, S. Snyder²⁹, R. Sobie^{174,ae},
 F. Socher⁴⁶, A. Soffer¹⁵⁹, A. Søgaard⁴⁸, D.A. Soh¹⁵⁵, G. Sokhrannyi⁸⁹, C.A. Solans Sanchez³⁵,
 M. Solar¹³⁸, E.Yu. Soldatov¹¹⁰, U. Soldevila¹⁷², A.A. Solodkov¹⁴⁰, A. Soloshenko⁷⁷,
 O.V. Solovyanov¹⁴⁰, V. Solovyev¹³⁴, P. Sommer⁵⁰, H. Son¹⁶⁸, A. Sopczak¹³⁸, D. Sosa^{59b},
 C.L. Sotiropoulou^{69a,69b}, R. Soualah^{64a,64c,j}, A.M. Soukharev^{120b,120a}, D. South⁴⁴, B.C. Sowden⁹¹,
 S. Spagnolo^{65a,65b}, M. Spalla^{69a,69b}, M. Spangenberg¹⁷⁶, F. Spanò⁹¹, D. Sperlich¹⁹, F. Spettel¹¹³,
 T.M. Spieker^{59a}, R. Spighi^{23b}, G. Spigo³⁵, L.A. Spiller¹⁰², M. Spousta¹³⁹, R.D. St. Denis^{55,*},
 A. Stabile^{66a,66b}, R. Stamen^{59a}, S. Stamm¹⁹, E. Stanecka⁸², R.W. Stanek⁶, C. Stanescu^{72a},
 M.M. Stanitzki⁴⁴, B.S. Stapf¹¹⁸, S. Stapnes¹³⁰, E.A. Starchenko¹⁴⁰, G.H. Stark³⁶, J. Stark⁵⁶, S.H. Stark³⁹,
 P. Staroba¹³⁷, P. Starovoitov^{59a}, S. Stärz³⁵, R. Staszewski⁸², P. Steinberg²⁹, B. Stelzer¹⁴⁹, H.J. Stelzer³⁵,
 O. Stelzer-Chilton^{166a}, H. Stenzel⁵⁴, G.A. Stewart⁵⁵, M.C. Stockton¹²⁷, M. Stoebe¹⁰¹, G. Stoica^{27b},
 P. Stolte⁵¹, S. Stonjek¹¹³, A.R. Stradling⁸, A. Straessner⁴⁶, M.E. Stramaglia²⁰, J. Strandberg¹⁵¹,
 S. Strandberg^{43a,43b}, M. Strauss¹²⁴, P. Strizenec^{28b}, R. Ströhmer¹⁷⁵, D.M. Strom¹²⁷, R. Stroynowski⁴¹,
 A. Strubig⁴⁸, S.A. Stucci²⁹, B. Stugu¹⁷, N.A. Styles⁴⁴, D. Su¹⁵⁰, J. Su¹³⁵, S. Suchek^{59a}, Y. Sugaya¹²⁹,
 M. Suk¹³⁸, V.V. Sulin¹⁰⁸, D.M.S. Sultan^{73a,73b}, S. Sultansoy^{4c}, T. Sumida⁸³, S. Sun⁵⁷, X. Sun³,
 K. Suruliz¹⁵³, C.J.E. Suster¹⁵⁴, M.R. Sutton¹⁵³, S. Suzuki⁷⁹, M. Svatos¹³⁷, M. Swiatlowski³⁶,
 S.P. Swift², I. Sykora^{28a}, T. Sykora¹³⁹, D. Ta⁵⁰, K. Tackmann^{44,aa}, J. Taenzer¹⁵⁹, A. Taffard¹⁶⁹,
 R. Tafirout^{166a}, N. Taiblum¹⁵⁹, H. Takai²⁹, R. Takashima⁸⁴, E.H. Takasugi¹¹³, T. Takeshita¹⁴⁷,
 Y. Takubo⁷⁹, M. Talby⁹⁹, A.A. Talyshев^{120b,120a}, J. Tanaka¹⁶¹, M. Tanaka¹⁶³, R. Tanaka¹²⁸, S. Tanaka⁷⁹,
 R. Tanioka⁸⁰, B.B. Tannenwald¹²², S. Tapia Araya^{144b}, S. Tapprogge⁹⁷, S. Tarem¹⁵⁸, G.F. Tartarelli^{66a},
 P. Tas¹³⁹, M. Tasevsky¹³⁷, T. Tashiro⁸³, E. Tassi^{40b,40a}, A. Tavares Delgado^{136a,136b}, Y. Tayalati^{34e},
 A.C. Taylor¹¹⁶, G.N. Taylor¹⁰², P.T.E. Taylor¹⁰², W. Taylor^{166b}, P. Teixeira-Dias⁹¹, D. Temple¹⁴⁹,
 H. Ten Kate³⁵, P.K. Teng¹⁵⁵, J.J. Teoh¹²⁹, F. Tepel¹⁸⁰, S. Terada⁷⁹, K. Terashi¹⁶¹, J. Terron⁹⁶, S. Terzo¹⁴,
 M. Testa⁴⁹, R.J. Teuscher^{165,ae}, T. Theveneaux-Pelzer⁹⁹, F. Thiele³⁹, J.P. Thomas²¹,
 J. Thomas-Wilsker⁹¹, A.S. Thompson⁵⁵, P.D. Thompson²¹, L.A. Thomsen¹⁸¹, E. Thomson¹³³,
 M.J. Tibbetts¹⁸, R.E. Ticse Torres⁹⁹, V.O. Tikhomirov^{108,am}, Yu.A. Tikhonov^{120b,120a}, S. Timoshenko¹¹⁰,
 P. Tipton¹⁸¹, S. Tisserant⁹⁹, K. Todome¹⁶³, S. Todorova-Nova⁵, S. Todt⁴⁶, J. Tojo⁸⁵, S. Tokár^{28a},
 K. Tokushuku⁷⁹, E. Tolley¹²², L. Tomlinson⁹⁸, M. Tomoto¹¹⁵, L. Tompkins¹⁵⁰, K. Toms¹¹⁶, B. Tong⁵⁷,
 P. Tornambe⁵⁰, E. Torrence¹²⁷, H. Torres¹⁴⁹, E. Torró Pastor¹⁴⁵, J. Toth^{99,ac}, F. Touchard⁹⁹,
 D.R. Tovey¹⁴⁶, C.J. Treado¹²¹, T. Trefzger¹⁷⁵, F. Tresoldi¹⁵³, A. Tricoli²⁹, I.M. Trigger^{166a},
 S. Trincz-Duvold¹³², M.F. Tripiana¹⁴, W. Trischuk¹⁶⁵, B. Trocmé⁵⁶, A. Trofymov⁴⁴, C. Troncon^{66a},
 M. Trottier-McDonald¹⁸, M. Trovatelli¹⁷⁴, L. Truong^{32b}, M. Trzebinski⁸², A. Trzupek⁸², K.W. Tsang^{61a},
 J.C.-L. Tseng¹³¹, P.V. Tsiareshka¹⁰⁵, G. Tsipolitis¹⁰, N. Tsirintanis⁹, S. Tsiskaridze¹⁴, V. Tsiskaridze⁵⁰,
 E.G. Tskhadadze^{157a}, K.M. Tsui^{61a}, I.I. Tsukerman¹⁰⁹, V. Tsulaia¹⁸, S. Tsuno⁷⁹, D. Tsybychev¹⁵²,
 Y. Tu^{61b}, A. Tudorache^{27b}, V. Tudorache^{27b}, T.T. Tulbure^{27a}, A.N. Tuna⁵⁷, S.A. Tupputi^{23b,23a},
 S. Turchikhin⁷⁷, D. Turgeman¹⁷⁸, I. Turk Cakir^{4b,u}, R. Turra^{66a}, P.M. Tuts³⁸, G. Ucchielli^{23b,23a},
 I. Ueda⁷⁹, M. Ughetto^{43a,43b}, F. Ukegawa¹⁶⁷, G. Unal³⁵, A. Undrus²⁹, G. Unel¹⁶⁹, F.C. Ungaro¹⁰²,
 Y. Unno⁷⁹, C. Unverdorben¹¹², J. Urban^{28b}, P. Urquijo¹⁰², P. Urrejola⁹⁷, G. Usai⁸, J. Usui⁷⁹,

L. Vacavant⁹⁹, V. Vacek¹³⁸, B. Vachon¹⁰¹, K.O.H. Vadla¹³⁰, A. Vaidya⁹², C. Valderanis¹¹²,
 E. Valdes Santurio^{43a,43b}, S. Valentini^{23b,23a}, A. Valero¹⁷², L. Valéry¹⁴, S. Valkar¹³⁹, A. Vallier⁵,
 J.A. Valls Ferrer¹⁷², W. Van Den Wollenberg¹¹⁸, H. Van der Graaf¹¹⁸, P. Van Gemmeren⁶,
 J. Van Nieuwkoop¹⁴⁹, I. Van Vulpen¹¹⁸, M.C. van Woerden¹¹⁸, M. Vanadia^{71a,71b}, W. Vandelli³⁵,
 A. Vaniachine¹⁶⁴, P. Vankov¹¹⁸, G. Vardanyan¹⁸², R. Vari^{70a}, E.W. Varnes⁷, C. Varni^{53b,53a}, T. Varol⁴¹,
 D. Varouchas¹²⁸, A. Vartapetian⁸, K.E. Varvell¹⁵⁴, G.A. Vasquez^{144b}, J.G. Vasquez¹⁸¹, F. Vazeille³⁷,
 T. Vazquez Schroeder¹⁰¹, J. Veatch⁵¹, V. Veeraraghavan⁷, L.M. Veloce¹⁶⁵, F. Veloso^{136a,136c},
 S. Veneziano^{70a}, A. Ventura^{65a,65b}, M. Venturi¹⁷⁴, N. Venturi³⁵, A. Venturini²⁶, V. Vercesi^{68a},
 M. Verducci^{72a,72b}, W. Verkerke¹¹⁸, A.T. Vermeulen¹¹⁸, J.C. Vermeulen¹¹⁸, M.C. Vetterli^{149,au},
 N. Viaux Maira^{144b}, O. Viazlo⁹⁴, I. Vichou^{171,*}, T. Vickey¹⁴⁶, O.E. Vickey Boeriu¹⁴⁶,
 G.H.A. Viehhauser¹³¹, S. Viel¹⁸, L. Vigani¹³¹, M. Villa^{23b,23a}, M. Villaplana Perez^{66a,66b}, E. Vilucchi⁴⁹,
 M.G. Vincter³³, V.B. Vinogradov⁷⁷, A. Vishwakarma⁴⁴, C. Vittori^{23b,23a}, I. Vivarelli¹⁵³, S. Vlachos¹⁰,
 M. Vogel¹⁸⁰, P. Vokac¹³⁸, G. Volpi^{69a,69b}, H. von der Schmitt¹¹³, E. Von Toerne²⁴, V. Vorobel¹³⁹,
 K. Vorobev¹¹⁰, M. Vos¹⁷², R. Voss³⁵, J.H. Vossebeld⁸⁸, N. Vranjes¹⁶, M. Vranjes Milosavljevic¹⁶,
 V. Vrba¹³⁸, M. Vreeswijk¹¹⁸, T. Šfiligoj⁸⁹, R. Vuillermet³⁵, I. Vukotic³⁶, T. Ženiš^{28a}, L. Živković¹⁶,
 P. Wagner²⁴, W. Wagner¹⁸⁰, J. Wagner-Kuhr¹¹², H. Wahlberg⁸⁶, S. Wahrmund⁴⁶, J. Wakabayashi¹¹⁵,
 J. Walder⁸⁷, R. Walker¹¹², W. Walkowiak¹⁴⁸, V. Wallangen^{43a,43b}, C. Wang^{15c}, C. Wang^{58b,e}, F. Wang¹⁷⁹,
 H. Wang¹⁸, H. Wang³, J. Wang¹⁵⁴, J. Wang⁴⁴, Q. Wang¹²⁴, R. Wang⁶, S.M. Wang¹⁵⁵, T. Wang³⁸,
 W. Wang^{155,p}, W.X. Wang^{58a,af}, Z. Wang^{58c}, C. Wanotayaroj¹²⁷, A. Warburton¹⁰¹, C.P. Ward³¹,
 D.R. Wardrope⁹², A. Washbrook⁴⁸, P.M. Watkins²¹, A.T. Watson²¹, M.F. Watson²¹, G. Watts¹⁴⁵,
 S. Watts⁹⁸, B.M. Waugh⁹², A.F. Webb¹¹, S. Webb⁹⁷, M.S. Weber²⁰, S.A. Weber³³, S.W. Weber¹⁷⁵,
 J.S. Webster⁶, A.R. Weidberg¹³¹, B. Weinert⁶³, J. Weingarten⁵¹, M. Weirich⁹⁷, C. Weiser⁵⁰, H. Weits¹¹⁸,
 P.S. Wells³⁵, T. Wenaus²⁹, T. Wengler³⁵, S. Wenig³⁵, N. Wermes²⁴, M.D. Werner⁷⁶, P. Werner³⁵,
 M. Wessels^{59a}, K. Whalen¹²⁷, N.L. Whallon¹⁴⁵, A.M. Wharton⁸⁷, A.S. White¹⁰³, A. White⁸,
 M.J. White¹, R. White^{144b}, D. Whiteson¹⁶⁹, B.W. Whitmore⁸⁷, F.J. Wickens¹⁴¹, W. Wiedenmann¹⁷⁹,
 M. Wielers¹⁴¹, C. Wiglesworth³⁹, L.A.M. Wiik-Fuchs⁵⁰, A. Wildauer¹¹³, F. Wilk⁹⁸, H.G. Wilkens³⁵,
 H.H. Williams¹³³, S. Williams³¹, C. Willis¹⁰⁴, S. Willocq¹⁰⁰, J.A. Wilson²¹, I. Wingerter-Seez⁵,
 E. Winkels¹⁵³, F. Winklmeier¹²⁷, O.J. Winston¹⁵³, B.T. Winter²⁴, M. Wittgen¹⁵⁰, M. Wobisch⁹³,
 T.M.H. Wolf¹¹⁸, R. Wolff⁹⁹, M.W. Wolter⁸², H. Wolters^{136a,136c}, V.W.S. Wong¹⁷³, S.D. Worm²¹,
 B.K. Wosiek⁸², J. Wotschack³⁵, K.W. Woźniak⁸², M. Wu³⁶, S.L. Wu¹⁷⁹, X. Wu⁵², Y. Wu¹⁰³,
 T.R. Wyatt⁹⁸, B.M. Wynne⁴⁸, S. Xella³⁹, Z. Xi¹⁰³, L. Xia^{15b}, D. Xu^{15a}, L. Xu²⁹, T. Xu¹⁴², B. Yabsley¹⁵⁴,
 S. Yacoob^{32a}, D. Yamaguchi¹⁶³, Y. Yamaguchi¹²⁹, A. Yamamoto⁷⁹, S. Yamamoto¹⁶¹, T. Yamanaka¹⁶¹,
 M. Yamatani¹⁶¹, K. Yamauchi¹¹⁵, Y. Yamazaki⁸⁰, Z. Yan²⁵, H.J. Yang^{58c,58d}, H.T. Yang¹⁸, Y. Yang¹⁵⁵,
 Z. Yang¹⁷, W-M. Yao¹⁸, Y.C. Yap¹³², Y. Yasu⁷⁹, E. Yatsenko⁵, K.H. Yau Wong²⁴, J. Ye⁴¹, S. Ye²⁹,
 I. Yeletskikh⁷⁷, E. Yigitbasi²⁵, E. Yildirim⁹⁷, K. Yorita¹⁷⁷, K. Yoshihara¹³³, C.J.S. Young³⁵, C. Young¹⁵⁰,
 J. Yu⁸, J. Yu⁷⁶, S.P.Y. Yuen²⁴, I. Yusuff^{31,a}, B. Zabinski⁸², G. Zacharis¹⁰, R. Zaidan¹⁴, A.M. Zaitsev^{140,al},
 N. Zakharchuk⁴⁴, J. Zalieckas¹⁷, A. Zaman¹⁵², S. Zambito⁵⁷, D. Zanzi¹⁰², C. Zeitnitz¹⁸⁰,
 G. Zemaityte¹³¹, A. Zemla^{81a}, J.C. Zeng¹⁷¹, Q. Zeng¹⁵⁰, O. Zenin¹⁴⁰, D. Zerwas¹²⁸, D. Zhang¹⁰³,
 F. Zhang¹⁷⁹, G. Zhang^{58a,af}, H. Zhang^{15c}, J. Zhang⁶, L. Zhang⁵⁰, L. Zhang^{58a}, M. Zhang¹⁷¹, P. Zhang^{15c},
 R. Zhang^{58a,e}, R. Zhang²⁴, X. Zhang^{58b}, Y. Zhang^{15d}, Z. Zhang¹²⁸, X. Zhao⁴¹, Y. Zhao^{58b,128,ai},
 Z. Zhao^{58a}, A. Zhemchugov⁷⁷, B. Zhou¹⁰³, C. Zhou¹⁷⁹, L. Zhou⁴¹, M.S. Zhou^{15d}, M. Zhou¹⁵²,
 N. Zhou^{15b}, C.G. Zhu^{58b}, H. Zhu^{15a}, J. Zhu¹⁰³, Y. Zhu^{58a}, X. Zhuang^{15a}, K. Zhukov¹⁰⁸, A. Zibell¹⁷⁵,
 D. Ziemińska⁶³, N.I. Zimine⁷⁷, C. Zimmermann⁹⁷, S. Zimmermann⁵⁰, Z. Zinonos¹¹³, M. Zinser⁹⁷,
 M. Ziolkowski¹⁴⁸, G. Zobernig¹⁷⁹, A. Zoccoli^{23b,23a}, R. Zou³⁶, M. Zur Nedden¹⁹, L. Zwalski³⁵.

¹Department of Physics, University of Adelaide, Adelaide; Australia.

²Physics Department, SUNY Albany, Albany NY; United States of America.

- ³Department of Physics, University of Alberta, Edmonton AB; Canada.
- ^{4(a)}Department of Physics, Ankara University, Ankara;^(b)Istanbul Aydin University, Istanbul;^(c)Division of Physics, TOBB University of Economics and Technology, Ankara; Turkey.
- ⁵LAPP, Université Grenoble Alpes, Université Savoie Mont Blanc, CNRS/IN2P3, Annecy; France.
- ⁶High Energy Physics Division, Argonne National Laboratory, Argonne IL; United States of America.
- ⁷Department of Physics, University of Arizona, Tucson AZ; United States of America.
- ⁸Department of Physics, University of Texas at Arlington, Arlington TX; United States of America.
- ⁹Physics Department, National and Kapodistrian University of Athens, Athens; Greece.
- ¹⁰Physics Department, National Technical University of Athens, Zografou; Greece.
- ¹¹Department of Physics, University of Texas at Austin, Austin TX; United States of America.
- ^{12(a)}Bahcesehir University, Faculty of Engineering and Natural Sciences, Istanbul;^(b)Istanbul Bilgi University, Faculty of Engineering and Natural Sciences, Istanbul;^(c)Department of Physics, Bogazici University, Istanbul;^(d)Department of Physics Engineering, Gaziantep University, Gaziantep; Turkey.
- ¹³Institute of Physics, Azerbaijan Academy of Sciences, Baku; Azerbaijan.
- ¹⁴Institut de Física d'Altes Energies (IFAE), Barcelona Institute of Science and Technology, Barcelona; Spain.
- ^{15(a)}Institute of High Energy Physics, Chinese Academy of Sciences, Beijing;^(b)Physics Department, Tsinghua University, Beijing;^(c)Department of Physics, Nanjing University, Nanjing;^(d)University of Chinese Academy of Science (UCAS), Beijing; China.
- ¹⁶Institute of Physics, University of Belgrade, Belgrade; Serbia.
- ¹⁷Department for Physics and Technology, University of Bergen, Bergen; Norway.
- ¹⁸Physics Division, Lawrence Berkeley National Laboratory and University of California, Berkeley CA; United States of America.
- ¹⁹Institut für Physik, Humboldt Universität zu Berlin, Berlin; Germany.
- ²⁰Albert Einstein Center for Fundamental Physics and Laboratory for High Energy Physics, University of Bern, Bern; Switzerland.
- ²¹School of Physics and Astronomy, University of Birmingham, Birmingham; United Kingdom.
- ²²Centro de Investigaciones, Universidad Antonio Nariño, Bogota; Colombia.
- ^{23(a)}Dipartimento di Fisica e Astronomia, Università di Bologna, Bologna;^(b)INFN Sezione di Bologna; Italy.
- ²⁴Physikalisches Institut, Universität Bonn, Bonn; Germany.
- ²⁵Department of Physics, Boston University, Boston MA; United States of America.
- ²⁶Department of Physics, Brandeis University, Waltham MA; United States of America.
- ^{27(a)}Transilvania University of Brasov, Brasov;^(b)Horia Hulubei National Institute of Physics and Nuclear Engineering, Bucharest;^(c)Department of Physics, Alexandru Ioan Cuza University of Iasi, Iasi;^(d)National Institute for Research and Development of Isotopic and Molecular Technologies, Physics Department, Cluj-Napoca;^(e)University Politehnica Bucharest, Bucharest;^(f)West University in Timisoara, Timisoara; Romania.
- ^{28(a)}Faculty of Mathematics, Physics and Informatics, Comenius University, Bratislava;^(b)Department of Subnuclear Physics, Institute of Experimental Physics of the Slovak Academy of Sciences, Kosice; Slovak Republic.
- ²⁹Physics Department, Brookhaven National Laboratory, Upton NY; United States of America.
- ³⁰Departamento de Física, Universidad de Buenos Aires, Buenos Aires; Argentina.
- ³¹Cavendish Laboratory, University of Cambridge, Cambridge; United Kingdom.
- ^{32(a)}Department of Physics, University of Cape Town, Cape Town;^(b)Department of Mechanical Engineering Science, University of Johannesburg, Johannesburg;^(c)School of Physics, University of the Witwatersrand, Johannesburg; South Africa.

- ³³Department of Physics, Carleton University, Ottawa ON; Canada.
- ^{34(a)}Faculté des Sciences Ain Chock, Réseau Universitaire de Physique des Hautes Energies - Université Hassan II, Casablanca;^(b)Centre National de l'Energie des Sciences Techniques Nucleaires (CNESTEN), Rabat;^(c)Faculté des Sciences Semlalia, Université Cadi Ayyad, LPHEA-Marrakech;^(d)Faculté des Sciences, Université Mohamed Premier and LPTPM, Oujda;^(e)Faculté des sciences, Université Mohammed V, Rabat; Morocco.
- ³⁵CERN, Geneva; Switzerland.
- ³⁶Enrico Fermi Institute, University of Chicago, Chicago IL; United States of America.
- ³⁷LPC, Université Clermont Auvergne, CNRS/IN2P3, Clermont-Ferrand; France.
- ³⁸Nevis Laboratory, Columbia University, Irvington NY; United States of America.
- ³⁹Niels Bohr Institute, University of Copenhagen, Copenhagen; Denmark.
- ^{40(a)}Dipartimento di Fisica, Università della Calabria, Rende;^(b)INFN Gruppo Collegato di Cosenza, Laboratori Nazionali di Frascati; Italy.
- ⁴¹Physics Department, Southern Methodist University, Dallas TX; United States of America.
- ⁴²Physics Department, University of Texas at Dallas, Richardson TX; United States of America.
- ^{43(a)}Department of Physics, Stockholm University;^(b)Oskar Klein Centre, Stockholm; Sweden.
- ⁴⁴Deutsches Elektronen-Synchrotron DESY, Hamburg and Zeuthen; Germany.
- ⁴⁵Lehrstuhl für Experimentelle Physik IV, Technische Universität Dortmund, Dortmund; Germany.
- ⁴⁶Institut für Kern- und Teilchenphysik, Technische Universität Dresden, Dresden; Germany.
- ⁴⁷Department of Physics, Duke University, Durham NC; United States of America.
- ⁴⁸SUPA - School of Physics and Astronomy, University of Edinburgh, Edinburgh; United Kingdom.
- ⁴⁹INFN e Laboratori Nazionali di Frascati, Frascati; Italy.
- ⁵⁰Physikalisch Institut, Albert-Ludwigs-Universität Freiburg, Freiburg; Germany.
- ⁵¹II. Physikalisch Institut, Georg-August-Universität Göttingen, Göttingen; Germany.
- ⁵²Département de Physique Nucléaire et Corpusculaire, Université de Genève, Genève; Switzerland.
- ^{53(a)}Dipartimento di Fisica, Università di Genova, Genova;^(b)INFN Sezione di Genova; Italy.
- ⁵⁴II. Physikalisch Institut, Justus-Liebig-Universität Giessen, Giessen; Germany.
- ⁵⁵SUPA - School of Physics and Astronomy, University of Glasgow, Glasgow; United Kingdom.
- ⁵⁶LPSC, Université Grenoble Alpes, CNRS/IN2P3, Grenoble INP, Grenoble; France.
- ⁵⁷Laboratory for Particle Physics and Cosmology, Harvard University, Cambridge MA; United States of America.
- ^{58(a)}Department of Modern Physics and State Key Laboratory of Particle Detection and Electronics, University of Science and Technology of China, Hefei;^(b)Institute of Frontier and Interdisciplinary Science and Key Laboratory of Particle Physics and Particle Irradiation (MOE), Shandong University, Qingdao;^(c)School of Physics and Astronomy, Shanghai Jiao Tong University, KLPPAC-MoE, SKLPPC, Shanghai;^(d)Tsung-Dao Lee Institute, Shanghai; China.
- ^{59(a)}Kirchhoff-Institut für Physik, Ruprecht-Karls-Universität Heidelberg, Heidelberg;^(b)Physikalisch Institut, Ruprecht-Karls-Universität Heidelberg, Heidelberg; Germany.
- ⁶⁰Faculty of Applied Information Science, Hiroshima Institute of Technology, Hiroshima; Japan.
- ^{61(a)}Department of Physics, Chinese University of Hong Kong, Shatin, N.T., Hong Kong;^(b)Department of Physics, University of Hong Kong, Hong Kong;^(c)Department of Physics and Institute for Advanced Study, Hong Kong University of Science and Technology, Clear Water Bay, Kowloon, Hong Kong; China.
- ⁶²Department of Physics, National Tsing Hua University, Hsinchu; Taiwan.
- ⁶³Department of Physics, Indiana University, Bloomington IN; United States of America.
- ^{64(a)}INFN Gruppo Collegato di Udine, Sezione di Trieste, Udine;^(b)ICTP, Trieste;^(c)Dipartimento di Chimica, Fisica e Ambiente, Università di Udine, Udine; Italy.

- ^{65(a)}INFN Sezione di Lecce;^(b)Dipartimento di Matematica e Fisica, Università del Salento, Lecce; Italy.
^{66(a)}INFN Sezione di Milano;^(b)Dipartimento di Fisica, Università di Milano, Milano; Italy.
^{67(a)}INFN Sezione di Napoli;^(b)Dipartimento di Fisica, Università di Napoli, Napoli; Italy.
^{68(a)}INFN Sezione di Pavia;^(b)Dipartimento di Fisica, Università di Pavia, Pavia; Italy.
^{69(a)}INFN Sezione di Pisa;^(b)Dipartimento di Fisica E. Fermi, Università di Pisa, Pisa; Italy.
^{70(a)}INFN Sezione di Roma;^(b)Dipartimento di Fisica, Sapienza Università di Roma, Roma; Italy.
^{71(a)}INFN Sezione di Roma Tor Vergata;^(b)Dipartimento di Fisica, Università di Roma Tor Vergata, Roma; Italy.
^{72(a)}INFN Sezione di Roma Tre;^(b)Dipartimento di Matematica e Fisica, Università Roma Tre, Roma; Italy.
^{73(a)}INFN-TIFPA;^(b)Università degli Studi di Trento, Trento; Italy.
⁷⁴Institut für Astro- und Teilchenphysik, Leopold-Franzens-Universität, Innsbruck; Austria.
⁷⁵University of Iowa, Iowa City IA; United States of America.
⁷⁶Department of Physics and Astronomy, Iowa State University, Ames IA; United States of America.
⁷⁷Joint Institute for Nuclear Research, Dubna; Russia.
^{78(a)}Departamento de Engenharia Elétrica, Universidade Federal de Juiz de Fora (UFJF), Juiz de Fora;^(b)Universidade Federal do Rio De Janeiro COPPE/EE/IF, Rio de Janeiro;^(c)Universidade Federal de São João del Rei (UFSJ), São João del Rei;^(d)Instituto de Física, Universidade de São Paulo, São Paulo; Brazil.
⁷⁹KEK, High Energy Accelerator Research Organization, Tsukuba; Japan.
⁸⁰Graduate School of Science, Kobe University, Kobe; Japan.
^{81(a)}AGH University of Science and Technology, Faculty of Physics and Applied Computer Science, Krakow;^(b)Marian Smoluchowski Institute of Physics, Jagiellonian University, Krakow; Poland.
⁸²Institute of Nuclear Physics Polish Academy of Sciences, Krakow; Poland.
⁸³Faculty of Science, Kyoto University, Kyoto; Japan.
⁸⁴Kyoto University of Education, Kyoto; Japan.
⁸⁵Research Center for Advanced Particle Physics and Department of Physics, Kyushu University, Fukuoka ; Japan.
⁸⁶Instituto de Física La Plata, Universidad Nacional de La Plata and CONICET, La Plata; Argentina.
⁸⁷Physics Department, Lancaster University, Lancaster; United Kingdom.
⁸⁸Oliver Lodge Laboratory, University of Liverpool, Liverpool; United Kingdom.
⁸⁹Department of Experimental Particle Physics, Jožef Stefan Institute and Department of Physics, University of Ljubljana, Ljubljana; Slovenia.
⁹⁰School of Physics and Astronomy, Queen Mary University of London, London; United Kingdom.
⁹¹Department of Physics, Royal Holloway University of London, Egham; United Kingdom.
⁹²Department of Physics and Astronomy, University College London, London; United Kingdom.
⁹³Louisiana Tech University, Ruston LA; United States of America.
⁹⁴Fysiska institutionen, Lunds universitet, Lund; Sweden.
⁹⁵Centre de Calcul de l’Institut National de Physique Nucléaire et de Physique des Particules (IN2P3), Villeurbanne; France.
⁹⁶Departamento de Física Teorica C-15 and CIAFF, Universidad Autónoma de Madrid, Madrid; Spain.
⁹⁷Institut für Physik, Universität Mainz, Mainz; Germany.
⁹⁸School of Physics and Astronomy, University of Manchester, Manchester; United Kingdom.
⁹⁹CPPM, Aix-Marseille Université, CNRS/IN2P3, Marseille; France.
¹⁰⁰Department of Physics, University of Massachusetts, Amherst MA; United States of America.
¹⁰¹Department of Physics, McGill University, Montreal QC; Canada.
¹⁰²School of Physics, University of Melbourne, Victoria; Australia.

- ¹⁰³Department of Physics, University of Michigan, Ann Arbor MI; United States of America.
- ¹⁰⁴Department of Physics and Astronomy, Michigan State University, East Lansing MI; United States of America.
- ¹⁰⁵B.I. Stepanov Institute of Physics, National Academy of Sciences of Belarus, Minsk; Belarus.
- ¹⁰⁶Research Institute for Nuclear Problems of Byelorussian State University, Minsk; Belarus.
- ¹⁰⁷Group of Particle Physics, University of Montreal, Montreal QC; Canada.
- ¹⁰⁸P.N. Lebedev Physical Institute of the Russian Academy of Sciences, Moscow; Russia.
- ¹⁰⁹Institute for Theoretical and Experimental Physics (ITEP), Moscow; Russia.
- ¹¹⁰National Research Nuclear University MEPhI, Moscow; Russia.
- ¹¹¹D.V. Skobeltsyn Institute of Nuclear Physics, M.V. Lomonosov Moscow State University, Moscow; Russia.
- ¹¹²Fakultät für Physik, Ludwig-Maximilians-Universität München, München; Germany.
- ¹¹³Max-Planck-Institut für Physik (Werner-Heisenberg-Institut), München; Germany.
- ¹¹⁴Nagasaki Institute of Applied Science, Nagasaki; Japan.
- ¹¹⁵Graduate School of Science and Kobayashi-Maskawa Institute, Nagoya University, Nagoya; Japan.
- ¹¹⁶Department of Physics and Astronomy, University of New Mexico, Albuquerque NM; United States of America.
- ¹¹⁷Institute for Mathematics, Astrophysics and Particle Physics, Radboud University Nijmegen/Nikhef, Nijmegen; Netherlands.
- ¹¹⁸Nikhef National Institute for Subatomic Physics and University of Amsterdam, Amsterdam; Netherlands.
- ¹¹⁹Department of Physics, Northern Illinois University, DeKalb IL; United States of America.
- ^{120(a)}Budker Institute of Nuclear Physics, SB RAS, Novosibirsk;^(b)Novosibirsk State University Novosibirsk; Russia.
- ¹²¹Department of Physics, New York University, New York NY; United States of America.
- ¹²²Ohio State University, Columbus OH; United States of America.
- ¹²³Faculty of Science, Okayama University, Okayama; Japan.
- ¹²⁴Homer L. Dodge Department of Physics and Astronomy, University of Oklahoma, Norman OK; United States of America.
- ¹²⁵Department of Physics, Oklahoma State University, Stillwater OK; United States of America.
- ¹²⁶Palacký University, RCPTM, Joint Laboratory of Optics, Olomouc; Czech Republic.
- ¹²⁷Center for High Energy Physics, University of Oregon, Eugene OR; United States of America.
- ¹²⁸LAL, Université Paris-Sud, CNRS/IN2P3, Université Paris-Saclay, Orsay; France.
- ¹²⁹Graduate School of Science, Osaka University, Osaka; Japan.
- ¹³⁰Department of Physics, University of Oslo, Oslo; Norway.
- ¹³¹Department of Physics, Oxford University, Oxford; United Kingdom.
- ¹³²LPNHE, Sorbonne Université, Paris Diderot Sorbonne Paris Cité, CNRS/IN2P3, Paris; France.
- ¹³³Department of Physics, University of Pennsylvania, Philadelphia PA; United States of America.
- ¹³⁴Konstantinov Nuclear Physics Institute of National Research Centre "Kurchatov Institute", PNPI, St. Petersburg; Russia.
- ¹³⁵Department of Physics and Astronomy, University of Pittsburgh, Pittsburgh PA; United States of America.
- ^{136(a)}Laboratório de Instrumentação e Física Experimental de Partículas - LIP;^(b)Departamento de Física, Faculdade de Ciências, Universidade de Lisboa, Lisboa;^(c)Departamento de Física, Universidade de Coimbra, Coimbra;^(d)Centro de Física Nuclear da Universidade de Lisboa, Lisboa;^(e)Departamento de Física, Universidade do Minho, Braga;^(f)Departamento de Física Teórica y del Cosmos, Universidad de Granada, Granada (Spain);^(g)Dep Física and CEFITEC of Faculdade de Ciências e Tecnologia,

- Universidade Nova de Lisboa, Caparica; Portugal.
- ¹³⁷Institute of Physics, Academy of Sciences of the Czech Republic, Prague; Czech Republic.
- ¹³⁸Czech Technical University in Prague, Prague; Czech Republic.
- ¹³⁹Charles University, Faculty of Mathematics and Physics, Prague; Czech Republic.
- ¹⁴⁰State Research Center Institute for High Energy Physics, NRC KI, Protvino; Russia.
- ¹⁴¹Particle Physics Department, Rutherford Appleton Laboratory, Didcot; United Kingdom.
- ¹⁴²IRFU, CEA, Université Paris-Saclay, Gif-sur-Yvette; France.
- ¹⁴³Santa Cruz Institute for Particle Physics, University of California Santa Cruz, Santa Cruz CA; United States of America.
- ¹⁴⁴(^a)Departamento de Física, Pontificia Universidad Católica de Chile, Santiago; (^b)Departamento de Física, Universidad Técnica Federico Santa María, Valparaíso; Chile.
- ¹⁴⁵Department of Physics, University of Washington, Seattle WA; United States of America.
- ¹⁴⁶Department of Physics and Astronomy, University of Sheffield, Sheffield; United Kingdom.
- ¹⁴⁷Department of Physics, Shinshu University, Nagano; Japan.
- ¹⁴⁸Department Physik, Universität Siegen, Siegen; Germany.
- ¹⁴⁹Department of Physics, Simon Fraser University, Burnaby BC; Canada.
- ¹⁵⁰SLAC National Accelerator Laboratory, Stanford CA; United States of America.
- ¹⁵¹Physics Department, Royal Institute of Technology, Stockholm; Sweden.
- ¹⁵²Departments of Physics and Astronomy, Stony Brook University, Stony Brook NY; United States of America.
- ¹⁵³Department of Physics and Astronomy, University of Sussex, Brighton; United Kingdom.
- ¹⁵⁴School of Physics, University of Sydney, Sydney; Australia.
- ¹⁵⁵Institute of Physics, Academia Sinica, Taipei; Taiwan.
- ¹⁵⁶Academia Sinica Grid Computing, Institute of Physics, Academia Sinica, Taipei; Taiwan.
- ¹⁵⁷(^a)E. Andronikashvili Institute of Physics, Iv. Javakhishvili Tbilisi State University, Tbilisi; (^b)High Energy Physics Institute, Tbilisi State University, Tbilisi; Georgia.
- ¹⁵⁸Department of Physics, Technion, Israel Institute of Technology, Haifa; Israel.
- ¹⁵⁹Raymond and Beverly Sackler School of Physics and Astronomy, Tel Aviv University, Tel Aviv; Israel.
- ¹⁶⁰Department of Physics, Aristotle University of Thessaloniki, Thessaloniki; Greece.
- ¹⁶¹International Center for Elementary Particle Physics and Department of Physics, University of Tokyo, Tokyo; Japan.
- ¹⁶²Graduate School of Science and Technology, Tokyo Metropolitan University, Tokyo; Japan.
- ¹⁶³Department of Physics, Tokyo Institute of Technology, Tokyo; Japan.
- ¹⁶⁴Tomsk State University, Tomsk; Russia.
- ¹⁶⁵Department of Physics, University of Toronto, Toronto ON; Canada.
- ¹⁶⁶(^a)TRIUMF, Vancouver BC; (^b)Department of Physics and Astronomy, York University, Toronto ON; Canada.
- ¹⁶⁷Division of Physics and Tomonaga Center for the History of the Universe, Faculty of Pure and Applied Sciences, University of Tsukuba, Tsukuba; Japan.
- ¹⁶⁸Department of Physics and Astronomy, Tufts University, Medford MA; United States of America.
- ¹⁶⁹Department of Physics and Astronomy, University of California Irvine, Irvine CA; United States of America.
- ¹⁷⁰Department of Physics and Astronomy, University of Uppsala, Uppsala; Sweden.
- ¹⁷¹Department of Physics, University of Illinois, Urbana IL; United States of America.
- ¹⁷²Instituto de Física Corpuscular (IFIC), Centro Mixto Universidad de Valencia - CSIC, Valencia; Spain.

- ¹⁷³Department of Physics, University of British Columbia, Vancouver BC; Canada.
- ¹⁷⁴Department of Physics and Astronomy, University of Victoria, Victoria BC; Canada.
- ¹⁷⁵Fakultät für Physik und Astronomie, Julius-Maximilians-Universität Würzburg, Würzburg; Germany.
- ¹⁷⁶Department of Physics, University of Warwick, Coventry; United Kingdom.
- ¹⁷⁷Waseda University, Tokyo; Japan.
- ¹⁷⁸Department of Particle Physics, Weizmann Institute of Science, Rehovot; Israel.
- ¹⁷⁹Department of Physics, University of Wisconsin, Madison WI; United States of America.
- ¹⁸⁰Fakultät für Mathematik und Naturwissenschaften, Fachgruppe Physik, Bergische Universität Wuppertal, Wuppertal; Germany.
- ¹⁸¹Department of Physics, Yale University, New Haven CT; United States of America.
- ¹⁸²Yerevan Physics Institute, Yerevan; Armenia.
- ^a Also at Department of Physics, University of Malaya, Kuala Lumpur; Malaysia.
- ^b Also at Borough of Manhattan Community College, City University of New York, NY; United States of America.
- ^c Also at Centre for High Performance Computing, CSIR Campus, Rosebank, Cape Town; South Africa.
- ^d Also at CERN, Geneva; Switzerland.
- ^e Also at CPPM, Aix-Marseille Université, CNRS/IN2P3, Marseille; France.
- ^f Also at Département de Physique Nucléaire et Corpusculaire, Université de Genève, Genève; Switzerland.
- ^g Also at Departament de Fisica de la Universitat Autonoma de Barcelona, Barcelona; Spain.
- ^h Also at Departamento de Física Teorica y del Cosmos, Universidad de Granada, Granada (Spain); Spain.
- ⁱ Also at Departamento de Física, Pontificia Universidad Católica de Chile, Santiago; Chile.
- ^j Also at Department of Applied Physics and Astronomy, University of Sharjah, Sharjah; United Arab Emirates.
- ^k Also at Department of Financial and Management Engineering, University of the Aegean, Chios; Greece.
- ^l Also at Department of Physics and Astronomy, University of Louisville, Louisville, KY; United States of America.
- ^m Also at Department of Physics, California State University, Fresno CA; United States of America.
- ⁿ Also at Department of Physics, California State University, Sacramento CA; United States of America.
- ^o Also at Department of Physics, King's College London, London; United Kingdom.
- ^p Also at Department of Physics, Nanjing University, Nanjing; China.
- ^q Also at Department of Physics, St. Petersburg State Polytechnical University, St. Petersburg; Russia.
- ^r Also at Department of Physics, University of Fribourg, Fribourg; Switzerland.
- ^s Also at Department of Physics, University of Michigan, Ann Arbor MI; United States of America.
- ^t Also at Dipartimento di Fisica E. Fermi, Università di Pisa, Pisa; Italy.
- ^u Also at Giresun University, Faculty of Engineering, Giresun; Turkey.
- ^v Also at Graduate School of Science, Osaka University, Osaka; Japan.
- ^w Also at Horia Hulubei National Institute of Physics and Nuclear Engineering, Bucharest; Romania.
- ^x Also at II. Physikalisches Institut, Georg-August-Universität Göttingen, Göttingen; Germany.
- ^y Also at Institucio Catalana de Recerca i Estudis Avancats, ICREA, Barcelona; Spain.
- ^z Also at Institut de Física d'Altes Energies (IFAE), Barcelona Institute of Science and Technology, Barcelona; Spain.
- ^{aa} Also at Institut für Experimentalphysik, Universität Hamburg, Hamburg; Germany.
- ^{ab} Also at Institute for Mathematics, Astrophysics and Particle Physics, Radboud University Nijmegen/Nikhef, Nijmegen; Netherlands.

ac Also at Institute for Particle and Nuclear Physics, Wigner Research Centre for Physics, Budapest; Hungary.

ad Also at Institute of Frontier and Interdisciplinary Science and Key Laboratory of Particle Physics and Particle Irradiation (MOE), Shandong University, Qingdao; China.

ae Also at Institute of Particle Physics (IPP); Canada.

af Also at Institute of Physics, Academia Sinica, Taipei; Taiwan.

ag Also at Institute of Physics, Azerbaijan Academy of Sciences, Baku; Azerbaijan.

ah Also at Institute of Theoretical Physics, Ilia State University, Tbilisi; Georgia.

ai Also at LAL, Université Paris-Sud, CNRS/IN2P3, Université Paris-Saclay, Orsay; France.

aj Also at Louisiana Tech University, Ruston LA; United States of America.

ak Also at Manhattan College, New York NY; United States of America.

al Also at Moscow Institute of Physics and Technology State University, Dolgoprudny; Russia.

am Also at National Research Nuclear University MEPhI, Moscow; Russia.

an Also at Novosibirsk State University, Novosibirsk; Russia.

ao Also at Ochanomizu University, Ochanomizu University, Tokyo; Japan.

ap Also at Physikalisches Institut, Albert-Ludwigs-Universität Freiburg, Freiburg; Germany.

aq Also at School of Physics, Sun Yat-sen University, Guangzhou; China.

ar Also at The City College of New York, New York NY; United States of America.

as Also at The Collaborative Innovation Center of Quantum Matter (CICQM), Beijing; China.

at Also at Tomsk State University, Tomsk, and Moscow Institute of Physics and Technology State University, Dolgoprudny; Russia.

au Also at TRIUMF, Vancouver BC; Canada.

av Also at Universita di Napoli Parthenope, Napoli; Italy.

* Deceased